Ecohydraulics of Instream Flow Alterations

Valentine Muhawenimana

Supervised by:

Dr. Catherine A.M.E. Wilson and Prof. Jo Cable

A thesis submitted to Cardiff University for the degree of

Doctor of Philosophy (PhD)

Department of Civil and Environmental Engineering

School of Engineering

Cardiff University, Wales, UK

October 2019

Acknowledgment

My deepest thanks to my supervisors Dr Catherine Wilson and Prof Jo Cable for having guided, supported, mentored and inspired me throughout my PhD, I am ever grateful. You have been awesome all the way and working with you has been an honour.

Thanks are extended to Pablo, Rhidian, Alex, Rhi, and Jelena with whom I have had the privilege of collaborating throughout the PhD. Special thanks to Amy for providing Tilapia and all in the CRIPES lab for caring for the fish.

Thanks to the School of Engineering for funding my PhD, it is greatly appreciated. I also thank the lab technicians Paul, Harry, and Carl who were always keen to assist during experiments. I am grateful to the undergraduate students Ana, Jak, and Nadine for assistance in collecting data. I also wish to thank colleagues and friends in the HRC in Engineering and CRIPES in Biosciences, for both fun and learning times.

For company and laughs, I thank my siblings Valery, Paci, Feza, Christine, Desire, all the friends from Radar, Joelle, Faith, Avinash, Shalini, Arthur, Ben, Mpinga, and of course Eunice; you patiently listened to my reports of up and downs and always encouraged me. To my dear Tony, forever thank you for always being my lighthouse.

To my amazing parents, maman Goretti and papa Bonaventure, I dedicate this PhD in gratitude for everything.

And to anyone reading these words, thank you!

Abstract

Increasingly sustainable river management efforts are underway to limit the damage on freshwater ecosystems caused by anthropogenic hydro-engineering activities. This is exemplified by engineered Woody debris dams (WDD) used Natural Flood Management (NFM) to attenuate flood flows, although design guidance and evidence of WDD flood attenuation are incomplete. Considering current questions of inefficient solutions in ecohydraulics, a trade-off is necessary to balance the introduction of new alterations with restoring river habitats and biodiversity. This thesis sought to (i) evaluate design options for WDD to maximise their performance for flood attenuation, and (ii) resolve questions pertaining to the hydrodynamics of flow alterations and resulting fish-flow interactions. Flood attenuation was found to depend on WDD streamwise length, geometric arrangement, and most importantly cross-sectional flow blockage ratio and porosity (Ch. 2). In the wake of an idealised WDD spanwise cylinder, turbulence length scale relative to fish size, direction and magnitude of Reynolds shear stresses and vorticity governed fish (Nile tilapia, *Oreochromis niloticus*) swimming stability, and habitat choice reflected avoidance of relatively highly turbulent areas (Ch. 3). Large Eddy Simulation showed that proximity of the spanwise cylinder to the ground determined the wake and near bed dynamics by affecting the separation of shear layers, creating a ground vortex that merged with the von-Karman vortex street rendering the wake asymmetrical, and resulting in lift forces, drag coefficients and Strouhal numbers higher than those of unbounded cylinders (Ch. 4). Furthermore, swimming performance and habitat choice of Pumpkinseed fish (*Lepomis gibbosus*) relative to velocity and turbulence was found to highly depend on temperature, as fish showed energy-saving behaviour at the lower temperature, while their time to fatigue increased with temperature (Ch. 5). In addition to quantifying WDD flood attenuation performance in relation to dam composition, arrangement of wood pieces and porosity, this thesis highlighted the importance of currently overlooked and ultimately consequential flow attributes such as the direction of turbulent shear stresses and vorticity, and temperature regimes in the current depiction on fish behaviour in anthropogenically altered flows.

Nomenclature

A_B	Cross-sectional flow blockage ratio
A_f	Cross-sectional flow area for uniform flow condition
A_L	Cross-section area of the LWD
A_p	Projected area of a log member of LWD
B_{fp}	Flood plain width
B_{mc}	Main channel width
C_D	Drag coefficient
C_L	Lift coefficient
D, D_i	Cylinder, Log diameter
d.f.	Degrees of freedom
f	vortex shedding peak frequency
F_D	Drag force
Fr	Froude number
G	Gap between channel bed and obstruction
GLM	Generalised Linear Model
GLMM	Generalised Linear Mixed Model
GV	Ground vortex
H	Flow depth
h_0	Uniform flow depth
h_t	Height of top log above the channel bed (Z direction)
LES	Large Eddy Simulation
L_u	The longitudinal turbulent integral length
WDD	Woody debris dam
L_x	Streamwise length of the dam (X direction)

PSD	Power Spectral Distribution
Q	Discharge
R_0	Hydraulic radius
Re	Reynolds number
SL, TL	Fish standard, and total length
St	Strouhal number
T_f	Time to fatigue for fish swimming
TI	Turbulence intensity
TKE	Turbulent kinetic energy
u^*	Friction velocity
u, v, w	streamwise, spanwise, and vertical velocity components
u', v', w'	streamwise, spanwise, and vertical components of velocity fluctuations
U_0	Cross-sectional averaged velocity
W	Fish weight
x, y, z	streamwise, spanwise, and vertical components of the coordinate system
ΔA	Upstream flow area increase
Δh	Upstream afflux
θ	Flow separation angle
ν	Fluid kinematic viscosity
ρ	fluid density
τ_{uv}	Spanwise Reynolds shear stress component
τ_{uw}	Vertical Reynolds shear stress component
ω_y	spanwise component of the vorticity vector
$\overline{(\ )}$	Time averaging symbol
$\langle\ \rangle$	Spatial averaging symbol

Table of contents

List of figures

List of tables

Chapter 1. General Introduction

1.1 Context

The world's river systems are currently severely impacted by extensive hydraulic engineering and water resources activities, including transportation, hydropower energy generation and flood risk management. The consequences of this widespread disruption of the natural environment are apparent in the fragmentation of river habitats, damages to biodiversity and loss of natural ecological processes, where hydraulic structures such as dams create fish migration barriers (Poff et al. 1997; Nilsson et al. 2005; Fuller et al. 2015). Furthermore, climate change impacts all aspects of the earth's environment, exacerbates the frequency and severity of floods, changes fluvial regimes and raises water and air temperatures, further modifying the aquatic habitats and populations (Poff et al. 2002; Daufresne and Boët 2007; Schneider et al. 2013).

To address these issues, ecohydraulics combines the fields of biology, ecology, civil and environmental engineering to asses and solve problems shared across these fields by providing solutions that are better suited to preserving aquatic biodiversity, while limiting and reversing the negative environmental impacts incurred thus far (Nestler et al. 2016; Silva et al. 2018). However, the field of ecohydraulics currently suffers from inefficient solutions, and must improve the sustainability of anthropogenic fluvial practices (Murchie et al. 2008; Cooke and Hinch 2013; Kemp 2016; Silva et al. 2018), while adapting to climate change and its added impact on ecosystems. It is,

therefore, essential that improvements to current and new solutions to river engineering questions be evaluated, using sustainable means, as exemplified by Natural Flood Management to remedy the effects of altering flow regimes on aquatic species. Detailed literature reviews of these subjects are provided in each subsequent chapter. This introductory chapter presents an overview of current problems, solutions and remaining questions related to the hydrodynamics of instream flow alterations and impacts on fish behaviour, after which the aims and objectives of this thesis are outlined.

1.2 Fragmentation of freshwater ecosystems and modifications to river habitats

Anthropogenic modifications to river environments for water supply and flow regulation, hydropower, navigation, irrigation and flood control have severely fragmented and damaged freshwater ecosystems (Poff et al. 1997; Fuller et al. 2015). Up to 80% of the main European rivers (Dynesius & Nilsson, 1994) and 50% of the world's large river systems are fragmented by dams with direct damages to ecosystem biodiversity (Nilsson et al. 2005). Alterations of natural flow regimes by hydro-engineering structures, such as dams, reservoirs, hydropower turbines, weirs and culverts, have changed the physical and ecological habitat features of otherwise natural flow regimes (O'Hanley et al. 2013; Fuller et al. 2015). Moreover, the lack of habitat connectivity has driven unfavourable changes to biodiversity by affecting fish throughout their life cycles whereby their short and long-distance migrations are limited to the isolated habitats, affecting fish populations and dispersion (Bunn and Arthington 2002; Fagan 2002; Moilanen and Nieminen 2002; Miyazono and Taylor 2013; O'Hanley et al. 2013). Freshwater ecosystems are further threatened by global climate change, which affects air and water temperature, as well as precipitation and river runoff patterns (Hulme et al. 2002; Poff et al. 2002; Schneider et al. 2013;

Masson-Delmotte et al. 2018). The hydrologic processes rendered extreme, also increase the frequency of flood events (Hulme et al. 2002; Masson-Delmotte et al. 2018). Furthermore, the cumulative effect of climate change results in immediate alterations to aquatic environments and disrupts ecosystem functions (Poff and Hart 2002; Daufresne and Boët 2007; Clarke 2009; Schneider et al. 2013; Masson-Delmotte et al. 2018).

Natural Flood Management (NFM) is amongst one of the most recent methods for managing the effects climate change in response to current natural flooding disasters, which cause major human disruption, economic loss and even mortalities (Pitt, 2008b). NFM has potential to complement traditional engineering flood defence methods, for example flood gates, by-pass channels, dams and reservoirs, with 'soft engineering' methods, such as earth bunds, woodland planting, ditches, storage ponds and Large woody debris dams (Pitt 2008; SEPA 2015; Burgess-Gamble et al. 2017). NFM offers sustainable cost-effective methods of hydrologically and hydraulically managing run-off and alleviating flood risk, along with ecosystem benefits by utilising natural processes, which emphasize the natural functions of rivers, floodplains and catchments (SEPA 2015; Burgess-Gamble et al. 2017; Dadson et al. 2017).

Instream flow attenuation structures such as engineered Woody debris dams (WDD) (shown in Figs. 1.1, and 1.2) used in NFM pose the risk of increasing channel obstruction and fragmentation. Engineered WDD are similar to, and inspired by naturally occurring WDD and beaver dams, which are classified as naturally occurring, non-anthropogenic barriers, whose cumulative damming effect has a river fragmentation impact (Naiman et al. 1988; Fuller et al. 2015). New physical alterations to the natural flow pattern could further fragment and strain freshwater ecosystems (Schneider et al., 2013), especially as ecosystems will be unable to adapt at the rapid rate of climate change (Poff et al. 2002).

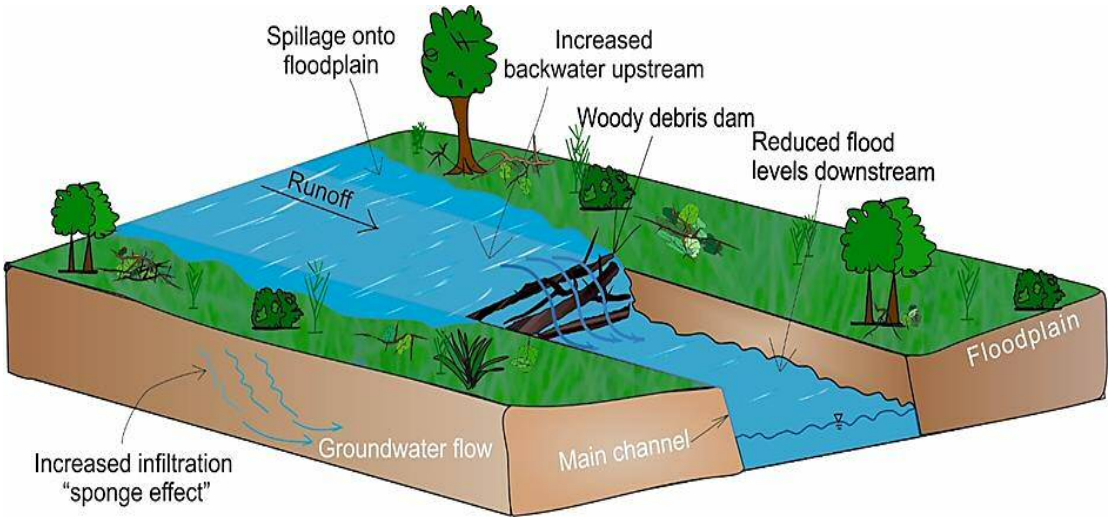

Figure 1.1. Diagram illustrating the flow attenuation process of woody debris dams where flow is temporally stored on upstream of the dam, spilling onto floodplains and increasing ground water infiltration and the resulting reduction of the downstream flow depths.

Figure 1.2. Field photograps of WDD (left) depticting backwater rise upstream of the dam (Source: Slow The Flow Calderdale, 2019) and (right) a series of WDD on Wilde Brook, part of 'Shropshire Slow the Flow'.

WDD's flood defence efficiency might only cover small flood events of up to 1 in 50 return periods, although they can successfully mitigate against high return period flood events when used in conjunction with other NFM methods such as offline storage areas (Burgess-Gamble et al. 2017). However, more evidence of this efficiency is necessary, particularly across different catchment types, gradients and land-uses, as well as design guidance to ensure that flood alleviation and habitats enhancement benefits are maximised (Nienhuis and Leuven 2001; Acreman et al. 2011; SEPA 2015; Burgess-Gamble et al. 2017). Hence, a trade-off between the need for natural flood management and the introduction of artificial obstructions in rivers, while efforts are being made to adapt to climate change, restore river connectivity and rehabilitate damaged ecosystems is necessary (Acreman et al. 2011; Barlow et al. 2014; Fuller et al. 2015; Burgess-Gamble et al. 2017).

1.3 Current solutions: river habitat restoration and fish passage

Current river environment engineering and practices intend to gradually restore degraded river ecosystems and their biodiversity functions either to their natural, pre-alteration state or to a newly adapted and sustainable state (Poff et al. 1997; Poff et al. 2002; Clarke 2009). Reviews of restoration methods and outcomes are provided by Roni et al. (2002) and Wohl et al. (2005). To increase habitat complexity, large woody structures are widely used instream (Kail et al. 2007; Nagayama and Nakamura 2010), as well as boulders and spawning gravel placed on river beds (Roni et al., 2002). The efficiency or successful outcomes of river restoration are currently disputed, in terms of the extent of reversed damage or creation of habitat heterogeneity since methods, timescales and reach or catchment scales of restorations and monitoring vary widely (Nienhuis and Leuven 2001; Roni et al. 2002; Palmer et al. 2010; Bernhardt and Palmer 2011; Wohl et al. 2005).

Defragmentation of river networks and increasing connectivity between isolated habitats towards more sustainable ecosystems resource management uses removal of fragmenting agents, or creation of passageways for fish. Methods of removal, especially of dams (reviewed by Kemp and O'Hanley 2010; Foley et al. 2017) opt to eliminate the obstructions entirely, although with the loss of the dam's function come socio-economic costs (Poff and Hart 2002; O'Hanley et al. 2013; Poff and Schmidt 2016; Foley et al. 2017). Post-dam removal habitats show more dynamic processes of streamflow, sediment and nutrients, as well as altered species movement and interactions (Foley et al. 2017). Other river obstructions such as weirs, sluices, deflectors and culvers are also removed or retrofitted to reduce flow blockage and improve the free passage of fish (Nienhuis and Leuven 2001; Roni et al. 2002; Kemp and O'Hanley 2010; Palmer et al. 2010).

Fish passes (also referred to as fishways) and fish ladders are restoration options designed to reduce interference with obstructing hydro-engineering structures, for example dams or hydropower stations, while creating pathways to facilitate the up- and downstream passage of fish over the obstructions (Larinier 2001; Armstron et al. 2010; Katopodis and Williams 2012; Silva et al. 2018). Although much progress has been made since the first designs, fish passes efficiency (i.e. percentage of fish entering the fish pass and successfully passing it; Roscoe and Hinch 2010; Bunt et al. 2012) remains on average 38 to 73% (Bunt et al. 2016), below recommended levels of 85% or an ideal 100% (Larinier 2001; Cooke and Hinch 2013; Silva et al. 2018). Efficiency of fish passes is highly variable and it is debated whether fish passes offer a practical and definitive solution to the problem of river habitat connectivity (Kemp 2016; Silva et al. 2018). It is generally perceived that fish passes have improved connectivity as continuous research has refined their design and performance, but problems persist such as the transference of species-specific fish passes designs to other geo- and biophysical systems across the world (Katopodis and Williams 2012;

Cooke and Hinch 2013; Kemp 2016; Silva et al. 2018) or the risk of ecological trapping (Pelicice and Agostinho 2008).

The high variability of fish pass efficiency is attributed to the lack of fully agreed upon implementation and monitoring standards (Bunt et al. 2016; Silva et al. 2018) and the focus on economically important salmonids at the potential detriment of other species (Roscoe and Hinch 2010; Noonan et al. 2012; Kemp 2016), as depicted in Figure 1.3. Other limiting factors include inadequate placement of fish passes, their design and resulting attraction or within fish passes flow hydraulics which are often unsuitable for fish (Williams et al. 2012). This is in turn attributable to the currently limited understanding of fish-flow interactions, where the flow hydraulics are defining characteristics of the environment that the fish inhabits and must navigate (Williams et al. 2012; Kemp 2016). Flow hydrodynamics in terms of discharge, velocity, and turbulence, along with fish swimming behaviour and physiology have formed the basis of design criteria for fish passes, and advances in these areas will guide the progress of fish pass design and improved efficiency (Larinier 2001; Murchie et al. 2008; Enders et al. 2009; Cooke and Hinch 2013).

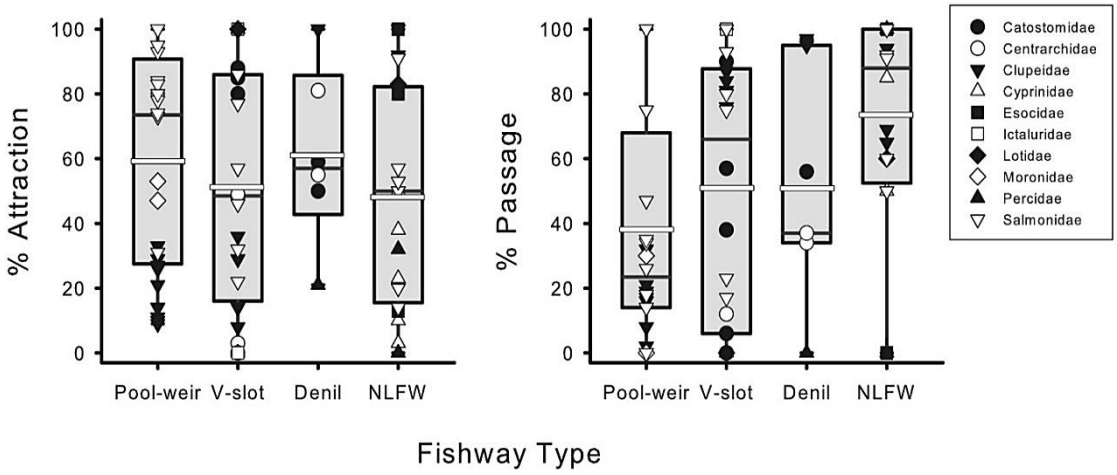

Figure 1.3. A summary of attraction and passage efficiencies of the main fishway types: Pool and weir, Vertical slot, Denil-type and Nature-like fishways (or NLFW).

Data shows from bottom to top: minimum, mean, median, and interquartile distributions. Figure reproduced from Bunt et al. (2016).

1.4 Altered flows, hydrodynamics and fish swimming behaviour

Physical alterations to river habitats change the natural regimes of discharge, flow depth, velocity, turbulence, temperature and water quality (Larinier 2001; Fuller et al. 2015). Understanding fish behavioural responses to these environmental stressors is key for the practical applications of preserving habitats and biodiversity (Larinier 2001; Kemp 2016; Silva et al. 2018). The challenge of linking biological, environmental and engineering aspects of the altered ecosystem is currently exemplified by the conflicting results in the study of fish-flow interactions (Nestler et al. 2016; Silva et al. 2018).

The swimming ability of a fish is generally characterised in terms of its critical, prolonged or sustained swimming velocity, indicating endurance and ability to navigate flow. The effect of altered flows on fish swimming kinematics is then linked to fish swimming behaviour. Negative effects of highly turbulent or accelerating flows are manifested by a decrease in swimming speed, swimming instability and increased energy expenditure whereas positive effects of turbulence allow fish to reduce their energy expenditure by taking advantage of the localised momentum generated from turbulent structures (Webb 1998; Enders et al. 2003; Liao et al. 2003; Smith et al. 2005; Liao 2007; Tritico and Cotel 2010). Fish exhibit complex habitat selection behaviour and chose their station holding positions and swimming path based on temporally and spatially predictable velocity and turbulence flow attributes, such as turbulence intensity (Pavlov et al. 2000; Cotel et al. 2006), turbulent kinetic energy (Smith et al. 2006), and Reynolds shear stresses (Silva et al. 2011). In addition, the extent of impact of turbulent flows depends on the physical size of eddies relative to the fish size (Pavlov et al. 2000; Tritico and Cotel 2010; Webb and Cotel 2011).

The scale gap between laboratory and field studies also makes it difficult to recreate turbulent flows, with turbulent kinetic energy, turbulence intensity, Reynolds shear stresses and vorticity that are representative of those experienced by fish *in situ* (Lacey et al. 2012).

Finally, swimming performance is inherently linked to water temperature (Beddow et al. 1995; Beveridge et al. 2010), an abiotic environmental factor subject to climate change, with immediate physiological effects on fish, directly affecting ecosystem biodiversity (Poff et al. 2002; Rahel and Olden 2008). This key variable, however, has been widely overlooked in ecohydraulics studies and could impact our current understanding of fish-flow interactions.

The cumulative effects of multiple stressors on ecosystems will exacerbate the ecological response to flow alterations (Poff and Zimmerman 2010). As global climate change impacts precipitation, runoff, temperatures, and seasonal variations (Poff et al. 2002), ecohydraulics solutions ought to adapt to these changes, to address the issues of habitat fragmentation and flow alterations, as well as thermal alterations. However, thus far studies of fish-flow interactions have not considered the collective effects velocities, turbulence, and temperature on fish behaviour. Ultimately, isolated approaches to habitat management restoration limit our understanding and solutions to the current issues, which are partly due to due to the aforementioned lack of comprehensive standards but also the incomplete understanding of fish behaviour upon which design and performance of fishways depends (Silva et al., 2018). Considering the physiological effects of temperature and swimming (Figure 1.4) (Lee et al. 2003), thermal barriers merit inclusion in fish kinematics studies to improve fish-friendly engineering.

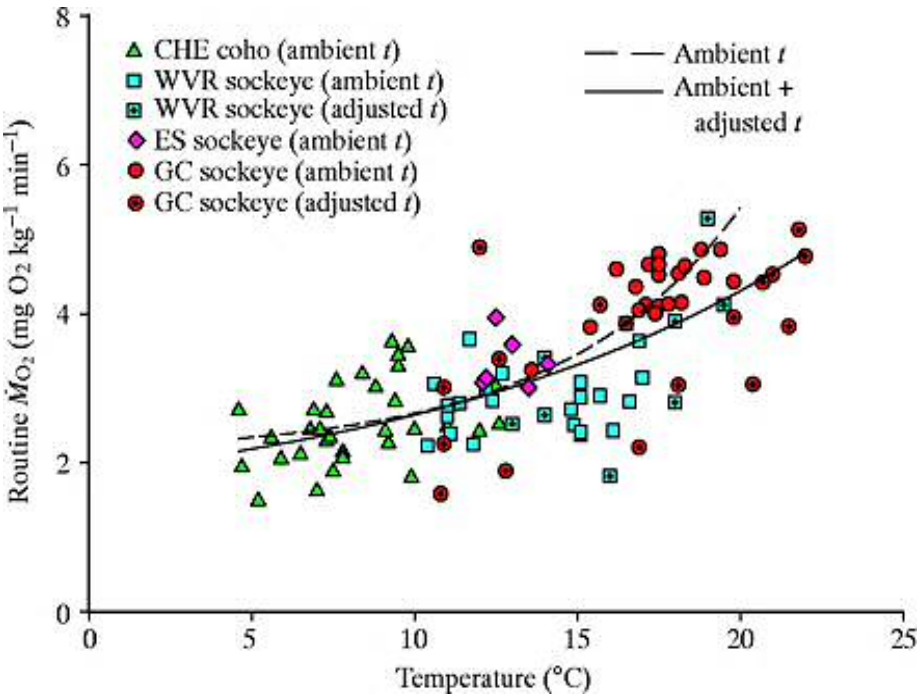

(A)

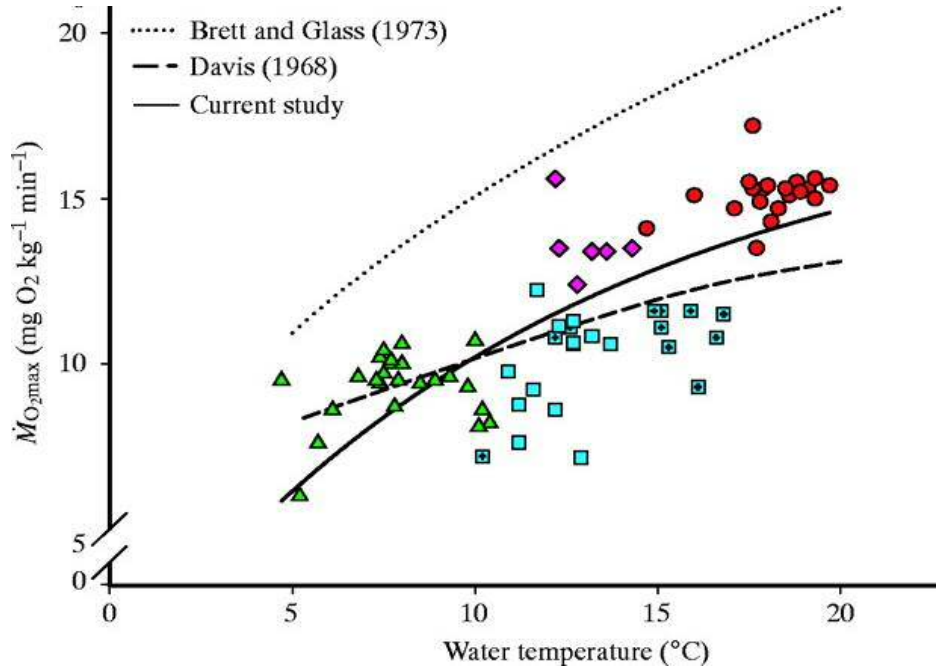

(B)

Figure 1.4. Rate of Oxygen consumption $\dot{M}O_2$ (mg O_2 $min^{-1}kg^{-1}$) relative to temperature, showing exponential increase of (A) routine and (B) maximum (for fish swimming at their critical velocity) Oxygen consumption with increasing temperature. Figures reproduced from Lee et al. (2003).

1.5 Thesis aims and objectives

This thesis addresses research gaps pertaining to the hydraulics of flow alteration by evaluating the flood attenuation performance of NFM features of WDD with regard to their design and physical characteristics, while evaluating their impact on fish behaviour in terms of fish-flow interactions. The following paragraphs outline the thesis structure and present the aims and objectives of each chapter.

In Chapter 2, various experimental designs of WDD were evaluated by their performance in terms of backwater flow area rise, addressing research gaps within design criteria, flood modelling, and practical implementations of NFM. Design parameters for the WDD in the experimental physical models included the length of the dams, the diameter, angle of orientation and distribution of logs, as well as solids volume fraction, porosity or blockage ratio and projected area of the dam. The hydraulics of woody debris dams were explored in a compound channel for 'Engineered dams' (uniformly distributed linear horizontal logs), 'Engineered natural dams' (diagonal logs forming truss like structures) and 'Naturally formed dams' (brush and driftwood accumulation from flood events). These dam designs were also tested under non-porous conditions for cases where brush, sediments, leaves and other debris have completely saturated the dam.

Since the use of WDD for natural flood risk management is expected to enhance river habitats and provide various ecoservices benefits, the effects on free passage of fish following further alteration of natural flow conditions in rivers due to engineered dams were considered. Hence, Chapter 3 of this thesis considered the hydrodynamics of altered flows and their impact on fish behaviour, habitat usage and swimming stability in the wake of a horizontal cylinder. This investigation tested the limiting conditions of velocity and turbulence that adversely affect fish swimming kinematics and stability in the altered flows, as well as their usage of the microhabitats surrounding the obstruction. The hydrodynamic characteristics of the habitats

associated with these behaviours was quantified to further understand the complex interactions of fish with their environments. The hydrodynamics of a spanwise flow obstruction, such as a WDD structure, placed near the channel bed were further studied using experiments and numerical modelling with Large Eddy Simulation to elucidate the fluid mechanics associated with bounded cylinder flow in Chapter 4.

Finally, Chapter 5 of the thesis considered thermal flow alterations, which alter ecosystems and increase pressures on biodiversity and have thus far been excluded from ecohydraulics studies of fish-flow interactions. The effects of water temperature on fish swimming performance and habitat usage were thus considered in relation to flow velocity and turbulence to highlight that this environmental factor affects our current understanding of fish swimming behaviour in altered flows.

Chapter 2. Flood attenuation hydraulics of Engineered Large Woody Debris Dams

A manuscript based on this chapter is currently under preparation aimed at publication in *Journal of Hydrology* as: Muhawenimana Valentine, Wilson Catherine A.M.E., Nefjodova Jelena, and Cable Jo (2019) Natural Flood management: Runoff Attenuation Hydraulics of Engineered Large Woody Debris Dams. V.M, C.W and J.C designed the experiments, V.M and J.N conducted the experiments, V.M processed and analysed the data. V.M wrote the text, with supervision and comments from C.W and J.C.

Summary

Natural flood management aims to enhance natural processes to build resilience into flood risk management alongside standard hard engineering methods of flood defence, using 'soft engineering' methods such as Woody debris dams (WDD). Understanding of the flood attenuation performance of WDD is however, still limited and the current study addresses the research gaps pertaining to the hydraulic effects of various dam designs and the physical characteristics which determine the extent of flood attenuation. Various porous and non-porous engineered WDD, whose designs varied by streamwise length, blockage ratio, mode of formation and distribution of components in linear arrays of horizontal or inclined members with constant or

varying diameters were tested in a symmetrical compound channel. Flow area afflux, defined as the upstream increase in flow area caused by the dam were compared to the initial uniform flow conditions without the dam and used to characterise the flood attenuation performance of the dam, under 80 and 100% bankfull discharges. Flow area afflux ranged from 0 to 30% and depended on cross sectional blockage ratio (A_B) of the flow by the dam, and the projected area of wood (A_L), the distribution of log diameters, the mode of formation of the dam, and the height of the dam in the water column. Streamwise length had a limited effect on afflux, unless it was accompanied by increases in blockage ratio, especially for the non-porous structures. The use of uniformly distributed equal diameter logs in the dams resulted in equal or higher afflux than the more irregular or complex dams that used varied diameters and log orientations. The non-porous structures resulted in at least twice the afflux compared to porous dams, indicating that over time, accumulation of organic matter and sediments, which render the engineered dams more water tight, will improve flood attenuation performance. The cross-sectional blockage ratio of the channel was the primary factor in increasing afflux, and hence, WDD designs which maximise channel obstruction will result in higher flood attenuation.

2.1 Introduction

Flooding is one of the most devastating and costly of all natural disasters. In this era of 'global weirding', globalization and urbanisation, flood risk management has ever increasing importance to reduce human suffering and economic loss. To meet this challenge, flood management has switched from defence to risk strategy (Pitt 2008; Dadson et al. 2017). Current solutions use hard engineering measures such as flood walls, channel widening, flood storage reservoirs, and by-pass channels and flood gates, but also new 'soft engineering' solutions in the form of Natural Flood Management (NFM) in an effort to build resilience into traditional methods (Pitt

2008; SEPA 2015; Burgess-Gamble et al. 2017; Dadson et al. 2017). NFM is a relatively new field that incorporates the use of various natural processes including earth bunds, ditches and storage ponds, Large woody debris dams, and woodland planting in previously unforested areas. All these measures increase groundwater infiltration, alter the hydraulic resistance and flood capacity of river channels and slow down the flow in downstream areas at risk of flooding (Nisbet et al. 2011; SEPA 2015; Burgess-Gamble et al. 2017; Dadson et al. 2017; Lane 2017). Perhaps one of the most cost-effective measures is the introduction of engineered Woody debris dams (WDD), or leaky dams, in middle and upper catchments that attenuate flood processes by diverting flow onto floodplains (Figs.1.1 and 1.2). The resulting backwater effect enables temporary water storage, which is slowly released through the porous dam, thereby attenuating surface runoff and retarding flooding downstream (Gippel 1995; Nisbet et al. 2011; Thomas and Nisbet 2012; Quinn et al. 2013; Wenzel et al. 2014). The terms in equation 2.1 are typically managed using the aforementioned hard engineering methods to reduce flood risk and flood levels, which can also be achieved through reduction of peak discharge by use of WDD as instream storage structures (Lane 2017).

, rearranged as — (2.1)

Where Q is the discharge, B is the channel width, is the mean velocity and is the mean flow depth, and is the stream bed elevation.

Man-made, designed and engineered woody debris dams, also known as, log jams or leaky dams, were inspired by beaver dams, which impound rivers and can retain large volumes of water (Nyssen et al. 2011; Wohl 2013; Giriat et al. 2016; Puttock et al. 2017) and naturally occurring large woody debris accumulations of trees and branches recruited from river banks, which partially or fully obstruct flow (Wallerstein and Thorne 1997; Abbe and Montgomery 1996; Manners et al. 2007;

Dixon and Sear 2014). Descriptions of naturally occurring Woody debris dams (WDD), with key components acting as support structures for the entire dam and smaller diameter and shorter length branches accumulating behind the key members are given by Wallerstein and Thorne (1997) and Manners et al. (2007). River management and restoration schemes have a complex history whereby large woody debris were removed from rivers to improve navigation or to reduce channel resistance as they were believed to increase flood risk (Young 1991; Gippel et al. 1992; Gippel 1995; Shields and Gippel 1995). This, however, was prior to recognition of the deterioration of fluvial habitats, the need to restore their natural processes, and the habitat complexity enhancing effects of WDD, which provide refugia and shade for fish, improved water quality, as well as trapped sediment, organic matter and nutrients (Gippel 1995; Gippel et al. 1996; Roni et al. 2015; SEPA 2015; Burgess-Gamble et al. 2017).

Pilot studies have shown that WDD which span the full channel width can provide flood alleviation by delaying flood peaks and increasing flood travel time (Gregory et al. 1985; Wenzel et al. 2014; Burgess-Gamble et al. 2017; Dadson et al. 2017) (Illustrated in Figure 1.1). Hydraulic models in particular, use hydraulic roughness or Manning's n roughness coefficient to model WDD (Kitts 2010; Odoni and Lane 2010; Thomas and Nisbet 2012; Dixon et al. 2016) even though the physical effects are more complex (Daniels and Rhoads 2007; Manners et al. 2007). Furthermore, previous research on large woody debris accumulations has focused on their river management and desnagging practices, rather than capacity for natural flood management (Gippel et al. 1992; Gippel 1995; Shields and Gippel 1995; Manners et al. 2007).

Unknown are the hydraulic changes that WDDs make to flood processes by altering the upstream surface water profile, constricting and diverting flow, and attenuating flow. Experimental studies of WDDs have only studied the effects of single large

woody structures (Young 1991; Gippel 1995). This does not accurately represent hydraulic complexity of flows through natural and engineered large woody debris dams, which are composed of multiple timbers (Daniels and Rhoads 2007; Manners et al. 2007; Schalko et al. 2018). The process and extent of these benefits, however, have yet to be effectively quantified, as there is currently limited evidence for WDD design and flood attenuation performance (Burgess-Gamble et al., 2017).

Here, we experimentally quantified the backwater flow area rise and flood attenuation performance of full-span WDD in relation to the dams' streamwise length, cross sectional area, blockage ratio, orientation and angle of dam members and dam configuration, under bankfull (100% bankfull) and near bankfull (80% bankfull) conditions for various porosity and flow blockage ratios. Quantitative analysis of the hydraulics of these WDDs also addresses the lack of standardised designs, and we provide recommendations of key physical attributes for optimising the performance of WDD.

2.2 Methodology

2.2.1 Flume and uniform flow conditions

Experiments were conducted in an open channel recirculating flume 10 m long, 1.2 m wide, and 0.3 m deep (L, B, D) set to a 1/1000 bed slope. PVC sheets partitioned the flume into a symmetric compound channel, with a rectangular main channel of width 0.6 m (B_{mc}) and total floodplain width (B_{fp}) of 0.6 m comprised of two 0.3 m wide floodplains on each side of the main channel. The main channel has a bankfull depth of 0.15 m (H) (Figure 2.1). A pump with 0.6 m^3s^{-1} capacity recirculated the water and controlled the discharge, while a sharp crested tailgate weir located at the downstream end of the flume maintained the surface water profile along the flume. An ultrasonic flow meter (TecFluid Nixon CU100) measured the discharge to a precision of ± 1.5%. A Vernier pointer gauge was used measure the flow depth (±0.2 mm). Prior to installation of the WDD, uniform flow conditions were established for

80% bankfull flow condition ($0.8Q_{bk}$) and bankfull flow condition (Q_{bk}), relating to discharges (Q) of 0.22 and 0.28 m^3s^{-1} and uniform flow depths h_0 of 0.13 and 0.15 m, respectively (Table 2.1). These flow conditions relate to subcritical conditions (Fr <1, the Froude number $Fr = U_0(gh)^{-0.5}$, where g is the gravity acceleration) and were used throughout all experiments. Subscripts mc and fp refer to the main channel and floodplain respectively, while 1 and 2 refer to cross-sections upstream and downstream of the WDD dam respectively.

Table 2.1. Uniform flow conditions prior to installation of the WDD. h_0, U_0, Re, R_0, and Fr relate to the flow depth in the main channel, cross-sectional average velocity, Reynolds number based on the hydraulic radius R_0 and the Froude number.

Flow Conditions	$Q(m^3s^{-1})$	h_0 (m)	U_0 (ms^{-1})	R_0 (m)	Re (-)	Fr (-)
(i) $0.8Q_{bk}$	0.022	0.13	0.28	0.09	25,600	0.29
(ii) Q_{bk}	0.028	0.15	0.31	0.10	31,100	0.31

Table 2.2. Log diameter composition of WDD arrangements. D_i is the log diameter (mm)

	Large woody debris dam configuration				
D_i (mm)	Linear	Pseudo-natural	Lattice	Alternating	Driftwood
9		x			x
12		x			
25	x	x	x	x	x
35		x			
Porous dam	x	x	x	x	x
Non-porous dam	x	x	-	-	-

2.2.2 Large woody debris dam arrangements

Five geometric arrangements of WDD referred to as Linear, Lattice, Pseudo-natural, Alternating, and Driftwood (see Figures 2.1 and 2.2) were tested through a series of tests for $0.8Q_{bk}$ and Q_{bk} discharges. The dams were constructed using wooden dowels or logs (diameters, D_i of 9, 12, 18, 25, and 35 mm) with diameter compositions shown in Table 2.2. Dowels were fixed to the sides of the main channel using silicone adhesive, with each dam spanning the full width of the main channel.

The geometric arrangements of the Linear dams consisted of arrays of constant diameter (25 mm) horizontal logs spanned the full width of the main channel, parallel to the flume bed. The height of linear dams, h_t, was the elevation from the top log's edge to the flume bed. 'Lattice' arrangements were comprised of logs orientated diagonally at an angle of 6^0 to the horizontal. 'Alternating' dams were a hybrid of the Linear and Lattice dams, where dowels alternated between a layer of horizontally orientated dowels followed by a layer of the inclined dowels. 'Pseudo-natural' dams refer to arrangements with varied log diameters, which emulate the natural accumulation of smaller logs behind a larger downstream key member (Manners et al. 2007) and represent the use of locally sourced wood logs in the field, which vary in diameter. These also imitate natural woody debris dams where a large woody debris falls into the river and other smaller logs drift and accumulate behind it (Manners et al. 2007; Thomas and Nisbet 2012). Two cases of Pseudo-natural dams, referred to as N1 and N2 were tested, where a streamwise gap (dx = 5 mm) was added between logs in N1, whereas N2 was without streamwise gaps (dx =0) to evaluate the effect of streamwise porosity. This also accounted for the impact of potential irregularities in locally sourced timbers, which would not be as cylindrical as the logs used in the current study and might result in an overall $dx > 0$. 'Driftwood' formations emulated the accumulation of 12 logs of diameter Di= 9 and 10 logs of Di = 12 mm,

released 3 m upstream of a linear dam which had a streamwise length of L_x =100 mm and vertical height of top edge h_t = 145 mm. Drift logs made a 32% increase in wood volume on the Linear formation. In total, 39 repeats for each discharge, 80% and 100% bankfull, were made for the driftwood accumulations, and analysed using a Linear Regression method.

All logs comprising the dam were oriented perpendicularly to the flow, except for the case of the driftwood formations. A vertical gap (G) of 50 mm height, one third of the main channel depth, between the dam's lowest log and the channel bed was maintained throughout all the WDD experiments and configuration. In previous studies this unoccupied gap between the riverbed and the dam serves to allow low flows to pass unobstructed through the cross-section and to allow the free movement and passage of fish (Nisbet et al. 2011; SEPA 2015). For the Linear, Lattice, Pseudo-natural and Alternating arrangements, the dam length (L_x) in the streamwise direction (XY plane) was increased by consecutively adding a layer of logs across the channel in the YZ plane (Figure 2.2). Details of the dam arrangements are shown in Table 2.3 and Figure 2.2).

Finally, for the Linear and Pseudo-natural arrangements, we tested a non-porous WDD by wrapping the porous dam in plastic film, rendering it impermeable to imitate the natural clogging and accumulation of sediment, leaves, small branches and other debris immediately behind the dam and thus emulating a solid body. When this occurs naturally, the organic material accumulation decreases the flow through the dam until it becomes completely saturated and more watertight (Manners et al. 2007; Schalko et al. 2018). Non-porous cases were trailed for the Lattice and Alternating arrangements, however due to the inclined logs not fully supporting the plastic film, it caved in above and below the dam as it filled with water, and hence these data were not included in the analysis.

Linear

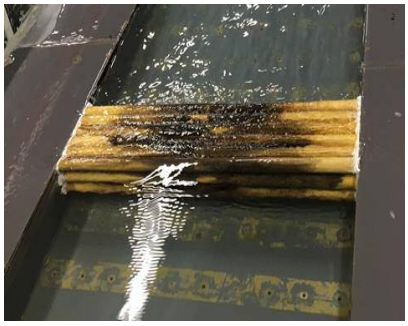

Pseudo-natural

Lattice

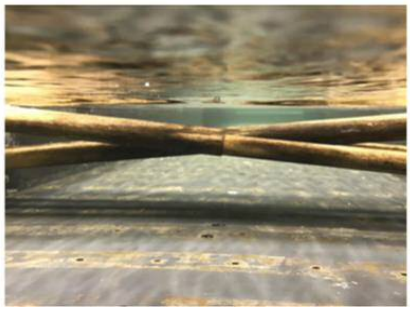

Alternating

Non-porous

Driftwood

Figure 2.1. Photographs of the experimental setups, showing the compound channel cross-section and indicating the position of the WDD for the various arrangements of woody debris dams, which are described in section 2.2 and figure 2.2 and 2.3.

(A) Side elevation

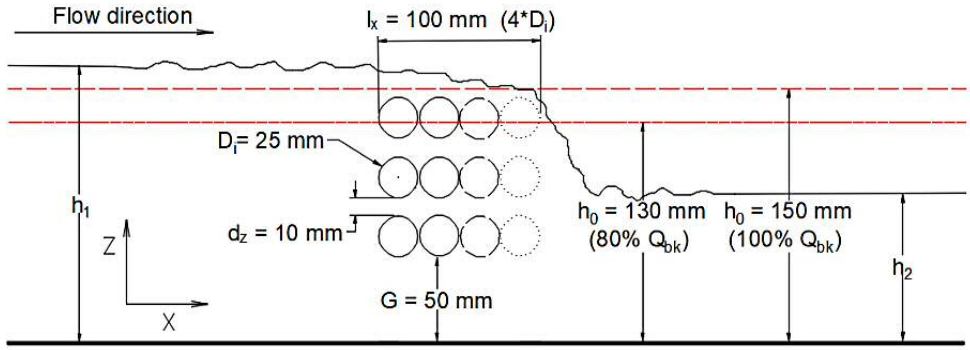

(B) Cross-sectional view

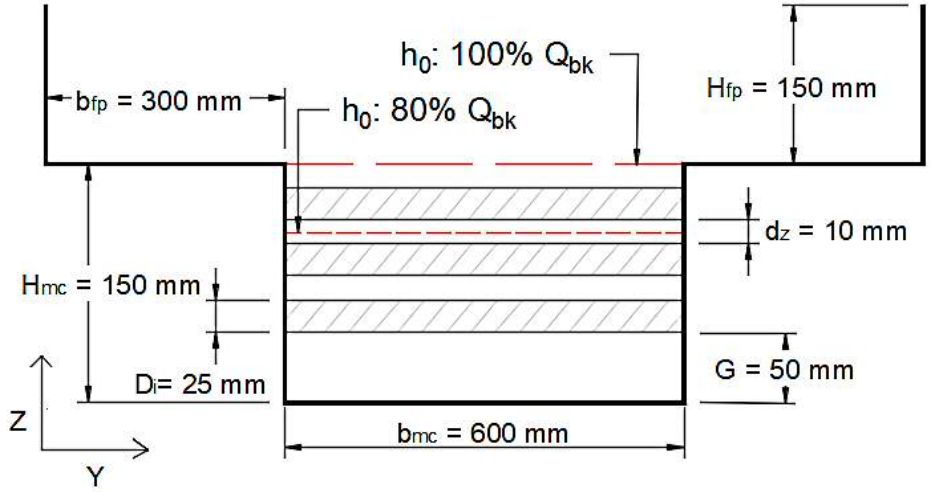

Figure 2.2. WDD configuration, geometry and arrangements for 'Linear' (A) Side elevation and (B) cross-sectional view (not to scale) of the channel and WDD configuration. The channel comprised of a symmetrical compound open channel of dimensions. A gap (*G*) was maintained between the lowest log of the dam and the flume bed. The dotted and dashed lines circles in (A) indicate the direction of removal of the logs as the dam was deconstructed from 8**Di* (200mm) to 1**Di* (9-25 mm)

(A) Linear WDD

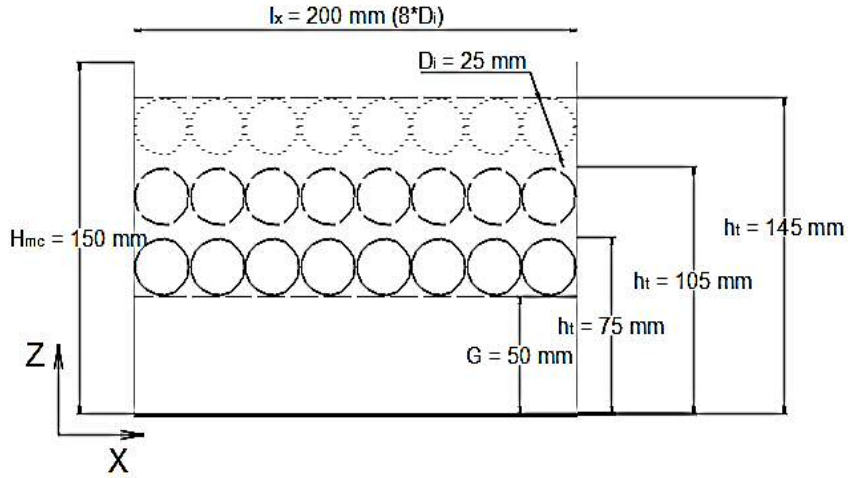

(B) Alternating WDD configuration

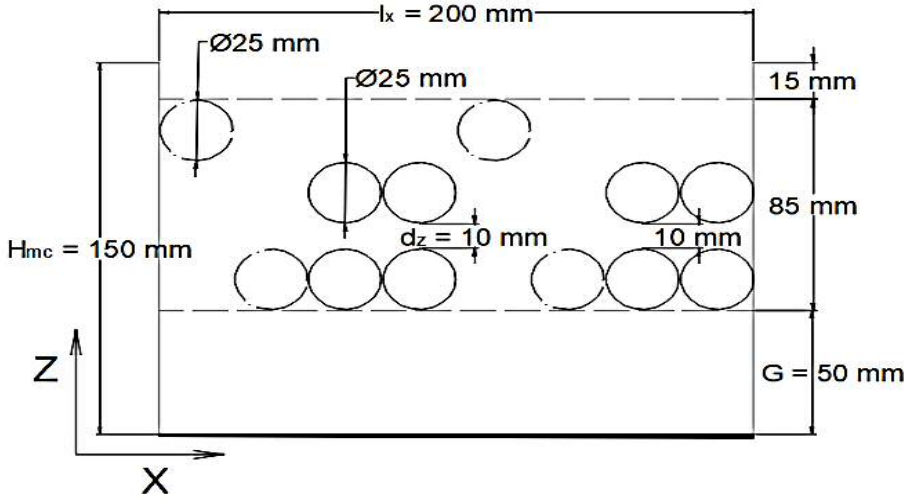

(C) Pseudo-Natural WDD configuration

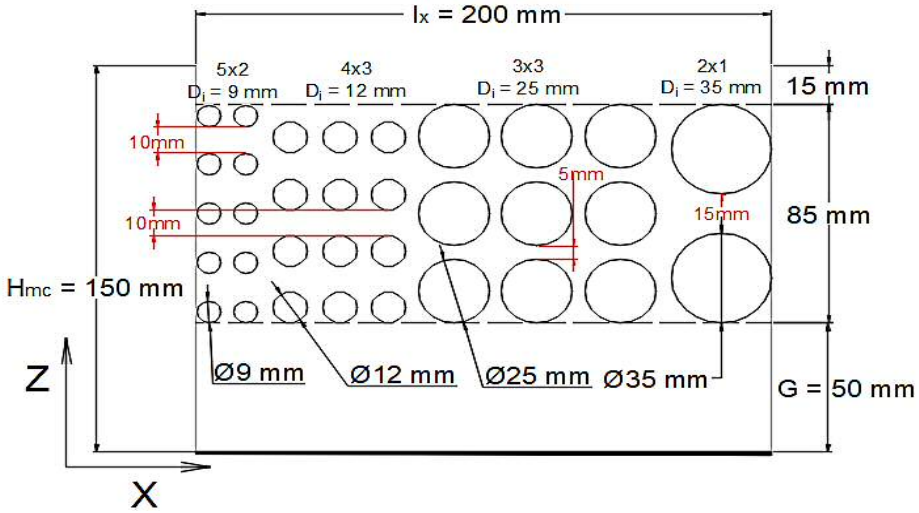

Figure 2.3. Side elevation view of the WDD arrangements, showing the distribution of logs comprising the dam WDD configuration, geometry and arrangements for 'Linear', 'Alternating' and 'Pseudo-natural N1'.

Table 2.3. Large woody debris dam sets of experiments where *Lx* is the streamwise length of the dam, *Di* is the log diameter, m is the number of logs, A_L is the cross-sectional area of the dam, A_B is the blockage ratio which is shown for 80% bankfull ($0.8Q_{bk}$) and 100% bankfull (Q_{bk}).'p' and 'np' indicate porous and non-porous dams respectively. Ranges cover the minimum (1 row) to the maximum (3 rows).

WDD design	L_x (mm)	D_i (mm)	m	(Z x dir)	A_L (m^2)	A_B (0.8 Q_{bk}) p	A_B (0.8 Q_{bk}) np	A_B (Q_{bk}) p	A_B (Q_{bk})np
Linear	25	25	1-3	1-3 x 1	0.015-0.045	0.186-0.559	0.186-0.746	0.168-0.506	0.168-0.675
	50	25	2-6	1-3 x 2	0.015-0.045	0.186-0.559	0.186-0.746	0.168-0.506	0.168-0.675
	75	25	3-9	1-3 x 3	0.015-0.045	0.186-0.559	0.186-0.746	0.168-0.506	0.168-0.675
	100	25	4-12	1-3 x 4	0.015-0.045	0.186-0.559	0.186-0.746	0.168-0.506	0.168-0.675
	125	25	5-15	1-3 x 5	0.015-0.045	0.186-0.559	0.186-0.746	0.168-0.506	0.168-0.675
	150	25	6-18	1-3 x 6	0.015-0.045	0.186-0.559	0.186-0.746	0.168-0.506	0.168-0.675
	175	25	7-21	1-3 x 7	0.015-0.045	0.186-0.559	0.186-0.746	0.168-0.506	0.168-0.675
	200	25	8-24	1-3 x 8	0.015-0.045	0.186-0.559	0.186-0.746	0.168-0.506	0.168-0.675
Lattice	25	25	1	1x1	0.0150	0.187	NA	0.169	NA
	50	25	2	1x2	0.0270	0.336	NA	0.305	NA
	75	25	3	1x3	0.0270	0.336	NA	0.305	NA
	100	25	4	1x4	0.0270	0.336	NA	0.305	NA
	125	25	5	1x5	0.0270	0.336	NA	0.305	NA
	150	25	6	1x6	0.0270	0.336	NA	0.305	NA
	175	25	7	1x7	0.0270	0.336	NA	0.305	NA
	200	25	8	1x8	0.0270	0.336	NA	0.305	NA
Pseudo-natural1	9	9	5	5x1	0.0270	0.336	0.634	0.304	0.574
	22	9	10	5x2	0.0270	0.336	0.634	0.304	0.574
	38	9, 12	14	4-5x 3	0.0288	0.358	0.634	0.324	0.574
	54	9, 12	18	4-5x4	0.0288	0.358	0.634	0.324	0.574
	70	9, 12	22	4-5x5	0.0288	0.358	0.634	0.324	0.574
	100	9,12,25	25	3-5x6	0.0450	0.560	0.634	0.507	0.574
	130	9,12,25	28	3-5x7	0.0450	0.560	0.634	0.507	0.574
	160	9,12,25	31	3-5x8	0.0450	0.560	0.634	0.507	0.574
	200	9,12,25,35	33	2-5x9	0.0450	0.560	0.634	0.507	0.574

Pseudo-natural2	9	9	5	5x1	0.0270	0.336	0.634	0.304	0.574
	18	9	10	5x2	0.0270	0.336	0.634	0.304	0.574
	27	9	15	5x3	0.0270	0.336	0.634	0.304	0.574
	40	9, 12	19	4-5x4	0.0288	0.358	0.634	0.324	0.574
	52	9, 12	23	4-5x5	0.0288	0.358	0.634	0.324	0.574
	64	9, 12	27	4-5x6	0.0288	0.358	0.634	0.324	0.574
	76	9, 12	31	4-5x7	0.0288	0.358	0.634	0.324	0.574
	88	9, 12	35	4-5x8	0.0288	0.358	0.634	0.324	0.574
	114	9, 12, 25	38	3-5x9	0.0450	0.560	0.634	0.507	0.574
	139	9, 12, 25	42	3-5x10	0.0450	0.560	0.634	0.507	0.574
	165	9, 12, 25	45	3-5x11	0.0450	0.560	0.634	0.507	0.574
	200	9, 12, 25, 35	47	2-5x12	0.0450	0.560	0.634	0.507	0.574
Alternating	25	25	1	1x1	0.0150	0.187	NA	0.169	NA
	50	25	2	1x2	0.0270	0.336	NA	0.305	NA
	75	25	4	1-2x3	0.0496	0.617	NA	0.559	NA
	100	25	6	1-2x4	0.0496	0.617	NA	0.559	NA
	125	25	7	1-2x5	0.0496	0.617	NA	0.559	NA
	150	25	8	1-2x6	0.0496	0.617	NA	0.559	NA
	175	25	10	1-2x7	0.0496	0.617	NA	0.559	NA
	200	25	12	1-2x8	0.0496	0.617	NA	0.559	NA
Driftwood	250-1780	9, 12, 25	34	3x4 *linear	_	_	NA	_	NA

Blockage ratio

Flow blockage ratio A_B (-) was defined by the proportion of the flow cross-sectional area occupied by the dam:

(2.2)

Where the cross-sectional area of the logs A_L is given by:

(2.3)

A_p is the projected area of each log and the flow cross sectional area A_f is:

(2.4)

Where B_{mc} is the main channel width and h_0 is the uniform flow depth.

2.2.3 Stage measurements and head loss

Water surface profiles were measured along the main channel centreline using a Vernier pointer gauge (nearest 0.1 mm) from a distance of 2 m from the upstream inlet until a distance 8 m from the inlet (2 m upstream of the downstream weir). The spatial resolution of the water surface level measurements in the longitudinal flow direction was such that spacing between measurements ranged from 2 mm to 500 mm, with higher spatial resolution measurements in the vicinity of the WDD. Temporal fluctuations in the surface water level in the proximity of the dam were not included in the calculations of mean flow depth. Time-averaged measurements of flow depth upstream (h_1) and downstream (h_2) of the dam were used for calculating the backwater stage afflux (Δh), and upstream flow area increase or flow area afflux (ΔA), which are given by:

(2.5)

and

(2.6)

Where A_1 is the upstream flow area and A_0 is the uniform flow cross section. These parameters were normalised by the uniform flow depth and flow area to obtain

and , respectively. Here on, afflux refers to flow area afflux (. A volumetric approach to the backwater effect of the WDD was adopted to comparatively evaluate the afflux including the overbank flows on the floodplains, which would not be adequately represented by the 1D approach of flow depth.

Predicted stage rise

Based on the momentum principle, and modelling woody debris as cylindrical obstructions, stage rise Δh is given by equation 2.7 (Ranga Raju et al. 1983; Gippel et al. 1996).

(2.7)

Where the Froude number (F_r) downstream of the WDD is

(2.8)

And the woody debris drag coefficient C_D is

(2.9)

Where F_D is the drag force, ρ=1000 kgm^{-3} is the density of water, U_1 and U_2 are the mean velocity upstream and downstream of the WDD, h_2 is the downstream mean flow velocity, A_p is the cross-sectional projected area of the WDD, F_D was obtained by force balance around the WDD (Manners et al. 2007), and the blockage ratio A_B is as shown in equation 2.2.

2.3 Results

2.3.1 Head loss and Drag coefficients

The observed stage rise was lesser than the predicted Δh from Eq. 2.7, shown in Figure 2.5 as the predicted Δh does not account for the porosity between logs comprising the dam, but rather utilises that cross-sectional projected area of a cylindrical object equivalent to the A_p of the dam. Therefore, the dam permeability reduces the extent of backwater effect that would otherwise be present. The lower measured Δh could be explained by additional energy losses occurring around the dam, which e *E*q. 2.7 does not account for.

Drag coefficient C_D increased with volume of wood for inbank flows for 'Linear' dams (Figure 2.6), but also decreased with increasing porosity (Figure 2.7), consistently with previous studies; indicating that WDD obstructions although porous result in drag coefficients similar to those of single cylinder obstructions. The vertical scatter of C_D values for the same blockage ratio is attributed to the effect of the WDD streamwise length, which increased surface drag, and therefore C_D.

'Linear' dams

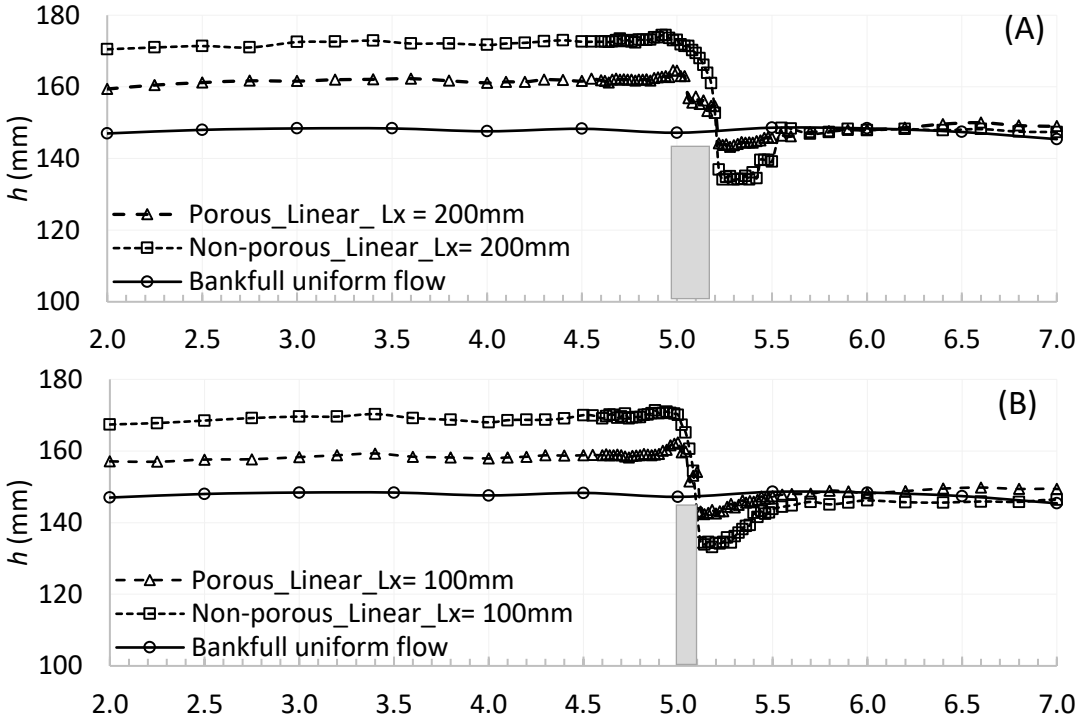

'Pseudo-natural' N2 dams

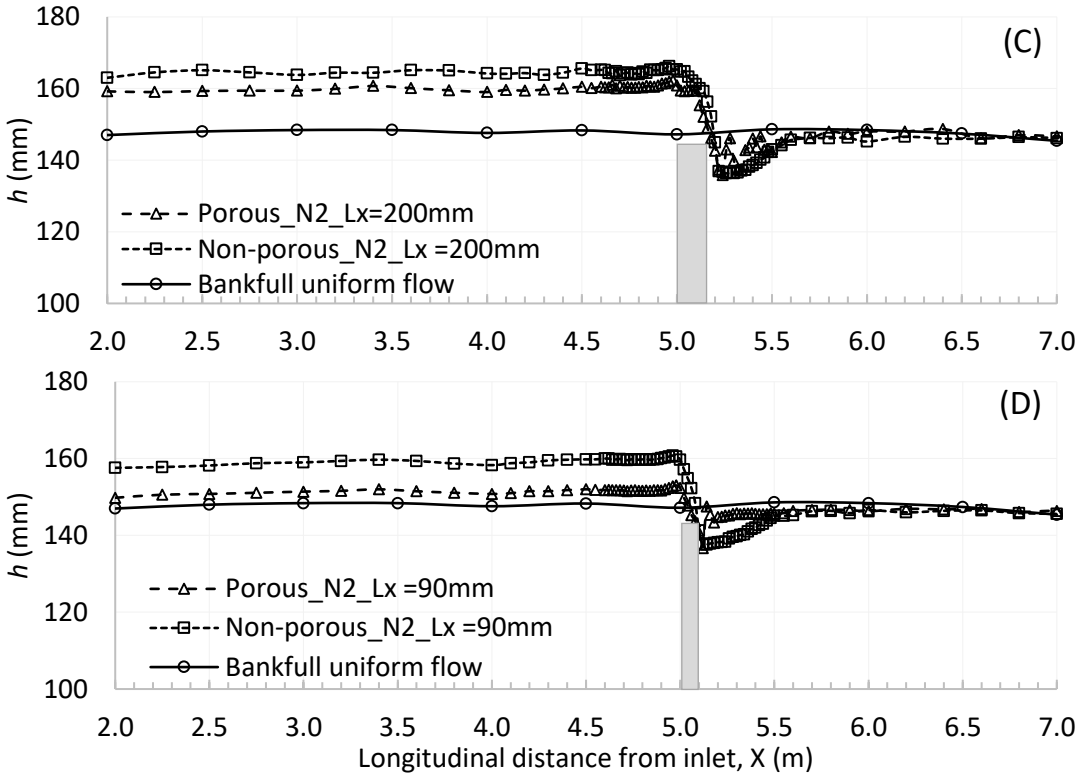

Figure 2.4. Surface water profiles: flow depth *h* (mm) relative to longitudinal distance X(m) for the 'Linear' (h_t=145mm) (A and B) and Pseudo-natural N1 for streamwise

lengths L_x= 200 mm (A and C) 100 mm (B) to 90 mm (D) for the 100% bankfull Q_{bk} discharge. The grey rectangular shape outlines the location of the non-porous dam.

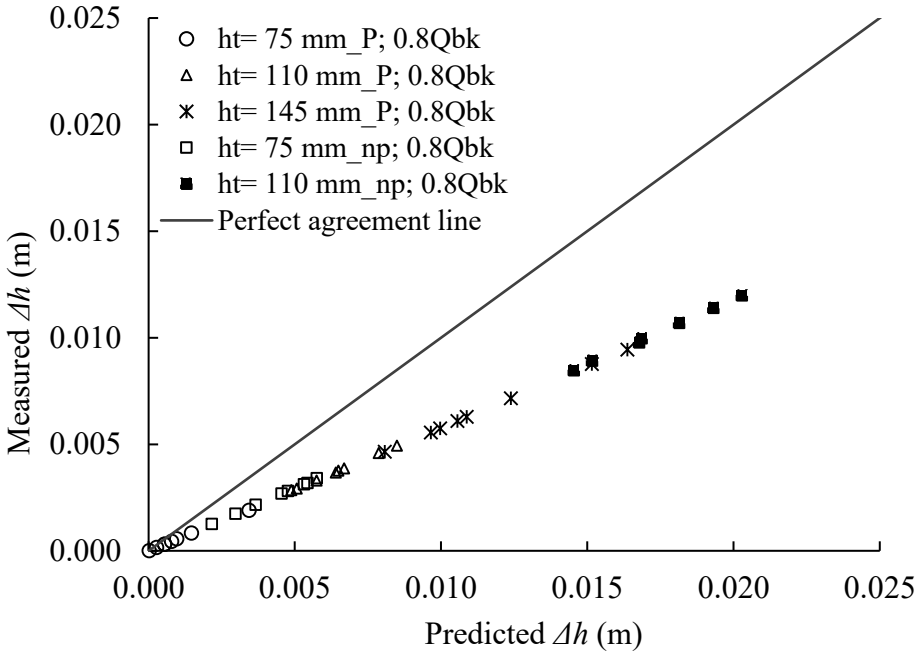

Figure 2.5. Stage rise measured for porous (h_t = 75, 110, and 145 mm) and non-porous (h_t = 75 and 110 mm) 'Linear' dams for inbank flows at the 80% bankfull discharge and stage rise predicted using Equation 2.4.

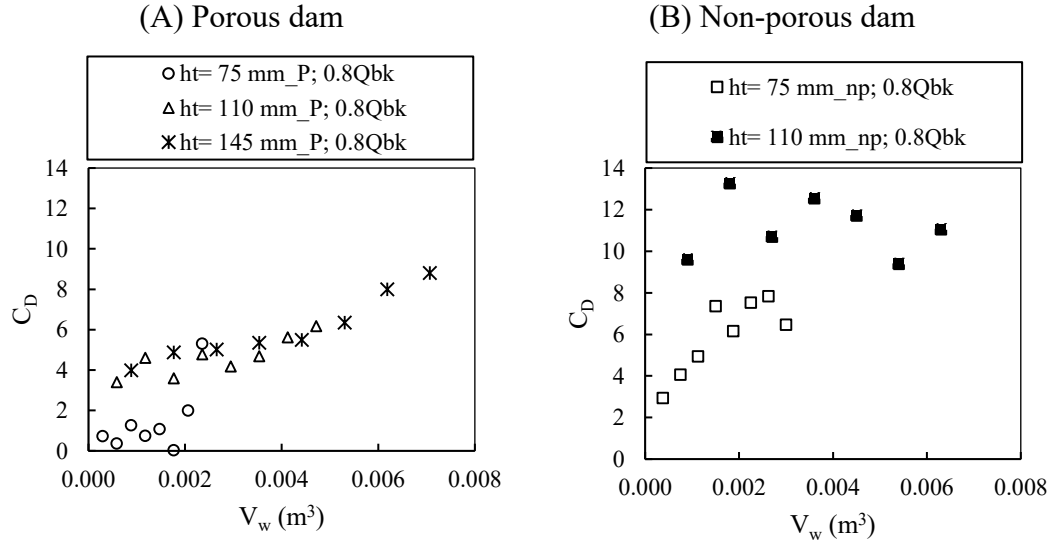

Figure 2.6. Variation of drag coefficient with volume of wood for the 80% bankfull discharge for porous (A) and non-porous (B) 'Linear' dams.

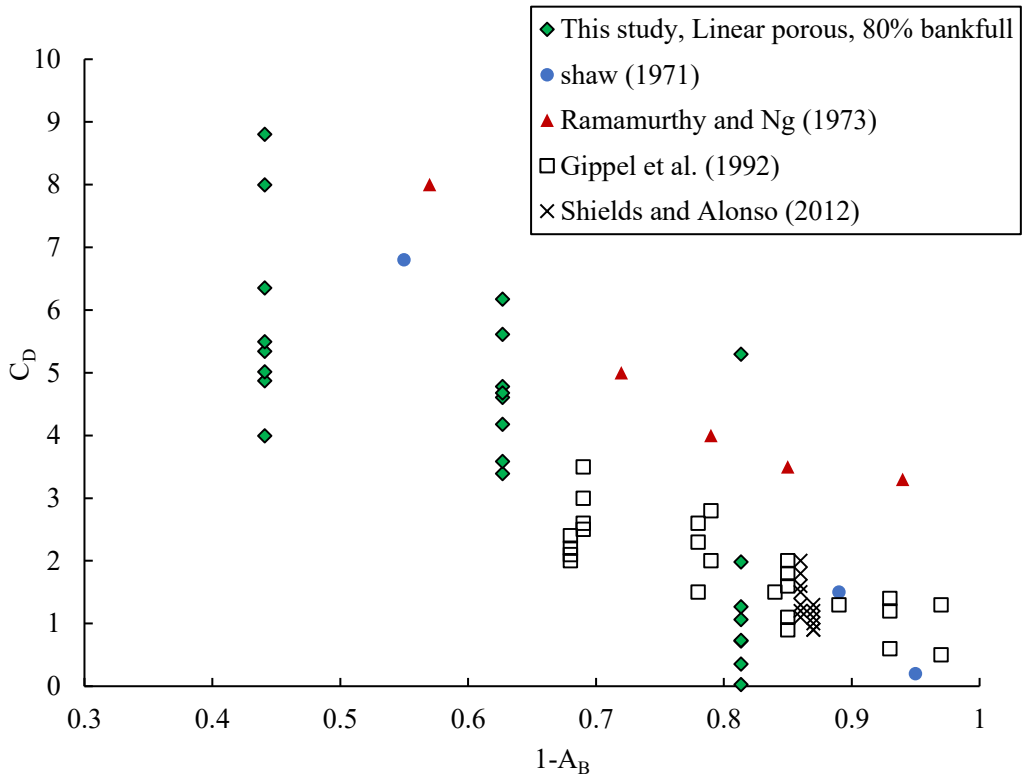

Figure 2.7. Drag coefficients calculated for Linear porous dams at $0.8Q_{bk}$ discharge, compared to literature data as shown in Shields and Alonso (2012).

2.3.2 Linear dam arrangement: effect of streamwise length of the dam on backwater

The linear dam configuration evaluated the effect of the distribution of logs in the XY and XZ planes with increasing volumes of wood on afflux. Increase in the dam's streamwise length (L_x) resulted in minor increases in afflux for the same h_t setting (Figure 2.8A). Afflux increased with increasing cross-sectional blockage area of the dam, as on average, the upstream wetted area afflux doubled when the A_L doubled, a pattern that was observed for both 80% and 100% bankfull discharges (Figure 2.8B). The non-porous dam showed significantly higher afflux than the non-porous structure.

Afflux increased with increasing blockage area (Figure 2.8C), corresponding to the increase in projected area of logs in the cross-sectional YZ plane and blockage ratio of the main channel cross-section. Increase of volume of logs in the longitudinal X direction (XZ plane) by increasing the streamwise length of the dam L_x (m), resulted in minor increases in local losses, as the flow streamlined between the voids and gaps of the dam. Amongst Linear dams of the same cross-sectional blockage ratio, increase of the streamwise length of the dam resulted in minor increases in afflux suggesting that distribution of the logs in the YZ plane is more efficient for blocking the flow and storing the water upstream of the dam than increased blockage in the streamwise direction.

For the non-porous WDD structures, the length of the dam played a more noticeable role together with the cross-sectional blockage of the main channel. With no flow through the voids, the afflux was twice that of porous dams. This effect was accentuated by increase in the blockage ratio of the dam, where increase in the number of logs in the vertical plane, and therefore h_t led to large increases in afflux. Afflux ranged between 0 and 15% for the porous dam, and 0 to 28% for the non-porous dam. This highlights how accumulation of debris, sediment and smaller branches may saturate the dam, with flood attenuation performance improving as the dam matures. The spread of afflux values for the same A_L (Figure 2.8B) and A_B (Figure 2.8C) was due to the differences in streamwise length of the dams with similar dam wood area and blockage ratios. Again, the changes in afflux due to the streamwise blockage are evident, however not as remarkable as the afflux due to the cross-sectional flow blockage ratio. This indicates that increases in wood volume and solid volume fraction are most beneficial for flood attenuation when the wood pieces are arranged in a manner that maximises the channel cross-section blockage area. The 80% bankfull discharge ($0.8Q_{bk}$) often resulted in higher afflux than the 100% bankfull discharge (Q_{bk}), this is attributed to afflux being normalised relative to the

uniform flow depth, which was lower for $0.8Q_{bk}$ than Q_{bk}, resulting in a greater proportional increase in afflux for the lower discharge condition compared to the higher discharge condition. Furthermore, the increase in wetted area in overbank flooding cases, which occurred more often for Q_{bk} than $0.8Q_{bk}$, induce greater skin friction losses and main channel/floodplain momentum exchange losses, which in turn diminished head loss.

2.3.3 Pseudo-natural dam arrangement: effect of streamwise porosity on backwater effect

The addition of gaps in the streamwise direction, (dx = 5mm) aimed to evaluate the performance of the dam with added porosity in the X direction for the Pseudo-natural N1 (dx = 5mm) and N2 (dx = 0) arrangements. Comparison of N1 and N2 (Figure 2.9) revealed that N1 showed slightly higher afflux than N2 for both $0.8Q_{bk}$ and Q_{bk}. The added porosity in the streamwise direction of N1 resulted in slightly higher afflux than the case without gaps, indicating that use of non-linear, irregular logs will not hinder dam performance, but might improve it. This is due to the water stagnating and occupying the gaps between columns of logs and provides additional flow blockage.

Afflux was a factor of two to four times greater in the non-porous case than for the porous dam case. The patterns of afflux relative to the WDD length were similar for 80% and 100% bankfull conditions. Afflux generally increased with increasing L_x, but no clear distinctions in the rate of increase were apparent between N1 and N2 cases when the frontal projected area and cross-sectional flow blockage ratio remain constant. The streamwise (dx) gaps (present in N1) resulted in a negligible difference in blockage ratio for dams of similar length. This highlights that as the dams mature and accumulate organic material, the performance of the N1 and N2 types of dams over time will likely become similar.

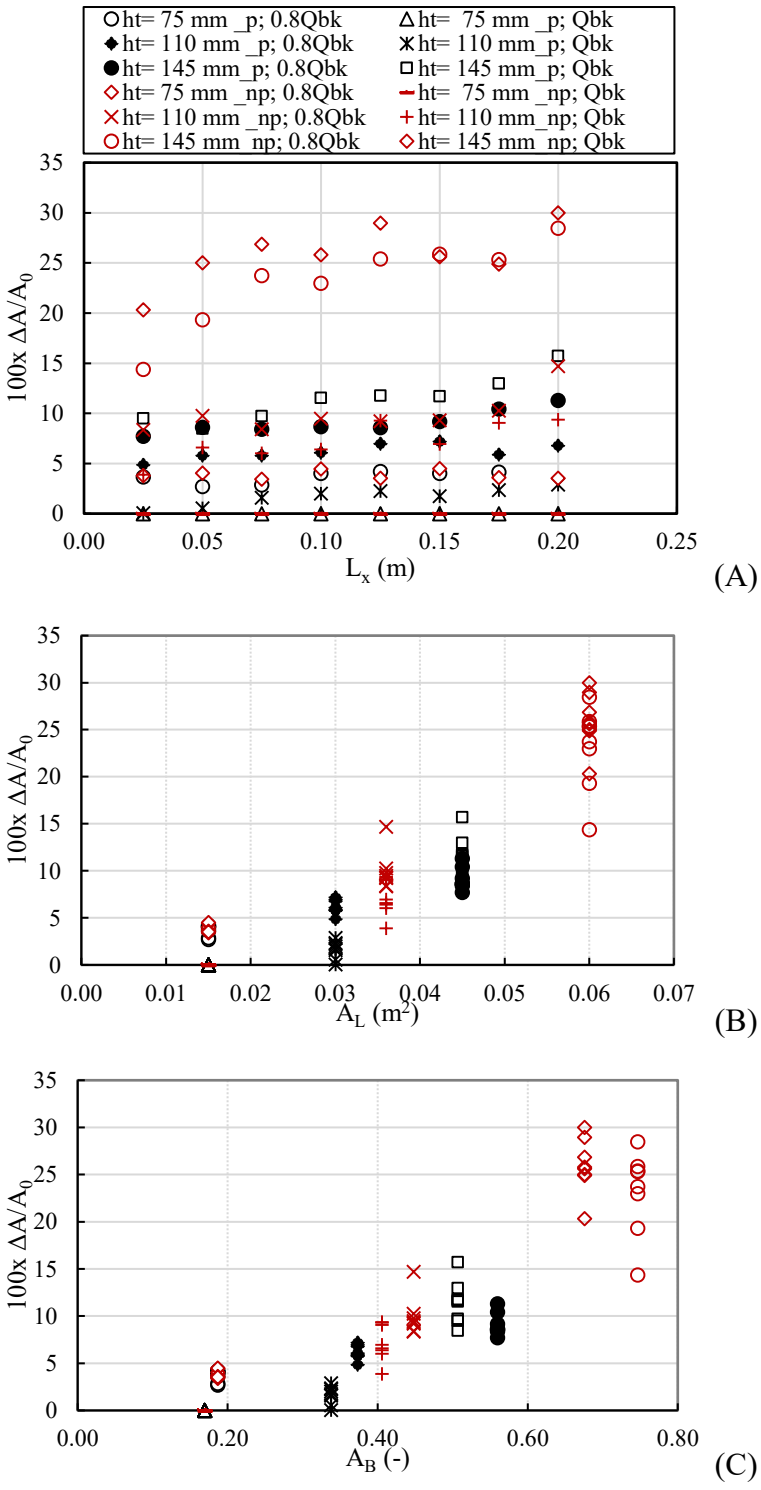

Figure 2.8. Effect of (A) dam streamwise length L_x (m), (B) the cross-sectional area of the dam A_L (m^2), (C) the cross-sectional flow blockage ratio due to the dam A_B (-) on backwater flow area rise (100x $\Delta A/A_0$) for h_t settings of 75, 110 and 145 mm for the 'Linear' dam configurations under 80% and 100% bankfull discharges ($0.8Q_{bk}$ and Q_{bk}, respectively). h_t is the vertical height of the edge of the top on the dam above

the channel bed. Standard error for backwater flow area rise was 0.7% and 1.5% for porous and non-porous dams respectively. “p” and “np” indicate porous (black markers) and non-porous (red markers) dam setups, respectively.

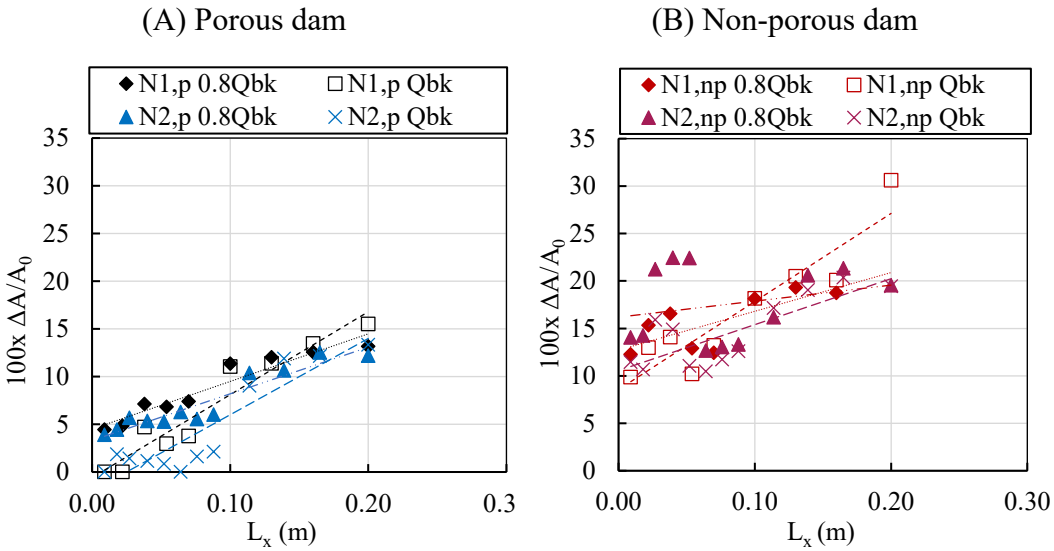

Figure 2.9. Backwater flow area rise for Pseudo-natural dam configurations N1 (which includes a streamwise gap dx = 5mm between logs) and N2 (for which dx = 0) for various dam streamwise lengths (L_x) under 80% and 100% bankfull discharges. “np” indicates non-porous dam (red markers) and “p” indicates porous dam (black markers). Standard error was 1.1% and 1.5% for porous and non-porous settings respectively.

2.3.4 Effect of WDD frontal projected area and orientation of logs on afflux

Linear, Lattice and Alternating dam configurations (Figures 2.2 and 2.3) were used to examine how the complexity of the arrangement and distribution of logs affected flood attenuation performance. These three configurations had similar solid volume fractions and volume of wood. Figure 2.10A, B and C show that more complex, i.e. less uniformly distributed log arrangements, of Lattice and Alternating dams resulted

in increased cross-sectional blockage area but similar afflux compared to the geometrically arranged Linear dams, with afflux ranging from 0 to 7%. In relation to streamwise length (L_x), there was a slight increase in afflux for all configurations with increasing L_x (Figure 2.10A). However, comparisons based on A_L (Figure 2.10B) revealed that Linear dams showed higher afflux than Lattice for similar A_L, and while Alternating dams had much higher A_L than the other configurations for similar Lx settings, they showed higher afflux than Lattice, but less than or equal to Linear dam afflux. Based on blockage ratio (Figure 2.10C), the Linear dam showed higher afflux than Lattice and Alternating dams for similar A_B magnitudes. The Alternating dam had overall lower afflux than Linear for the bankfull discharge despite having a higher blockage ratio. Variations in afflux are evident between 80% and 100% bankfull, particularly for the Alternating configuration, probably because of the previously mentioned impact of skin friction and exchange momentum losses due to overbank flow, which were more prominent for Q_{bk} than $0.8Q_{bk}$.

2.3.5 Linear and Pseudo-natural dam configurations: effect of log diameter mixture on afflux

Overall, afflux increased with increasing length Lx more in the Pseudo-natural than the Linear dams (Figure 2.11A). For the same streamwise lengths, however, Linear dams showed higher afflux than natural dams. This was due to Linear dams having greater cross-sectional area A_L and flow area blockage ratio A_B than Pseudo-natural ones (Figure 2.11B and C). Furthermore, for similar A_L and A_B magnitudes, Pseudo-natural dams showed lower afflux than Linear dams, probably due to the smaller diameter of Pseudo-natural dam components resulting in different hydrodynamic processes than the larger log diameters in the Linear configuration. This is attributed to the fact that many, small logs in the vertical direction have more gaps and allow more flow through the dam. Across all the Pseudo-natural and Linear dam data series, there is a strong positive correlation between the WDD blockage ratio A_B and flow

area afflux, highlighting that the cross-sectional flow blockage A_B is the primary governing parameter, while the streamwise blockage L_x is secondary.

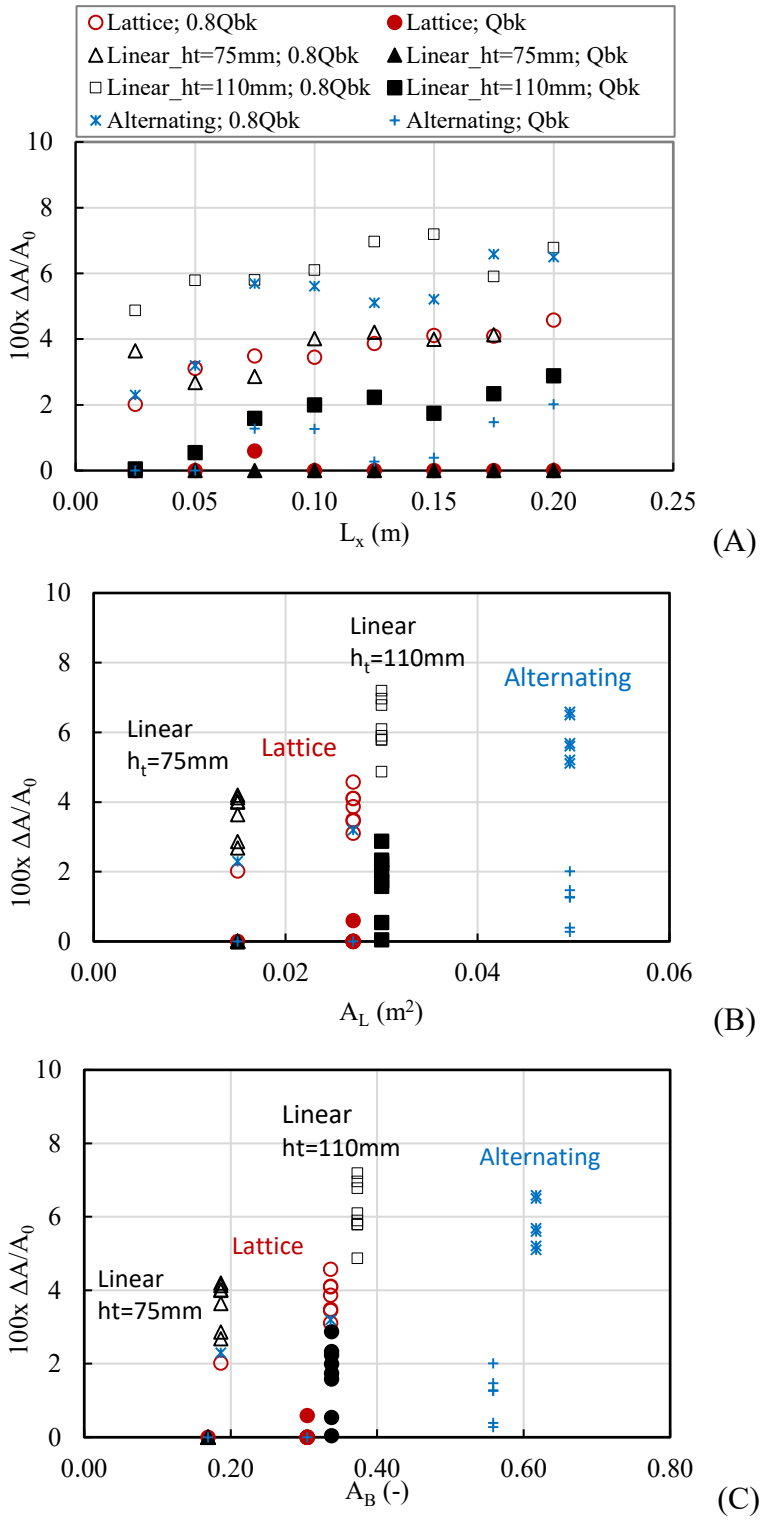

Figure 2.10. Effect of 'Linear', 'Lattice' and 'Alternating' WDD design on backwater flow area rise (100x $\Delta A/A_0$), showing the performance of similar (a) streamwise

lengths L_x, (b) WDD cross-sectional area A_L and (C) flow blockage ratio A_B. All data points shown here are for the porous dam setup. These show effect of configuration, geometry, angle of orientation and arrangement, as well as the resulting projected areas and blockage ratios on the performance of the WDD dam. Standard error was 0.7%, 0.6% and 0.7% for 'Linear', 'Lattice' and 'Alternating' dams respectively.

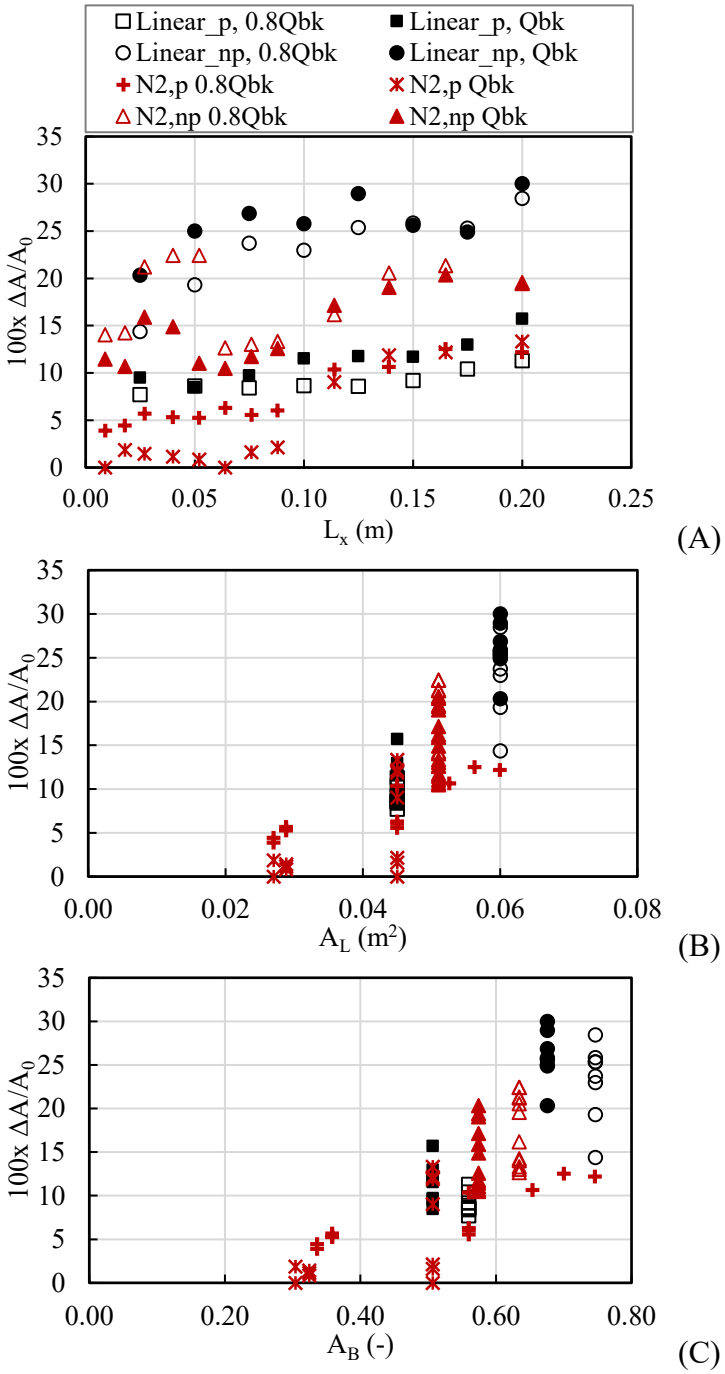

Figure 2.11. Effect of log diameter mixture i.e. constant log diameter in the 'Linear' configuration compared to varied log diameter in the 'Pseudo-natural' arrangement

(dx = 0) on the performance of the WDD dam. Figures display the variations in backwater flow area rise (100x $\Delta A/A_0$) relative to (a) streamwise length L_x, (b) cross-sectional area of the dam A_L and (c) blockage ratio A_B. Np and p indicate porous and non-porous setups, respectively. Standard error was 0.7% (porous), 1.5% (non-porous) for 'Linear', 1.1% (porous) and 1.5% (non-porous) for 'Pseudo-natural'. "np" indicates non-porous dam (red markers) and "p" indicates porous dam (black markers).

2.3.6 Natural driftwood formation: Effect of driftwood on the performance of the WDD

With constant volume of wood and various dam lengths, the effect of driftwood accumulations on the performance of the WDD was tested to simulate natural accumulation of small log pieces on engineered WDD. Figure 2.12 shows natural driftwood accumulation of 12 Di = 9 mm and 10 Di = 12 mm on the Linear dam Lx = 100mm and h_t = 145 mm and resulting afflux. The randomised distribution of drift logs (Figure 2.12B), with some interlocking between the Linear dam gaps, or at times nearly parallel to the flow direction, increased the overall length of the dam, which was the distance between the downstream face of the dam and the furthest reaching log. Based on the 39 experimental runs of driftwood accumulations, the measured flow area afflux ($\Delta A/A_0$) and corresponding streamwise length (L_x), linear regression provided a predictive relationship between L_x and 100x $\Delta A/A_0$ where afflux is negatively correlated with L_x (Figure 2.12A). This indicated that the random distribution of the driftwood widely varied the overall longitudinal length of the dam (L_x) where some log pieces extended further upstream than others. These elongated dams had higher L_x despite the constant volume of wood in all driftwood tests. Therefore, the dam's increased streamwise length had limited effect on the afflux due to the negligible increase in cross-sectional flow blockage since the greater dam

lengths were a result of driftwood logs reaching the fixed dam in directions parallel with the flow direction, with minimal flow blockage effects.

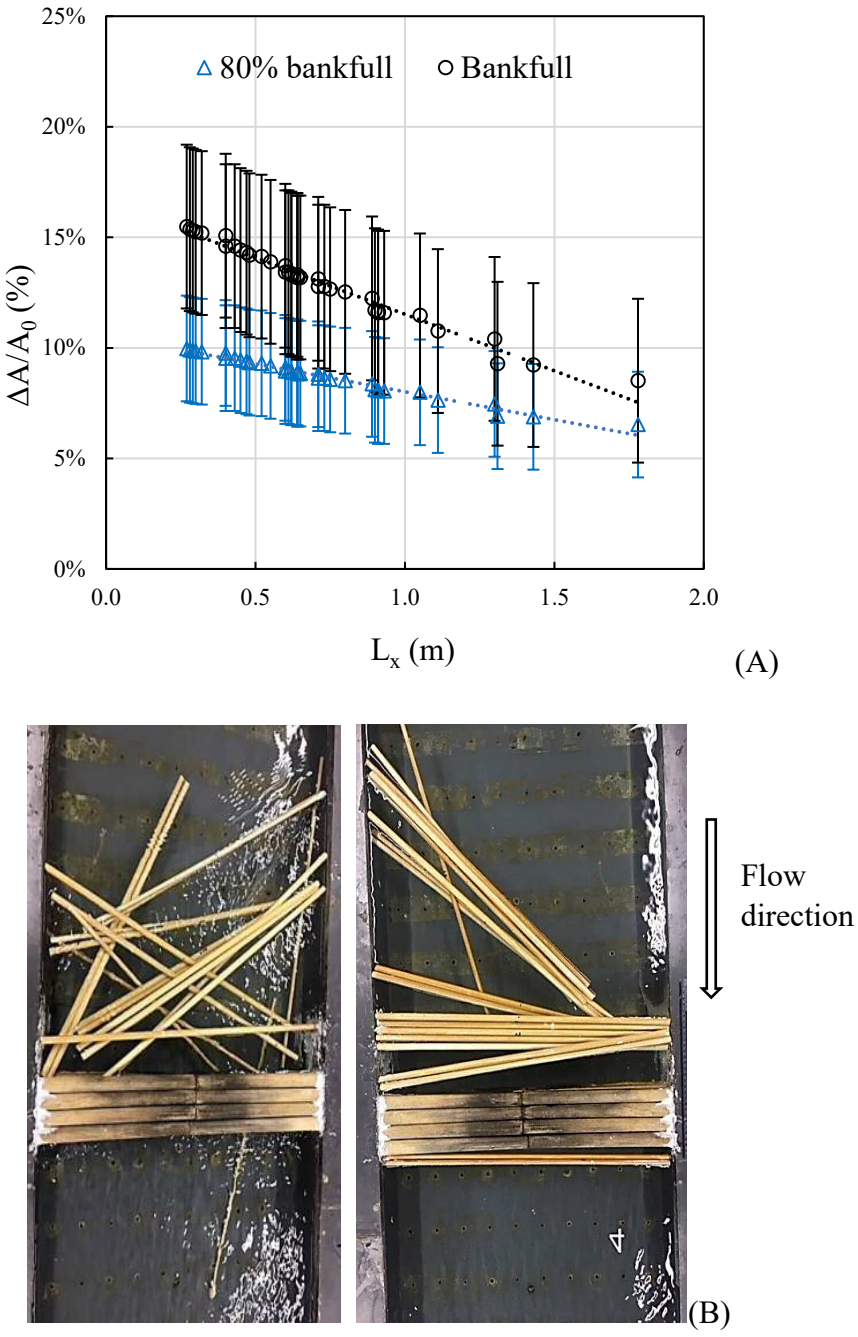

Figure 2.12. (A) Flow area backwater rise (100x $\Delta A/A_0$) resulting from driftwood accumulation of 12 and 10 logs of diameter Di = 9 mm and 12 mm respectively on a linear dam (streamwise length L_x = 100mm and vertical height of top edge h_t = 145 mm) under 0.8Q_{bk} and Q_{bk} discharges. Plotted is the linear regression analysis of the afflux relative to streamwise length of the dam from 39 runs at each discharge. Error

bars represent standard error (±2%). (B) Driftwood accumulation experiment showing the scattered distribution of the logs around the dam.

2.4 Discussion

The hydraulic effects of various designs of porous and non-porous engineered Large woody debris dams (WDD) were studied, by varying their physical characteristics of streamwise length, blockage ratio, mode of formation and distribution of components in linear arrays of horizontal or inclined members with constant or varied diameters. Overall, afflux increased with increasing streamwise length, and flow blockage ratio. However, unless accompanied by increases in dam cross-sectional area (A_L) and blockage ratio (A_B), increase in the dam's streamwise length resulted in minor increases in afflux. In the non-porous case, the streamwise blockage showed minor increases in afflux. Furthermore, results highlighted that the vertical, cross-sectional flow blockage (YZ plane) of the main channel is a more important parameter than channel blockage in the streamwise direction (XY plane) as afflux was highest for arrangements where h_t, A_L and A_B were highest for both porous and non-porous dams. The flow attenuation performance of the WDD was dependent on cross-sectional blockage ratio (A_B) of the flow by the dam, or the frontal projected area of wood (A_L), the distribution of log diameters, the mode of formation of the dam, and the height of the dam in the water column.

Alternating, Lattice, and Pseudo-natural dam configurations use different angles of orientations or varied log diameters, making them more structurally complex than the uniformly distributed arrays of the Linear configuration. Results indicated that the complex dams resulted in afflux less than or equal to afflux of Linear dams. This suggests that dam complexity is not necessarily an indicator of improved flood attenuation, since Linear dams result in similar, if not greater afflux than more complex dams, provided that streamwise length and blockage ratio were maximised.

Hence, it might be most beneficial in the design of engineered Large woody debris dams to distribute logs in such a way that greatest cross-sectional blockage area (YZ plane) is achieved, maximising A_B and consequently afflux. As non-porous dams mature and becomes more water-tight through the accumulation of branches, leaves and sediments (Wallerstein and Thorne 1997; Manners et al. 2007), their flood attenuation performance will improve and differences amongst different dam designs will likely converge.

For the Driftwood formations, the orientation of logs was crucial to the dam's afflux, which was negatively correlated with the dam's streamwise length for both discharges. Indeed, logs perpendicular to the flow result in higher flow depth afflux than those more parallel to the flow direction (with a streamwise angle $<90^0$) in cases of single cylindrical pieces (Young 1991; Gippel et al. 1996). Therefore, the driftwood logs which arrived at the dam more parallel than perpendicular to the flow direction lengthened the dam and diminished the backwater effect of the dam. However, *in situ* driftwood accumulations will likely be accompanied by leaves, sediments, organic material and debris, which will increase the flow blockage area and render the dam less porous (Wallerstein and Thorne 1997; Manners et al. 2007; Thomas and Nisbet 2012). Therefore, the afflux and streamwise length relationship in Figure 2.12A will probably change as the dam matures, not as a result of the extended streamwise length, but due to the flow blockage ratio (Schalko et al. 2018).

Variations in afflux for 80% and 100% bankfull discharges were attributed to friction and momentum exchange losses for overbank flow, which occurred more frequently in the 100% bankfull cases. Momentum exchange, flow depth and velocity differences between the main channel and floodplains contributes to friction losses as well as increased wetted perimeter for out of bank flow (Knight and Demetriou 1983; Shiono and Knight 1991; Yen 2002). Additionally, higher flow depth ratio between the main channel and flood plain, results in higher ratio of the respective

friction factors (Shiono & Knight, 1991). Measurements of the hydrodynamic flow fields in the presence of WDD could further explain this phenomenon.

The backwater effect and increased flow depth upstream implies decreased local velocities, which would be favourable to fish seeking refuge areas (Wallerstein and Thorne 1997; Shields et al. 2004; Manners and Doyle 2008; Floyd et al. 2009). However, although a vertical gap was left below the dam for base flows and the free passage of fish, the flow through this gap will likely be high due to the flow acceleration induced by constriction from the dam and hence might form a velocity barrier to fish during high discharge flood events (Castro-Santos 2005; Sniffer 2010). This flow acceleration is also likely to result in high shear stresses, which will exacerbate local scour on the channel bed below and downstream of the dam, and the subsequent changes in bed level might influence runoff attenuation of the dam (Abbe and Montgomery 1996; Wallerstein and Thorne 1997; Manners et al. 2007; Quinn et al. 2013). Such geomorphological effects of Large woody debris dams, are postulated to enhance fish habitat heterogeneity and their creation might result in ecosystem services benefits by providing refuge areas and trapping nutrients (Abbe and Montgomery 1996; Floyd et al. 2009; Dadson et al. 2017; Burgess-Gamble et al. 2017; SEPA 2015).

For flood modelling applications, a relationship between discharge, WDD characteristics and backwater needs to be established using experimental or numerical methods, based on the findings shown in the current experiments as to the parameters which maximise WDD backwater and flood attenuation. The backwater effect, surface storage and increased infiltration directly alter surface storage and groundwater flow upstream of each dam and therefore affect flood routing outcomes. Furthermore, in a catchment-based approach, evaluating series of multiple WDD on each channel and their cumulative flood attenuation effect could provide further understanding of the wider potential and practice of using WDD in NFM.

2.5 Conclusion

The hydraulics of flood attenuation performance of engineered WDD were studied by evaluating the backwater effects of different WDD designs with under 80% and 100% bankfull discharges. WDD designs varied by physical characteristics of streamwise length, blockage ratio, and mode of formation and distribution of components in linear arrays of horizontal or inclined members with constant or varied diameters. Afflux was dependent on the dam's streamwise length, especially when accompanied by increases in flow blockage ratio. However, despite lengthening the dam, driftwood which were not perpendicular to the flow direction reduced the dam's afflux. Furthermore, the use of uniformly distributed equal diameter logs in the dams resulted in equal or higher afflux than the more irregular or complex dams that used varied diameters and log orientations. Non-porous representations of WDD showed at least twice the afflux compared to porous dams, indicating that as the engineered dams become more watertight through the accumulation of organic matter and debris, their flood attenuation performance will improve. The cross-sectional blockage ratio of the channel occupied by the dam was the most primary factor that determined afflux, and hence, distributing logs to maximise channel obstruction will increase flow attenuation.

Chapter 3. Spanwise rollers and fish swimming kinematics

A manuscript based on this chapter has been accepted (11 October 2019) in Water Resources Research as: Muhawenimana Valentine, Wilson Catherine A.M.E., Pablo Ouro, and Cable Jo (2019). Spanwise cylinder wake hydrodynamics and fish behaviour. *Water Resources Research.* V.M, C.W, and J.C designed the experiment, V.M conducted the experiments and processed the data. V.M and P.O analysed and plotted the data. V.M wrote the text with comments from C.W, P.O and J.C.

Summary

Flows generated near hydro-engineering structures are characterised by energetic three-dimensional flow structures that are markedly different from naturally occurring fish habitats. The current study evaluated the interaction of Nile tilapia (*Oreochromis niloticus*) with spanwise rollers in the turbulent wake of a cylinder in both the wake bubble and the vortex shedding further downstream. The flow field hydrodynamics were measured using an Acoustic Doppler Velocimeter for Reynolds number (Re_D) regimes ranging from 3,730 to 33,590, over a streamwise length of $6D$ downstream of the cylinder and revealed a pair of alternating vortices rotating about a spanwise axis, which were rendered asymmetric by the bed boundary proximity. Fish avoided areas where vorticity, turbulence intensity, turbulent kinetic energy, eddy size and Reynolds shear stress were highest. Events of stability loss, referred to as spills, were significantly correlated to the turbulence integral length scale relative

to fish standard length, with the peak number of spills occurring when the eddy length approached 45 to 50% of the fish length. Spill events significantly depended on Re_D, Reynolds stress and vorticity, and varied according to fish length and weight. Amongst zones of similar Reynolds stress and vorticity magnitude, the frequency of spills depended on Reynolds shear stress and eddy vorticity direction, highlighting the physical importance of direction and orientation in determining the hydrodynamic forces that affect fish swimming stability. Recommendations are made for the inclusion of these metrics in the design and refinement of hydro-engineering schemes.

3.1 Introduction

Modifications to river habitats through hydraulic structures have significantly affected aquatic species by creating unnatural flows. Fragmentation of riverine habitats is particularly problematic for fish species, disrupting short and long distance migrations (Jager et al. 2001; Fagan 2002; Katopodis and Williams 2012; Fuller et al. 2015) and creating extreme conditions that may impact fish habitat preferences, feeding, spawning, swimming ability and swimming kinematics (Morita and Yokota 2002; Enders et al. 2005; Murchie et al. 2008; Williams et al. 2012; Hockley et al. 2014). River restoration schemes attempt to restore the aquatic environment back to natural conditions, and fish passes facilitate movement of migratory species with varying efficiency (Larinier 2001; Noonan et al. 2012). Such restorations, however, only achieve semi-natural conditions and often create a wider range of flow heterogeneity in terms of velocities, turbulence and turbulent shear stresses, particularly problematic for smaller or weaker swimmers (Wang et al. 2010; Silva et al. 2011; Lacey et al. 2012).

Both field and laboratory studies indicate that altered and turbulent flows can be both beneficial and detrimental to fish (Pavlov et al. 2000; Webb, 1998; Enders et al.

2004, 2003; Nikora et al. 2003; Haro et al. 2004; Liao 2007; Tritico and Cotel 2010) affecting their swimming behaviour, aggregation and migration (Pavlov et al. 2000; Kemp et al. 2005; Liao 2007; Pavlov and Skorobogatov 2009; Lacey et al. 2012). Fish can take advantage of turbulent flows to reduce energy expenditure (Webb 1998; Enders et al. 2003; Liao et al. 2003a, b; Liao 2007; Taguchi and Liao 2011; van der Hoop et al. 2018). Fish also choose low momentum paths available in the wake of an object and synchronise their swimming trajectory by "Karman gaiting" between von-Kármán-type alternating vortex shedding, therefore exploiting the rotating motion of these rollers to propel themselves upstream (Liao et al. 2003a, b). Fish use their lateral line to sense the velocity and pressure field properties in their environment, as well as vortices generated by the movement of other fish (Franosch, Hagedorn, Goulet, Engelmann, & van Hemmen, 2009) and those in the wake of an obstruction. Conversely, negative effects of turbulence on fish swimming ability manifest as highly turbulent flows create swimming instabilities, increase energy expenditure, and decrease swimming performance (Webb 1998; Pavlov et al. 2000; Enders et al. 2003; Nikora et al. 2003; Liao et al. 2003a, b; Lupandin 2005; Smith et al. 2005; Cotel et al. 2006; Smith et al. 2006; Liao 2007; Plew et al. 2007; Tritico and Cotel 2010; Maia et al. 2015; Wang and Chanson 2018). The conflicting findings of whether turbulence and large-scale vortices are beneficial or detrimental might be explained by the different intensity, periodicity, orientation and scale characteristics of the turbulent flows, which have varied across studies (Murchie et al. 2008; Lacey et al. 2012).

Losses in swimming stability in response to perturbations are important to evaluate (Lauder, 2011) because fish expend energy and time recovering from instabilities while navigating challenging flows at the cost of swimming speed; effects which vary depending on flow velocity, turbulence vorticity characteristics and fish length (Pavlov et al. 2000; Cada and Odeh 2001; Lupandin 2005; Tritico and Cotel 2010;

Maia et al. 2015), as well as turbulence intensity and shear stresses (Cotel et al. 2006; Silva et al. 2011). Tritico and Cotel (2010) identified a relationship between turbulence eddy diameter and fish body length, where eddies over 75% of fish length destabilised the fish, confirming previous investigations into the effects of turbulence on the swimming ability of fish (Pavlov et al. 2000; Cada and Odeh 2001; Liao 2007). This ratio of turbulent length scale to fish length that destabilise the fish has also been identified as 66% (Lupandin 2005), and in the range of 50 to 100% (Paul W. Webb & Cotel, 2011). Vertical rollers are shed from vertically orientated objects, spanwise rollers are shed from objects with axes that span the cross-flow direction and streamwise rollers have axes of rotation parallel to the flow direction; all incite different adverse responses from fish (Tritico and Cotel 2010; Maia et al. 2015). Indeed, the orientation of flow obstructions and the axis of rotation of their wake eddies is vital since spanwise rollers have a greater impact on swimming stability and critical swimming speed than vertical rollers by requiring more recovery manoeuvres from the fish (Tritico and Cotel 2010).

Cylindrical shaped objects, often used in hydrodynamic research, are abundant in fluvial environments, including vegetation, woody debris, pipes, or bridge piers. They generate coherent and periodic turbulent flow structures against which fish swimming behaviour can be studied. Recent research focus on flow around horizontal cylinders has shown that these can exhibit different vortex shedding regimes compared to vertical cylinders (Lehmkuhl, Rodríguez, Borrell, & Oliva, 2013). In addition to the Reynolds number, the characteristics of the unsteady wake behind a horizontal cylinder depends on its proximity to the solid boundary and the approaching boundary layer thickness which affects the cylinder hydrodynamic and lift forces, the location of frontal stagnation points and shear separation layers, the extent of the recirculation bubble, and symmetry of the von-Kármán street (Price et al. 2002; Oner et al. 2008; Sarkar and Sarkar 2010).

Our understanding of the threshold of hydrodynamic conditions that lead to disruption of fish swimming kinematics is incomplete. Therefore, to further investigate the swimming stability and habitat usage of fish in altered turbulent flows, the current study tested fish swimming kinematics in the wake of a horizontal cylinder model. The cylinder wake's hydrodynamic properties were measured, and fish of various length were tested under a wider range of cylinder Reynolds numbers.

3.2 Materials and Methods

3.2.1 Flume setup and test area

Experiments were performed in an open channel recirculating Armfield flume with glass walls (1000 cm length, 30 cm width, and 30 cm height) in the Cardiff School of Engineering Hydro-environmental Research Centre laboratory. The flume was set to a slope of 1/1000. An electromagnetic flowmeter (Euromag MUT1100) measured the water discharge (±0.3% Ls^{-1}). A cylinder, 5 cm diameter (D) was placed transversally across the flume width and fixed to the flume walls using silicon adhesive, with its centre at 5 cm from the flume bed. The ratio of the gap distance between the cylinder and the flume bed (G) relative to the cylinder diameter (G/D) equal to 0.5 and corresponds to a vertical distance whereby the proximity to the bed affects the vortex shedding mechanisms whilst not too confined to suppress the shedding phenomenon (Oner et al. 2008). Flow over and under the cylinder generated a turbulent wake that was used to test the fish swimming kinematics. Honeycomb flow diffusers bounded the test section, 5 cm upstream and 30 cm downstream of the cylinder, with the upstream flow diffuser located 380 cm from the upstream end of the flume (Figure 3.1). A constant flow depth (H) of 15 cm, measured using a Vernier pointer gauge (± 0.1 mm), was maintained for all tests using a tailgate weir located downstream of the flume, resulting in cross-sectional averaged velocities and Reynolds numbers shown in Table 3.1. Flow discharges (Q) ranged from 3 to 27 Ls^{-}

[1] and cross-sectional averaged velocities ranged from 6.67 to 60 cms^{-1} (Table 3.1). The wake of the cylinder was within Re_D ranges of the sub-critical regimes and was fully turbulent (Douglas, Gasiorek, Swaffield, & Jack, 2011). A Logitech HD web camera, C920 with a 720p-1080p resolution at 30 frames per second positioned on the glass side of the flume recorded a side elevation view of the fish swimming behaviour.

Table 3.1. Details of the velocity step test used for fish swimming behaviour with time increments (each 600 s) and flow rate (Q) with corresponding cross-sectional averaged velocity (U_0), Froude number (Fr) and cylinder Reynolds number (Re_D), vortex shedding peak frequency (f), and Strouhal number (St) at 25^0C.

Time [min]	Q [Ls^{-1}]	U_0 [cms^{-1}]	Fr	Re_D	f [s^{-1}]	St [-]
0-10	3	06.67	0.05	3,730	0.46	0.34
10-20	6	13.33	0.11	7,470	0.85	0.32
20-30	9	20.00	0.16	11,200	1.21	0.30
30-40	12	26.67	0.22	14,930	1.61	0.30
40-50	15	33.33	0.27	18,660	2.00	0.30
50-60	18	40.00	0.33	22,400	2.62	0.32
60-70	21	46.67	0.38	26,130	3.04	0.32
70-80	24	53.33	0.44	29,860	3.05	0.28
80-90	27	60.00	0.49	33,590	4.05	0.33

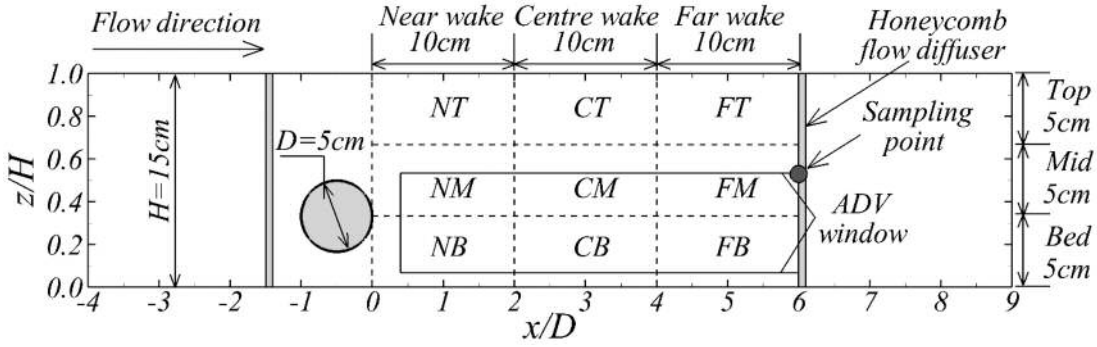

Figure 3.1. Side view of the fish behaviour observation test section, located 3.8 m downstream of the flume inlet and subdivided into flow volume zones of equal demensions, with length of 10 cm and 5 cm in the streamwise (x) and vertical (z) directions respectively. The origin of the x axis corresponds to the edge of the cylinder and the flume bed for the z axis. Flow volume zones are named: NB for the Near wake bed, NM for the Near wake Mid-water column, and NT for the Near wake Top water column. Similary, CB, CM, CT, FB, FM, and FT refer to the Bed, Mid, and Top water colum zones in the Centre and Far wakes of the cylinder, respectively. The spectral analysis sampling point located at x/D =6, z/H =0.53 is shown.

3.2.2 Fish swimming behaviour tests

Nile tilapia (*Oreochromis niloticus*, Silver strain; n=28; fork length (11.78±2.11 cm); standard length, herein referred to as L_{fish} (9.52±1.77 cm) and weight (31.6±17.5 g)) sourced from a commercial facility (FishGen Ltd), were maintained in aquaria facility in the Cardiff School of Biosciences at 25±0.5^{0}C. This temperature was also maintained during acclimatisation of the fish in the flume and for all swimming tests. Individual swimming tests were conducted using a ramped step velocity test after each fish was acclimatised in an area downstream of the test section in the flume for 30 min, at the lowest discharge of 1.5 Ls^{-1}. The acclimatisation space was also delimited by honeycomb flow diffusers, which were lifted to allow fish to swim in the test section at the beginning of the velocity step test and behaviour observations.

Discharges were increased from 3 to 27 Ls^{-1} in step increments of 3 Ls^{-1} and each velocity step was maintained for a test time of 10 min during which fish swimming kinematics were observed. Fish maintenance and behavioural tests were all approved by Cardiff University Animal Ethics Committee and conducted under Home Office licence PPL 303424.

Videos of the swimming behaviour were reviewed and habitat preference, as well as swimming behaviours were logged using JWatcher V1.0 software to record the amount of time fish spent in each flow volume of the test section, the time or velocity step and the volume zone where spills occurred. The body centre was used to locate the fish. Flow volume zones were defined by dividing the test section into nine subsections of equal dimensions. Three sections (10 cm length) along the streamwise direction delimited the near, centre and far wakes, while three sections (5 cm height) in the vertical direction delimited the water column into bed, mid and top-water column volume zones (see Figure 3.1). Spills, events of loss of balance, were defined by Tritico and Cotel (2010) as involuntary swimming behaviour where the fish's head rotates more than 45^0 in yawing motion, followed by drifting downstream over a distance longer than half of its body length. Recovery manoeuvres from the spill follow as the fish realigns its body length to the longitudinal flow direction. A measure of the rate of spill occurrence used in this study was the ratio of the number of spills over the amount of time spent in each flow volume, referred to as spill frequency (min^{-1}).

3.2.3 ADV velocity data acquisition

The hydrodynamic characteristics of the cylinder wake were measured using an Acoustic Doppler Velocimeter (ADV), a downward-looking Nortek Vectrino Plus (V.1.31+) at a sampling rate of 200Hz. The flow was seeded with neutrally buoyant sphericel hallow glass silicate powder with 10 μm mean diameter and 1.1 ±0.05g/cm^3

density (Potters Industries Inc.). The sound to noise ratio and correlation were maintained above 20 dB and 70% respectively by adding the seeding material to the water to ensure good quality data. Recorded velocities were in three dimensions of xyz coordinates, x longitudinal, y transverse and z vertical flow directions. The spatial resolution of the velocity sampling grid was such that 15 points were measured equispaced by 2 cm in the x direction and 15 points, 0.5 cm apart in the z direction. A constant sampling time of 300 s was used for all data points. The geometry of the ADV probe did not permit velocity measurements within 2.5 cm distance from the edge of the cylinder, and in a distance greater than 8 cm from the flume bed, which meant that parts of the Mid water column and Top layer of the water column (see Figure 3.1) were not included in the velocity measurements.

3.2.4 ADV data filtering and post processing

The Velocity Signal Analyser (MAJVSA version V1.5.62) was used to filter and despike the ADV data using limits of 15 dB and 70% for the Sound to Noise Ratio (SNR) Correlation (COR) respectively (Nortek, 2009). Further despiking used the Phase-Space Thresholding method by Goring and Nikora (2002) (revised by Wahl 2003) as well as a 12-point average spike replacement (Jesson et al. 2013). On average, the percentage of good samples after filtering and despiking was 80%. A FORTRAN script was used to perform the autocorrelation function integration and calculation of the turbulence length scale (Pope, 2000). The autocorrelation function is:

(3.1)

Where s is the lag time and u' denotes velocity fluctuation values. The longitudinal turbulent integral length scale L_u is given by:

(3.2)

Where T is the time at which the autocorrelation function becomes firstly negative, i.e., =0, and $\overline{u}$ is the mean streamwise velocity at the evaluated point. Vorticity was calculated using the time-averaged streamwise $\overline{u}$ and vertical velocities $\overline{w}$ as:

(3.3)

where ω_y is the spanwise component of the vorticity vector. Strouhal number is defined by:

(3.4)

where f is the dominant shedding frequency with the highest spectral energy in the Fast Fourier Transform (FFT), D is the cylinder diameter and U_0 is the cross-sectional averaged velocity (Pope, 2000). Turbulence characteristics calculated using MAJVSA included the turbulent kinetic energy (, longitudinal turbulence intensity , and Reynolds shear stresses and ( ) for the spanwise and vertical components respectively. Note that overbar ( ) denotes time-averaging.

3.2.5 Statistical analysis

Fish behaviour data in relation to hydrodynamic parameters were analysed in R statistics software (3.5.0) (R Core Team 2018) via RStudio (Version 1.1.447) (RStudio Team 2016). Mean, standard deviation and quartiles of each variable were summarised, and Shapiro tests used to evaluate the data distributions. Generalised Linear Mixed Models (GLMMs) are multivariate regression models that evaluate the statistical significance of relationships between dependent and independent variables (Thomas et al. 2013). GLMMS, where Fish ID accounted for repeated measures of fish, were used to evaluate the number of spills in each zone as explained by the fish

characteristics (length and weight), the amount of time spent in each zone, the longitudinal and vertical distance of the zone where the spill occurred, the Reynolds number, and the flow velocity and turbulence properties which are spatially-averaged for each zone ($\overline{u}$, $\overline{v}$, $\overline{w}$, , , , , , , , and L_u). Note the angle brackets denote spatial-averaging. Similar GLMMs were used to evaluate, the proportion of time and the frequency of spills in each flow volume zones for each fish. The GLMM models used Lmer and Lme4 R packages (Bates, Mächler, Bolker, & Walker, 2015), and were refined by minimising the Akaike information criterion (AIC).

3.3 Results

3.3.1 Turbulent wake dynamics

Swimming stability and microhabitat use of Nile tilapia was studied in the wake of a horizontal cylinder in a step velocity test with nine Reynolds numbers ranging from $3{,}730 \leq Re_D \leq 33{,}590$. Under these conditions, the cylinder flow is within the sub-critical regime in which the laminar shear layer breakdown off the walls of the cylinder generated coherent alternating von-Kármán vortex shedding with vortices with spanwise axes of rotation (Williamson, 1996). As the flow accelerated over and under the cylinder, clockwise and counter-clockwise rotating vortices formed off the upper and lower cylinder walls respectively.

The normalised time-averaged hydrodynamics developed in the cylinder wake were similar for all Reynolds numbers and Figure 3.2 presents those corresponding to the Re_D = 16,800 case. A wake bubble was generated immediately downstream of the cylinder as depicted from the contours of $\overline{u}$ in Figure 3.2a, which reduced in streamwise extent with increasing Reynolds number. The impact of the small gap between the cylinder and flume bed induced large vertical velocities $\overline{w}$ and turbulence

intensities which in turn contributed to the asymmetric formation and shedding of the von Kármán type vortices in the cylinder wake. Indeed, across the range of Re_D tested, the gap between the cylinder and the bed resulted in asymmetric vorticity field with predominantly clockwise vortices over the wake length as indicated by the large area occupied by negative vorticity which correlate well with the regions of highest Reynolds shear stress (Figure 3.2e and f). The large-scale vortical structures dissipated with increasing downstream distance from the cylinder such that the near wake ($x/D < 2$) showed higher magnitudes of longitudinal (Figure 3.2c), lateral and vertical turbulence intensities than the centre and far wakes (see Figure 3.1 for notation).

The recurrent generation of instantaneous turbulent structures were identified via Power Spectral Density (PSD) analysis of the time series of velocities at the sampling point x = 6D, z = 0.53H in the cylinder wake. Each time history was divided into six consecutive segments with each segment spanning 50 s and the resulting spectra are the average of the PSD from each segment. At each discharge the frequency of these energy peaks related to the von Kármán type vortex shedding and increased linearly with increasing Re_D with frequencies ranging from 0.46 to 4.05 s^{-1}, and corresponding Strouhal numbers remarkably constant irrespective of Re_D with a mean value of 0.31 ± 0.02 (mean ± s.d.) (Table 3.1). Note that these St values are higher than those for unbounded cylinder flows (St = 0.21) due to the proximity of the bed, in addition to the effects of free-surface dynamics. Such wake development is asymmetric as the vortices are constrained by the proximity of the bed and thus bottom vortices can only be horizontally propagated in the streamwise direction. This complex flow pattern of energetic turbulent structures spaned across the entire flume's width and occupied a large extent of the water column.

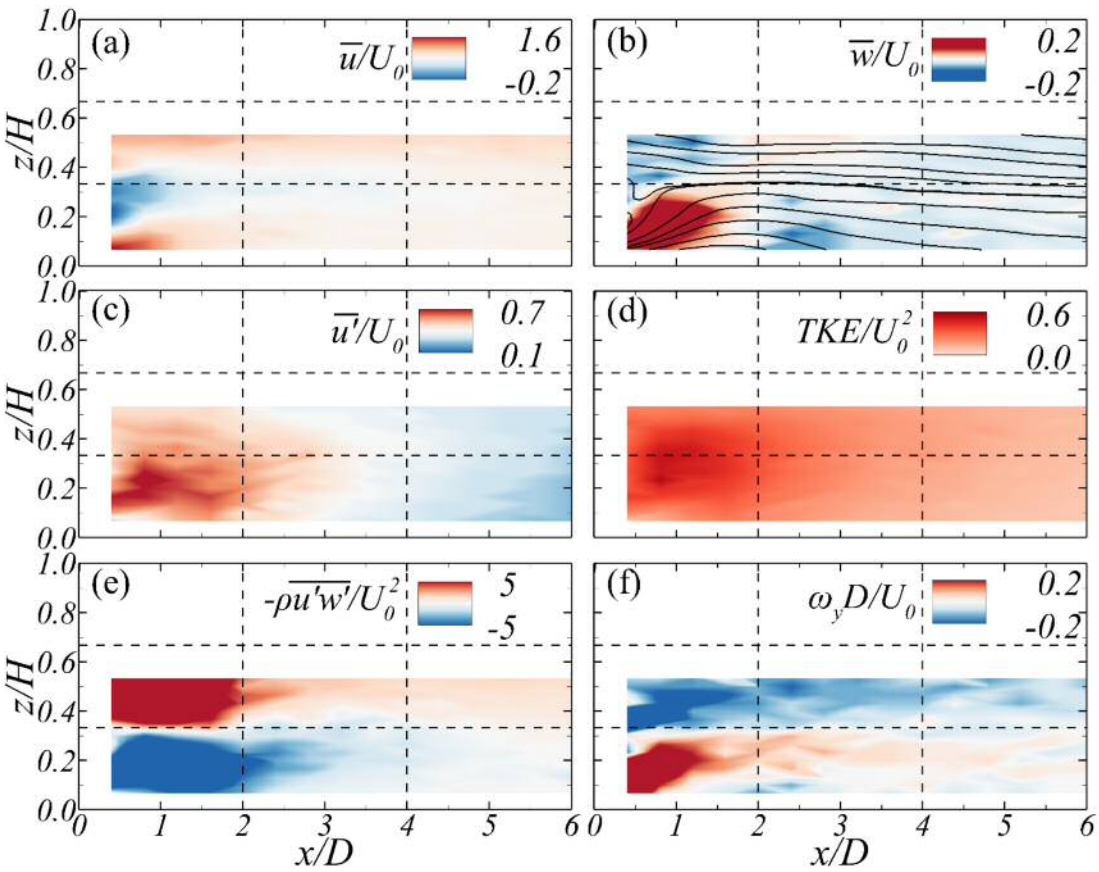

Figure 3.2. Time-averaged (a) streamwise velocity $\overline{u}$, (b) vertical velocity $\overline{w}$, (c) streamwise turbulence intensity(d) turbulent kinetic energy *TKE*, (e) principal Reynolds shear stress , and (f) spanwise vorticity ω_y for the Re_D = 18,600 case.

3.3.2 Fish behaviour

Distribution of habitat usage over the step velocity test

Habitat usage (percentage of time) did not vary significantly with cylinder Reynolds number throughout the step velocity test (GLMM, d.f.1, P>0.05) as the proportion of time fish spent in each flow volume zone (defined in Figure 3.1) remained uniform with increasing Re_D (Figure 3.3). Spatially, however, the percentage of time spent increased with increasing longitudinal distance from the cylinder (GLMM, d.f.1, P<0.001) and decreased with increasing vertical distance, as fish stayed closer to the flume bed instead of swimming higher in the water column (GLMM, d.f.1, P<0.001).

Hence, the most preferred zone, FB where fish spent 55% of time was furthest from the cylinder and closest to the flume bed (Figure 3.4a). Less than 2% of time was spent in each of the near wake zones, which are the most unstable regions with the highest magnitudes of turbulence intensity, turbulent kinetic energy, Reynolds shear stress and vorticity, as shown in Figure 3.2. The percentage of time spent in each zone increased with increasing L_w/L_{fish}, indicating that the fish preferred zones where the turbulent length scale was much less than half their length. When $L_w/L_{fish} \geq 0.4$, the percentage of time starts to decrease, as fish begin to avoid zones where the turbulent length scale approached 50% of the fish length (Figure 3.6a). Fish could station hold in zones of low turbulence intensity, with a preference for the range $0.3<TI_u<0.4$, a preference that was less evident with increasing TI_u. For all Re_D steps, percentage time decreased with increasing turbulence intensity (TI_u) as fish spent less time in zones of higher TI_u (GLMM, d.f.1, P <0.001).

Distribution of spill occurrences over the test area

For all 28 fish tested, 317 spills were recorded in total and distributed in the flow volume zones as depicted in Figure 3.4b. The number of spills per fish was dependent on fish length and weight, since larger fish spilled less than small fish (GLMM, d.f.1, P=0.033). Higher values of turbulence integral length scale to standard fish length ratio (L_w/L_{fish}) corresponded to higher numbers of spills (Figure 3.6a). Spanwise vortices with a length scale range of $0 \leq L_w/L_{fish} \leq 0.55$ were present in the cylinder wake, and spills were observed across the whole range, with the number of spills generally increasing with L_w/L_{fish} ratio and the maximum spills occurring towards the upper limit of the range where $L_w/L_{fish} = 0.55$ (Figure 3.6a). Similarly, high numbers of spills were recorded in the near wake zones of highest vertical Reynolds shear stress τ_{uw}, and vorticity (Figure 3.4b and c). The number of spills gradually increased with increasing Re_D, reaching a maximum at Re_D = 14,930 (U_0 = 30 cm/s)

and decreased slightly for the remaining Re_D steps (Figure 3.7). For U_0 < 30 cm/s the number of spills increased with each velocity step and was found to correlate with increasing cross-sectionally averaged velocity per volume zone (GLMM, d.f.1, P<0.001) and the higher the amount of time the fish spent in the zone, the higher the likelihood of spills occurring, which is evident in the FB and CB zones (GLMM, d.f.1, P<0.001; Figure 3.5). For U_0 = 30 cm/s, the number of spills significantly depended on the velocity step U_0 (GLMM, d.f.1, P=0.004), the ratio of velocity/fish length (body-length per second, based on fish total length) (GLMM, d.f.1, P=0.005), the fish's momentum (fish mass*) (GLMM, d.f.1, P=0.031), as well as the downstream distance from the cylinder (GLMM, d.f.1, P<0.001) (not shown here). The distribution of spills became less predictable at U_0 steps >30 cm/s as opposed to the near linear relationship of the number of spills with Re_D for U_0 <30 cm/s (R^2= 0.993) (Figure 3.5). Therefore, occurrence of spills depended on the fish's length and weight, and was significantly affected by the Re_D, the Reynolds stresses and the vorticity (Figure 3.6b and c).

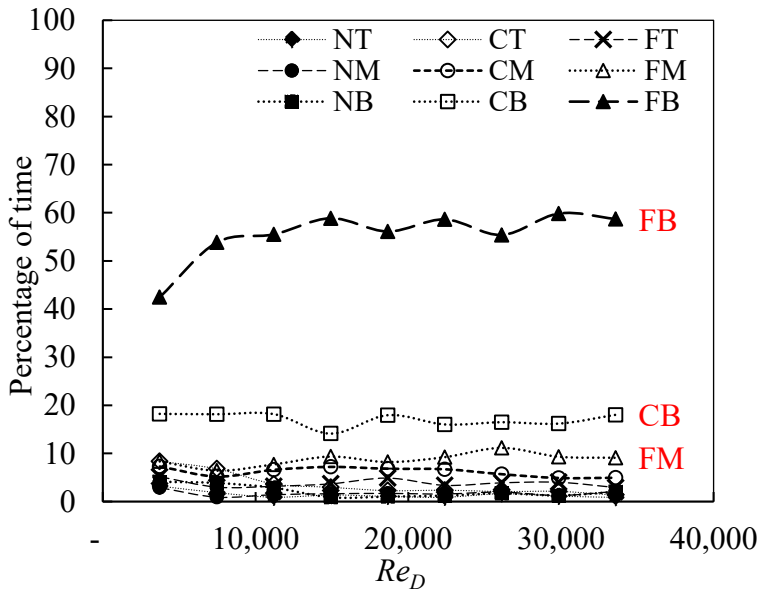

Figure 3.3. Percentage of time fish spent in each zone at different Re_D steps. ▲, □, and Δ markers indicate percentage time the fish spent in volume zones defined in

Figure 1 where FB is the far bed volume, CB is the central bed volume and FM is the far middle-depth volume.

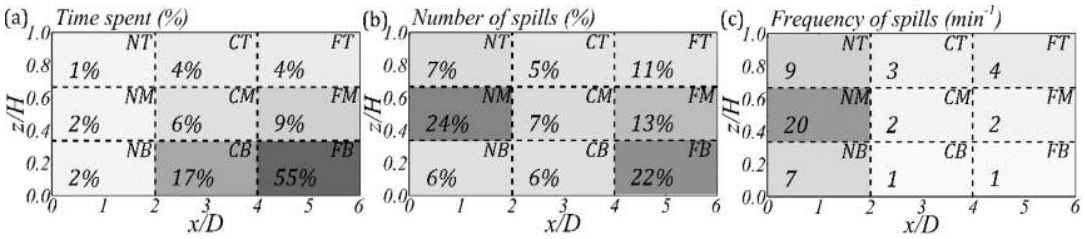

Figure 3.4. Distributions of percentage of (a) time spent, (b) spills and (c) spill frequency (min^{-1}) in each flow volume zone (outlined in Figure 1). The zones with the highest proportion of time, spills and frequency of spills are shaded in grey.

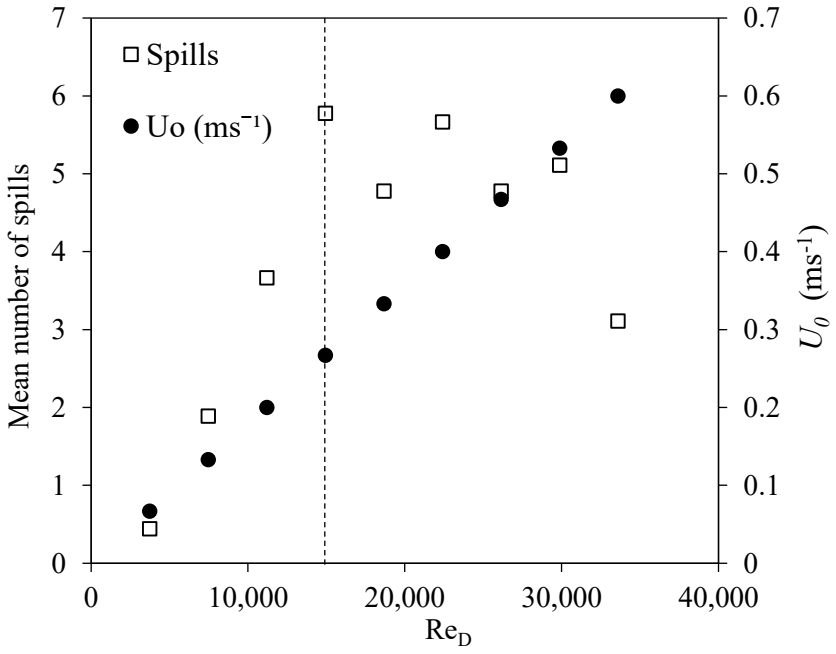

Figure 3.5.. Mean number of spills relative to the cylinder Reynolds number and the cross-sectionally averaged velocity U_0 (ms^{-1}). The dashed line indicates the Re_D =14,930 (U_0 = 0.3ms^{-1}) after which the number of spills remains relatively constant, before decreasing at the last velocity step.

Frequency of spill events over the step velocity test

Zones furthest from the cylinder, where the wake turbulence intensities had decayed were the preferred fish refuge due to the reduced likelihood of spills occurring (Figure 3.4c). The frequency of spills (spills per min) decreased with increasing downstream distance from the cylinder (GLMM, d.f.1, $P<0.001$). The near wake zones, where the fish spent the least amount of time, featured the highest spill frequency. The proportion of time that fish spent in each zone increased with increasing downstream distance from the cylinder, and increased with proximity to the bed (Figure 3.4a). Overall, the highest percentage of spills occurred in the far wake, followed by the near wake and the centre wake. The flow zones with the most spills were NM (24%) and FB (22%). In the NM zone, in particular, fish spilled the most but spent the least amount of time here, so they spilled almost immediately after swimming into this area, and therefore tended to avoid this area. The FB zone was the preferred station holding zone for the fish as they spent over half their time there, resulting in a proportionately high number of spills but the lowest frequency of spills (Figure 3.7).

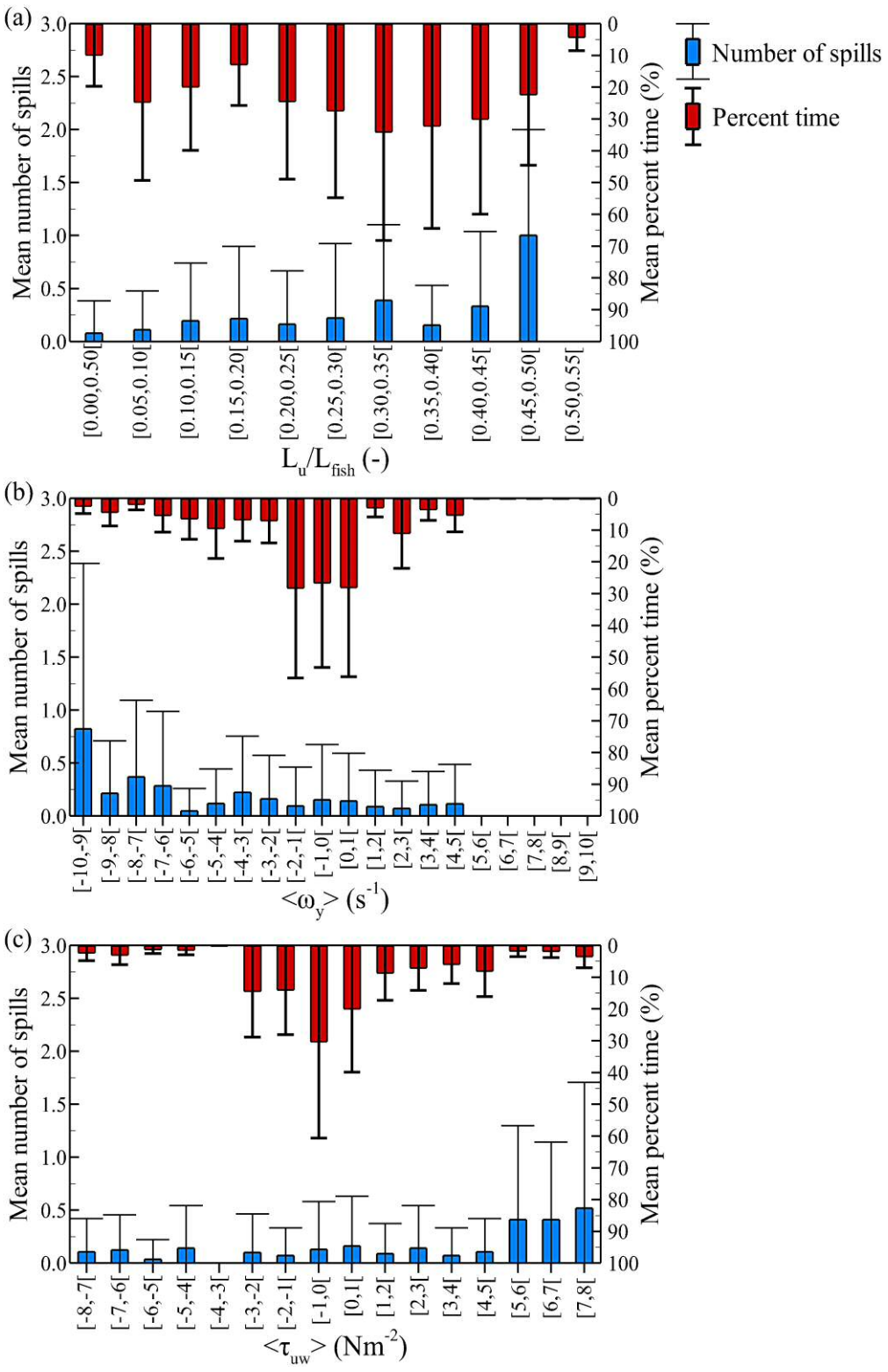

Figure 3.6. Mean number of spills and mean proportion of time (%) the fish spent (mean ± s.d.) relative to the flow characteristics of (a) the ratio of turbulence length scale over fish length L_u/L_{fish} in 0.05 intervals, (b), zone averaged y-vorticity

component ω_y in $1s^{-1}$ intervals, and (c) vertical Reynolds shear stress τ_{uw} in $1Nm^{-2}$ intervals. Error bars represent the standard deviation.

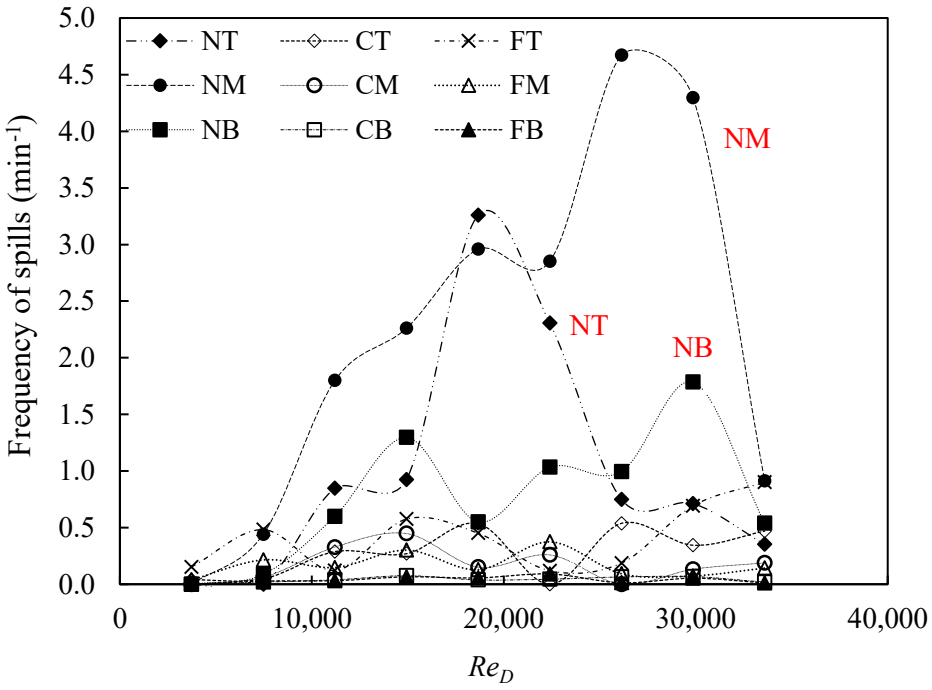

Figure 3.7. Variation of frequency of spills (min^{-1}) per Re_D and flow volume zones shows that the near wake zones (NB, NM, NT) had the highest ratio of spill occurrence over amount of time the fish spent in the zone, and this frequency changed with increasing Re_d. The **C**entre and **F**ar wake zones (CB, CM, CT, FB, FM, FT) where fish preferred to station hold show little to no variation in frequency of spills over the range of Re_D.

The frequency of spills significantly varied with Re_D (Figure 3.7) and vorticity (GLMM, d.f.1, $P<0.05$) and was significantly dependent on the fish's length ($P<0.001$), as well as the momentum of the fish (mass*) (GLMM, d.f.1, $P<0.001$). Furthermore, the frequency of spills increased with increasing ratio of turbulence length scale to cylinder diameter (L_w/D) but increased with decreasing L_w/L_{fish} (GLMM, d.f.1, $P<0.05$). Zones of higher τ_{uw} also showed increased frequency of spills ($P<0.001$). Furthermore, the highest spatial variation of vorticity was in the NB

and NM zones, with the remaining zones showing lesser standard deviation, highlighting the predominance of negative vorticity (clockwise eddies) in the NM zone, since only the NB zone contained positive vorticity (counter-clockwise rollers) (Figure 3.8). This considerably affected the frequency of spills, which was highest in the NM and NB zones where vorticity standard deviation was greater than 2.78 (more than 60% of the cross-sectionally averaged vorticity) (Figure 3.9). This result suggests that the near wake had less predictable flows due to the higher flow unsteadiness, leading to the lower preference of the fish to station hold in these zones and to the higher frequencies of spills observed.

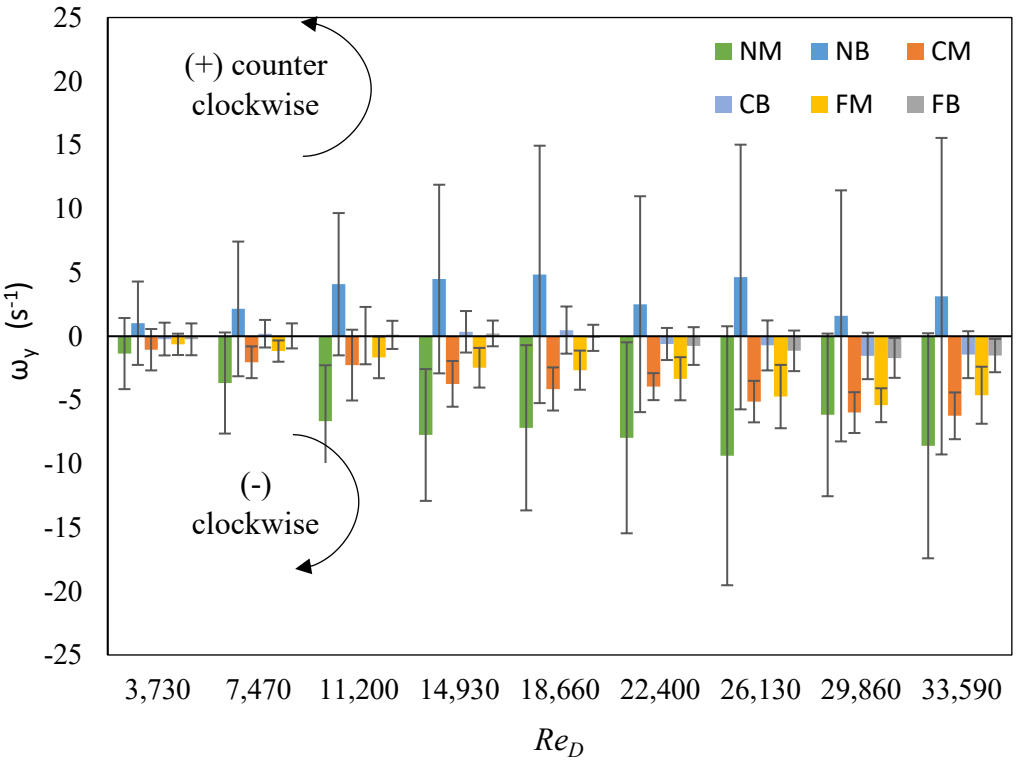

Figure 3.8. Zone-averaged vorticity ω_y (mean± s.d.) distribution by flow volume zones for each Re_D. Positive vorticity indicates vortices rotating in the counter clockwise direction, while negative values denote eddies rotating in the clockwise direction. Flow volume zones are outlined in Fig 1. Error bars represent the standard deviation.

The near wake, where highest fluctuations of vorticity above the mean were present (Figure 3.8), was characterised by the highest spill frequencies (Figure 3.9), suggesting that these flows were significantly unpredictable for the fish compared to the other zones. These near wake zones also had the highest instances of τ_{uv}, and τ_{uw} from the shear layer breakdown from the cylinder. The horizontal orientation of the cylinder considered in this study created a vortex shedding regime in which the XZ plane was most dominant, with mean $|\tau_{uv}| \leq 1.5$ Nm^{-2} and $|\tau_{uw}| \leq 8 Nm^{-2}$ (| | indicate absolute value), making Reynolds shear stress in the XZ plane over five times stronger than those in the XY plane. Due to the ground proximity which rendered the wake vortex shedding assymetric, the NM zone, where rollers were clockwise (negative) and τ_{uw} was downwards (positive), was among the least frequented zones, yet showed the highest number of spills and twice the frequency of spills of any other zone. In contrast, the NB zone of the lower shear layer was similarly frequented (Figure 3.4a) and had similar magnitude of Reynolds shear stresses and vorticity, but these were in opposite directions to those in the upper shear layer of NM (Figure 3.2). As a result, the NB zone showed significantly lower numbers of spills as well as a lower frequency of spills than the NM zone, which suggests that the directions of the shear forces and eddy vortices acting on the fish are of great importance to the swimming stability of fish. A summary figure which illustrates the interactions of the fish and the spanwise vortex dynamics as well as the distribution of forces acting on the fish is given in Figure 3.10.

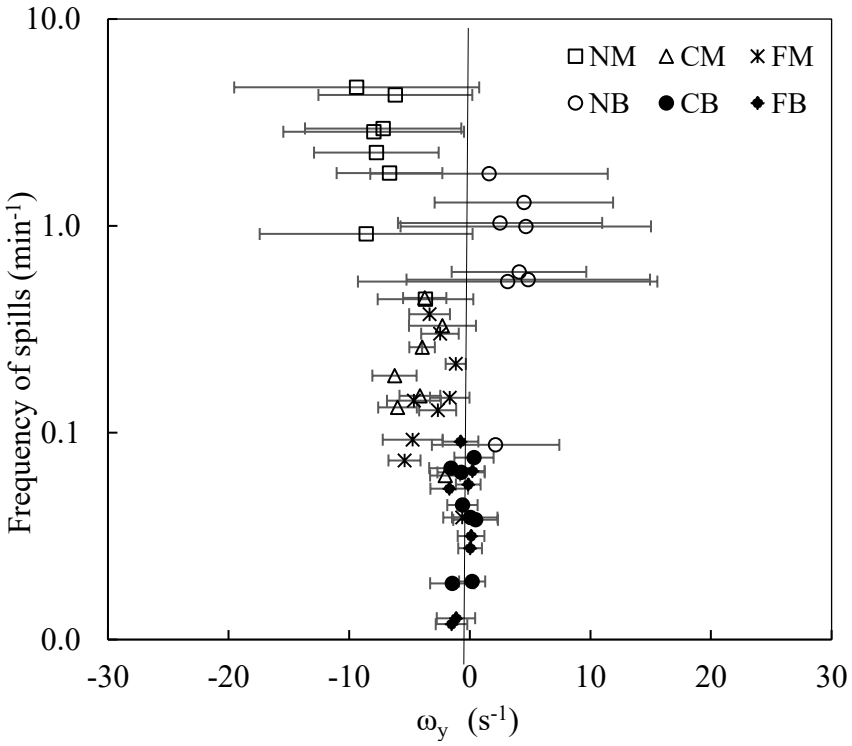

Figure 3.9. Semi-log plot of average frequency of spills relative to the zone averaged y-vorticity ω_y (mean±s.d.).

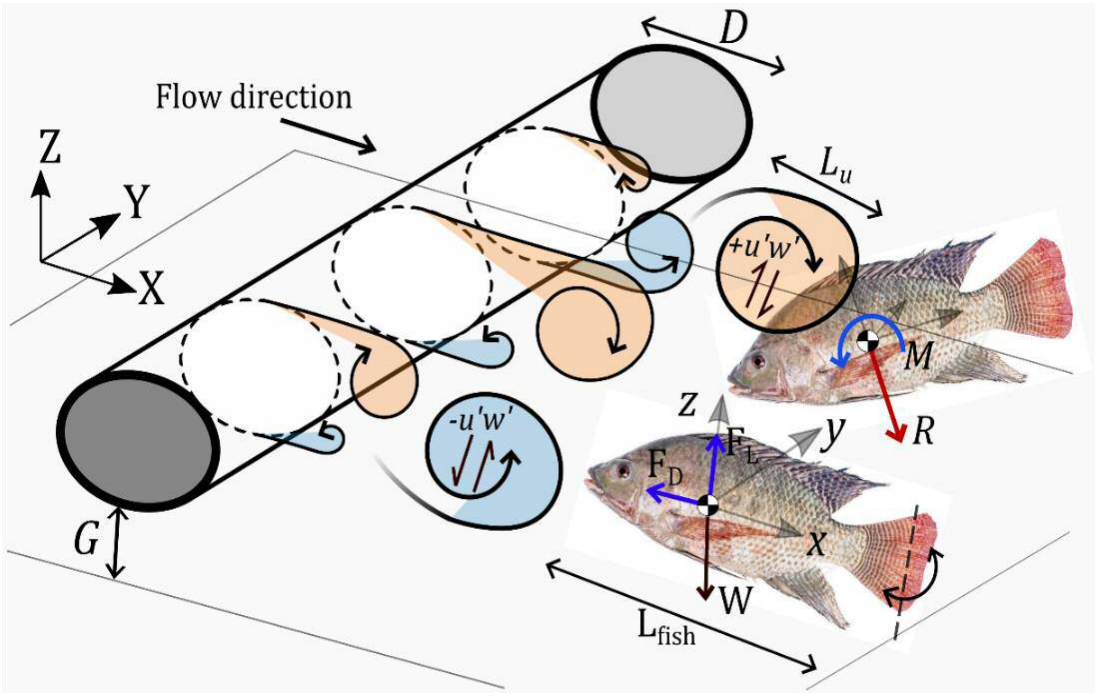

Figure 3.10. Schematic of the interaction between the alternating vortex shedding developed behind the horizontal cylinder and the fish including the force balance,

where F_D is drag force, F_L is lift force, W is fish's weight, L_u is the length scale of a given vortex, L_{fish} is the fish's length and R and M are the force vector and resulting moment, which causes a turning reaction when the fish becomes unbalanced, and *u'w'* illustrates the Reynolds shear stress.

3.4 Discussion

The swimming stability and habitat usage of Nile tilapia fish in the turbulent wake of a horizontal cylinder were investigated to evaluate fish interaction with turbulence characteristics under Reynolds numbers (Re_D) ranging from 3,730 to 33,590. Fish habitat preference was significantly influenced by local velocity, turbulence intensity, turbulent kinetic energy, turbulence integral length scale, vorticity, and Reynolds shear stresses. For all Re_D steps, fish spent less time in zones of higher turbulence intensity, to avoid the high swimming costs associated with elevated turbulence intensities (Pavlov et al. 2000; Odeh et al. 2002; Enders et al. 2003; Hockley et al. 2014). The change in spill occurrence after the intermediate Re_D level of 14,930 (Figure 3.5) is perhaps due to changes in the shape of eddies as turbulent shedding regimes vary with Re_D. In addition, Nile tilapia do respond positively to behavioural conditioning (Mesquita & Young, 2007) and therefore could have adjusted their spill responses through learned behaviour in the step velocity test, similar to behaviours of adjustment to turbulence observed by Maia et al. (2015). Fish were assumed to be within the critical swimming capabilities (Alsop, Kieffer, & Wood, 1999), and showed no signs of fatigue in the swimming observations.

Although other researchers have found that habitat preference varies with flow cross-sectional averaged velocity (U_0) (Pavlov et al. 2000; Odeh et al. 2002; Enders et al. 2003; Tritico and Cotel 2010), here, the percentage of time spent in each zone did not vary significantly with increasing Re_D, as also reported by Maia et al. (2015). This could be attributed to the relatively similar distribution of velocities and turbulence

in all zones throughout the step test and the FB (far bed) zone remained the preferred region due to the lower τ_{uw}, τ_{uv}, and ω_y. Furthermore, the threshold for the distribution of habitat choice and occurance of spills of L_u/L_{fish} being 50% (Figure 3.6a) supports the idea of there being an ideal ratio of turbulence length scale to fish length as fish are predicted to prefer turbulent length scales that are either much smaller or much greater than their body length (Pavlov et al. 2000; Odeh et al. 2002; Lupandin 2005; Webb and Cotel 2011; Tritico and Cotel 2010). This is also in keeping with the turbulence length scale to fish length ratio threshold of 0.66 reported by Pavlov et al. (2000) and Lupandin (2005), although small variations of this threshold might be due to interspecies differences, as fish species behave differently in similar settings, individual fish shape and hydrodynamic measurements techniques and calculations of turbulent length scale (Liao 2007; Lacey et al. 2012; Cotel and Webb 2015). Similar to other studies, the high preference for zones furthest from the cylinder was due to the presence of lowest vorticity, Reynolds shear stresses (Silva, Katopodis, et al. 2012; Hockley et al. 2014); and turbulent kinetic energy (Smith et al., 2006).

Tritico and Cotel (2010) demonstrated that the axis of rotation of the dominating vortices, vertical axis for vertical cylinders, and spanwiseaxis for horizontal spanwise cylinders yields different effects on swimming stability as spanwise rollers resulted in more spills than vertical rollers, for eddies over 75% of the fish length. The Kármán gaiting swimming behaviour described by Liao et al. (2003a, b) was not observed in the current study, as fish were unable to take advantage of the von-Kármán street typically composed of vertical rollers, which are not present in horizontal cylinder flow. This is because the eddy's plane of orientation (XZ plane) is perpendicular to the fish's spine and axis of undulation, which is employed in swimming, along with fin oscillations to propel longitudinally and produce lateral movements of their body (XY plane) (Pavlov et al. 2000; Webb 2002; Webb 2004; Epps and Techet 2007; Lauder and Madden 2007) and hence the main eddy torque and vorticity work against

the fish by dominating the plane (XZ plane) where motor control is most limited. This proposed reasoning is shown in Figure 3.10.

Reynolds shear stresses are of substantial physical importance in the fish's environment, yet often omitted in fish swimming behaviour studies (Lacey et al. 2012). Reynolds stresses are key parameters in injury mechanisms (Deng et al., 2005), and often fatal for turbine passed fish in hydropower focused studies (Coutant and Whitney 2000; Neitzel et al. 2000; Cada and Odeh 2001; Odeh et al. 2002). In fish pass studies, Reynolds stresses are the most significant flow characteristic influencing transit time and successful passage, particularly for small fish (Silva et al. 2011; Silva, Santos, et al. 2012). Even though the Reynolds shear stresses of the current experiment are lower than those in rivers (Lacey et al. 2012), current results clearly show that the physical characteristics of forces, shear stresses, are important to consider in fish-turbulence interaction studies (Figure 3.10). The balance of forces, resulting torques, and moments acting on the fish challenge its ability to maintain posture and swim unimpeded (Drucker and Lauder 1999; Pavlov et al. 2000; Odeh et al. 2002; Webb 2002; Lupandin 2005; Cotel et al. 2006; Liao 2007; Tritico and Cotel 2010; Webb and Cotel 2010; Silva, Katopodis, et al. 2012 ; Wang and Chanson 2018). However, considering the orientation plane of vortices and magnitude of hydrodynamic forces requires the inclusion of their direction, which this study has demonstrated to be essential.

The force balance to a swimming fish are intricate; the fish uses coordinated propulsive manoeuvres to overcome spanwise hydrodynamic forces (F_D), uplift forces (F_L) from the fluid dynamics and to compensate against its weight (W) as well as vertical or horizontal turbulent shear stresses dependent on an obstable's orientiation (Figure 3.10). The unbalanced resultant forces create overturning moments that affect the fish's locomotion (Drucker and Lauder 1999; Nauen and Lauder 2002; Webb 2002). Therefore, distribution, intensity, and direction of

hydrodynamic forces exerted on the fish will aid propulsion, or hinder swimming kinematics; whether the force is towards or counter to the fish, works for or against the fish's propulsive manoeuvres. The direction of the dominant Reynolds stresses, which characterise turbulence momentum transport, and eddies that are characteristic of rotational flow represent important physical attributes of the flow within which the fish swims. The interdependence of eddy vorticity and Reynolds shear stresses cannot be neglected, and as our results suggest, downward Reynolds shear stresses, and rollers with clockwise rotation destabilise the fish more often than those of similar extent but opposite direction (Figure 3.8).

Emphasis on the Reynolds stresses in fish swimming kinematics studies could then explain the size dependent responses from the fish since different sized fish will have different reaction forces to the turbulent shear stresses, resulting therefore in more frequent losses of posture and balance for smaller fish whose locomotion is overwhelmed by torques larger than their reaction forces capabilities or stabilisation manoeuvres by fin movement (Pavlov et al. 2000; Cada and Odeh 2001; Lupandin 2005; Webb 2002). Individual, physiological differences, in addition to size, life stage and species related variations (e.g. Pavlov et al. 2000; Plew et al. 2007), could become clearer when the direction of local Reynolds stresses and eddy vorticity, which have been overlooked in fish swimming studies (Lacey et al. 2012), are accounted for in the hydrodynamic propertites and quantification of turbulent flows.

3.5 Conclusion

In summary, in order to evaluate the turbulence metrics that govern fish swimming behaviour, swimming kinematics and habitat preference of fish were investigated in the turbulent wake of a horizontal cylinder. Habitat preference was determined by the turbulence intensity, turbulent kinetic energy, vorticity, Reynolds shear stress, and turbulent length scale relative to fish length as fish avoided areas of relatively high

turbulence. Similarly, these parameters influenced the occurrence of spills in addition to the Reynolds number, and the fish size and weight, with smaller fish being more perturbed than larger ones. The number of spills generally increased with L_u/L_{fish} ratio with the maximum spills occurring towards the upper limit where the eddy length was 45 to 50% of the fish length. The highest rate of spill occurrence was in the zones where the upper shear layer had highest magnitudes of downward-acting Reynolds stresses and negative vorticity (clockwise). Furthermore, physical reasoning was given to why spanwise rollers yield different effects on swimming stability compared to vertical vortices, in that the main eddy torque and vorticity work against the fish by dominating the plane where motor control is most limited.

Therefore, in addition to the scale of eddies and the plane of dominant eddy rotation and the magnitude of Reynolds shear stresses, we highlight that the direction of eddy rotation and the direction of Reynolds stresses are key physical flow characteristics that impact fish swimming kinematics. Their inclusion will yield a more holistic view of the hydrodynamic properties of turbulent flow and a better understanding of how the fish interact with altered flows and their environment in general. These results further our understanding of fish swimming behaviour, and can inform design and refinement of fish-friendly structures including fish passes, hydropower turbines, as well as restorations of fluvial environments. In fish passes and altered environments the prevention of flow dominated by spanwise rollers and downward turbulent shear stresses could benefit fish movement and passage. While the employment of spanwise rollers downstream of hydropower schemes (e.g. Archmedis screw turbines) could benefit fish guidance efforts to deter fish from turbine blades and perilous flows.

Chapter 4. Wake dynamics of a horizontal cylinder in proximity to a solid boundary

A manuscript based on this chapter has been accepted (27 September 2019) in Physical Review Fluids as: Ouro Pablo, Muhawenimana Valentine, Wilson Catherine A.M.E. (2019). Asymmetric wake of a horizontal cylinder in close proximity to a solid boundary for Reynolds numbers in the subcritical turbulence regime. *Physical Review Fluids*. V.M and C.W designed the study. P.O conducted the LES modelling and post-processed the numerical results. V.M conducted the experiments and analysed the experimental results.

Summary

The wake dynamics developed in the near wake behind a horizontal cylinder with wall proximity effects are elucidated from laboratory experiments and Large-Eddy Simulations (LES). A fixed vertical gap to diameter ratio (*G/D*) of 0.5 was chosen for Reynolds numbers equal to 6,666, 10,000 and 13,333. The LES results agreed well with the experimental measurements for the time-averaged flow quantities and captured the upward flow motion developed over the lower half of the flow depth as a consequence of the near-wall effect. The presence of the gap between the cylinder and the bed significantly influenced the dynamics of the vortex generation and shedding which, in consequence, led to an increasingly pronounced asymmetric wake distribution with increasing Reynolds number. The Kelvin-Helmholtz instability developed in the upper and lower shear layers was shown to be decoupled as their

instantaneous laminar-to-turbulent transition occurred at different downstream distances at any given time. Spanwise rollers were shown to form with an undulating pattern and they presented irregularly located vortex dislocations. Furthermore, a ground-vortex induced during the early stages of the lower roller's generation in the unsteady wake was shown to lift-off the ground and merge with the von-Karman vortices to form a single vortical structure. Experimental and LES Strouhal number values were in agreement, ranging between 0.30 and 0.32, while the computed drag coefficient values were lower than those typical for unbounded cylinder flows, and a positive uplift force was present on the cylinder. All these effects are a result of the proximity of the cylinder to a solid boundary.

4.1 Introduction

The wake structure around a vertically orientated cylinder has been the subject of research for more than a century due to the abundance of curved bodies in nature as well as in civil, mechanical and aeronautical engineering. Recent research efforts have also focused on the flow structure in the wake of a horizontal-orientated cylinder (Nishino et al. 2007; Oner et al. 2008). The dependency of the wake dynamics on the Reynolds number has been studied extensively for vertical cylinders and to a lesser extent for horizontal cylinders. This knowledge is critical to our understanding of how the dynamic forces imposed by the fluid on the body change as a function of flow regime and fluid viscosity, as pertaining to fluid-body interactions.

Flow around a horizontal cylinder can exhibit different behaviour compared to a vertical cylinder as the latter can be embedded in different flow conditions, such as in boundary layer flows (Takafumi Nishino et al., 2007), or subject to the influence of its proximity to the ground (Oner et al., 2008). Nonetheless, the flow features developed around the cylinder are still governed by the Reynolds numbers irrespective of its orientation. Through laboratory experimental and numerical

simulations, it has been observed that the shear layers separating from the cylinder's sides become unstable at Reynolds number ($Re = UD/\nu$) around 1,200 (Prasad & Williamson, 1996). Several studies focusing on the sub-critical flow regime ($3*10^2 < Re < 1*10^5$) have highlighted the higher shedding frequency of the shear layer (*SL*) generated vortices (f_{SL}) compared to that of the large-scale von Karman-type (*VK*) vortices (f_K) where the frequency of *VK* vortices occur at a factor of 6.7 to 8.0 times greater than the *SL* ones, although this ratio of f_{SL}/f_K can also depend on the Reynolds number (Unal and Rockwell 1984; Chyu et al. 1995; Prasad and Williamson 1996; Lehmkuhl et al. 2013; Aljure et al. 2017). A transition in the sub-critical wake dynamics occurs at a Reynolds number of around 5,000 to 5,500 where a distinct change in the shedding typology has been observed in both experimental and numerical studies (Norberg 1994; Prasad and Williamson 1996; Aljure et al. 2017). This transition is distinguished by the presence of undulations in the vortex filaments shedding across the cylinder span and the occurrence of vortex dislocations (Norberg 1994; Aljure et al. 2017) which also lead to a change in parallel to oblique vortex shedding (Prasad and Williamson 1996). With increasing Reynolds number greater than 5000 the wake typology remains unchanged up to a Reynolds number of $2*10^5$ which marks the beginning of the supercritical flow regime where there is a significant change in the flow separation that reduces the drag coefficient from values ranging from 1.0 to 1.4 to between 0.2 to 0.4 (Roshko 1961; Lehmkuhl et al. 2014). A detailed summary of the wake dynamics dependency on Reynolds number is given in Williamson (1996) and Sumner (2013).

A cylindrical body is often in the close proximity of a solid boundary, for example, a pipeline or a large woody structure across an erodible river or sea bed, a bridge-pier close to an abutment or a mast located close to a building. Only a few studies have examined the close proximity of a solid boundary on a horizontal cylinder wake's flow structure (Bearman and Zdravkovich 1978; Price et al. 2002; Nishino et al. 2007;

Oner et al. 2008; Kirkgoz et al. 2009; Sarkar and Sarkar 2010). In this configuration, the ratio of the horizontal cylinder diameter (D) and the vertical gap between the bed and the cylinder (G), referred to hereafter as the gap ratio (G/D), is highly influential on the vortex dynamics developed downstream. For small gap ratios, e.g. $G/D \leq 0.5$, the wake is asymmetric as a result of the difference in acceleration of the flow over and under the cylinder, and the interaction of the under flow with the wall boundary layer. As the gap ratio decreases the ground-effect increases, which causes the separation point on the upper cylinder wall to move upstream while the separation point on the lower cylinder wall moves downstream (Sarkar and Sarkar 2010). Furthermore, the frontal stagnation point moves towards the bed and an uplift force which increases with decreasing G/D ratio is generated on the cylinder (Roshko et al. 1975; Choi and Lee 2000; Nishino et al. 2007) while the lower vortex is drawn upwards into the water column immediately behind the cylinder (Oner et al. 2008; Sarkar and Sarkar 2010). This leads to a separation bubble forming close to the bed immediately downstream of the wake bubble, which rapidly reduces in vertical and longitudinal extent with increasing gap ratio (Sarkar and Sarkar 2010). At smaller gap ratios (G/D =0.25) and relatively low Reynolds numbers, a bubble can also be formed at the wall immediately upstream of the cylinder which rapidly reduces in extent with increasing G/D ratio (Sarkar and Sarkar 2010). As the gap ratio (G/D) approaches unity, the ground-effect vanishes causing the flow separation on the upper and lower cylinder walls to occur at a similar longitudinal position and the upper and lower vortices to become more aligned, with the recirculation bubble tending towards symmetry (Oner et al. 2008; Sarkar and Sarkar 2010).

The proximity of the wall alters the hydrodynamic forces on the horizontal cylinder and the von Karman-type vortex shedding frequency depends on both the thickness of the boundary layer and the gap ratio (Zdravkovich 1985; Lei et al. 1999). The uplift force on the cylinder is accompanied by a reduction in the drag coefficient which

decreases with decreasing gap ratio (Choi and Lee 2000). The proximity of the wall also alters the dominant vortex shedding frequency, resulting in complex vortex-boundary interactions. At lower Reynolds numbers ($1.2*10^3 < Re < 1.44*10^3$) and gap ratios ($G/D < 0.5$), two distinct peaks observed in the power spectra of the root mean square (rms) streamwise velocity have been attributed to the difference in motion between the upper and lower vortices shed from the upper and lower cylinder sides respectively, resulting in vortex-boundary interactions different from the unbounded cylinder condition (Price et al. 2002; Sarkar and Sarkar 2010). Indeed, for smaller gap ratios, the rms of the fluctuating lift coefficient is significantly lower for higher *G/D* ratios as a consequence of the suppression of the VK vortex shedding at the smaller *G/D* ratios (Sarkar and Sarkar 2010). The higher values of Strouhal number reported in these studies than those from unbounded cylinder flow are therefore a result of the different development of the vortex shedding and shear layers instability. With increasing gap ratio, the two peaks in the shedding frequency merge into one single dominant peak (Sarkar and Sarkar 2010) and periodic symmetric vortex shedding occurs. Hence, at a critical gap ratio in the range of $0.5 \leq G/D \leq 1.0$, the Strouhal number becomes independent of the gap ratio, approaching a value of around 0.2 commonly found in cylinder flows unaffected by boundary effects (Angrilli et al. 1982; Taniguchi and Miyakoshi 1990; Choi and Lee 2000; Price et al. 2002; Sarkar and Sarkar 2010).

Additionally, at higher Reynolds numbers ($4*10^4 < Re < 10^5$) a small gap ratio can not only suppress *VK* vortex shedding but completely stop it (Takafumi Nishino et al., 2007). For a cylinder with aspect ratio (*L/D*) 8.33, the VK vortex shedding becomes intermittent at a gap ratio of 0.4 before completely ceasing at a gap ratio of 0.3. At this lower gap ratio, a larger recirculation zone is bounded by two nearly parallel shear layers from the cylinder sides, with no *VK* vortices observed and only small-scale vortices generated from shear layers. The change in wake dynamics at

G/D = 0.3 is reflected in the drag coefficient reduction, which reaches a minimum at this gap ratio, and remains constant with decreasing *G/D* ratio (Takafumi Nishino et al., 2007).

Irrespective of the experimental measurement technique and numerical model, it is commonly agreed that the accurate measurement and prediction of the time-averaged high-order flow statistics in the near wake is highly challenging (Nishino et al. 2008; Lehmkuhl et al. 2013; Sumner 2013). It has been postulated that there are different modes of low-frequency meandering of the near wake that may be responsible for the large scattering of flow statistics (Lehmkuhl et al., 2013), which need to be resolved together with the high-frequency turbulence in the flow. Therefore, emphasis has been placed on the need to perform direct numerical simulations (DNS) or large-eddy simulations (LES) capable of resolving these flow characteristics conducted over a large number of shedding cycles in order to capture all the high- and low-frequency periodic motions. Numerical studies using LES and DNS have identified the wake's three-dimensionality by using different spanwise-length domains to capture the wavelength of the vortical structures across the cylinder span. For Reynolds numbers $\leq$ 5,000 a spanwise length of $2\pi D$ accurately captures the flow behaviour including the dynamic forces on the cylinder (Aljure et al., 2017) whereas a πD spanwise length only captures the turbulence structures in the shear layer region (Breuer 1998; Ma et al. 2000; Lehmkuhl et al. 2013).

There are few experimental and numerical test cases that have investigated a horizontal cylinder wake in the close proximity of a bed boundary at moderate Reynolds numbers. The present study combines an experimental study with high-fidelity Large-Eddy Simulations (LES) in order to further elucidate the near wake flow structure of a horizontal cylinder with wall proximity effects. A fixed vertical gap to diameter ratio (*G/D*) of 0.5 is chosen for Reynolds numbers (*Re*) equal to 6,666, 10,000 and 13,333. To the best of our knowledge, this specific vertical gap

cylinder to diameter ratio has not yet been investigated for Reynolds numbers higher than the threshold (Re = 5,000) at which there is a distinct shift in the vortex shedding dynamics found in cylinder flows unaffected by boundary effects.

4.2 Experimental set-up and data processing

The experiments were conducted in a recirculating flume with glass sidewalls in the hydraulics laboratory at Cardiff University, United Kingdom. The flume had a rectangular cross-section, and was 10 m long, 0.3 m wide and 0.3 m deep. A horizontal cylinder of diameter (D) 0.05m and length 0.3 m was fixed 3.85 m downstream from the upstream inlet. The vertical gap (G) between the flume bed and the cylinder wall was 0.025 m giving a G/D ratio of 0.5. The flow structure in the cylinder wake was examined for three different flow discharges (Q) of 6, 9 and 12 Ls^{-1}, which equated to cross-sectional bulk velocities of U_0 = 0.133, 0.200 and 0.266 ms^{-1} respectively. The mean flow depth (H) along the flume centreline remained fixed at 0.15 m for each flow condition and this was achieved by adjusting the downstream tailgate weir. The bed slope of the flume remained fixed at 1:1000. Table 4.1 presents details of the Reynolds numbers ($Re = U_0D/\nu$) and Froude number ($Fr = U_0(gH)^{-0.5}$, where g is the gravity acceleration) for the different flow conditions studied. The local flow depth (H_L) was measured in streamwise increments of 5 cm to characterise the effects of the cylinder and shallowness of the flow, on the surface water profile.

Velocity measurements were collected using a Nortek 10 MHz Vectrino Plus Acoustic Doppler Velocimeter (ADV) at a sampling rate of 200 Hz and 300 s sampling time. The cylindrical sampling volume (6 mm diameter and 7 mm height) was located at 50 mm from the probe transmitter. Thresholds of sound-to-noise ratio (SNR) and correlation (COR) >20 dB and >70%, respectively, were maintained by seeding the water with silicate powder (10 μm average diameter and 1.1 Kgm^{-3} density) and used for filtering the velocity time series. Despiking of time series used

the Phase-Space Thresholding (PST) method by Goring and Nikora (2002) as well as a 12-Point polynomial (12PP) (Jesson et al., 2013). Furthermore, by examining the velocity variances, data points identified as weak spots, which are errors resulting from acoustic pulse-to-pulse interference (Cea, Puertas, & Pena, 2007) were removed from the dataset.

Table 4.1. Details of the flow conditions studied: flow discharge (Q), Reynolds number (Re), bulk velocity (U_0), Froude number (Fr) and estimated friction velocity (u_*).

Q [ls^{-1}]	Re [-]	U_0 [ms^{-1}]	Fr [-]	u_* [ms^{-1}]
6	6,666	0.1333	0.110	0.020
9	10,000	0.2000	0.165	0.027
12	13,333	0.2667	0.220	0.033

An ADV measurement grid resolution of 0.005 m and 0.02 m was used in the vertical (z) and streamwise (x) directions, respectively in the cylinder wake. The velocity structure in the wake was measured along the channel centreline over a downstream distance of 0.3 m. In the following, the symbols <·> indicates time-averaging operation.

Flow visualisation of the cylinder wake dynamics used tracers composed of 2% Cetyltrimethylammonium salicylate (C_{16}TASal) and 0.5% Polyethylene oxide ($C_{2n}H_{4n+2}O_{n+1}$) solutions in water mixed with white emulsion paint colouring, following methods of Hoyt and Sellin (2000). Methylene blue standard stain (C.I.52015) was added to the tracer solution for contrast.

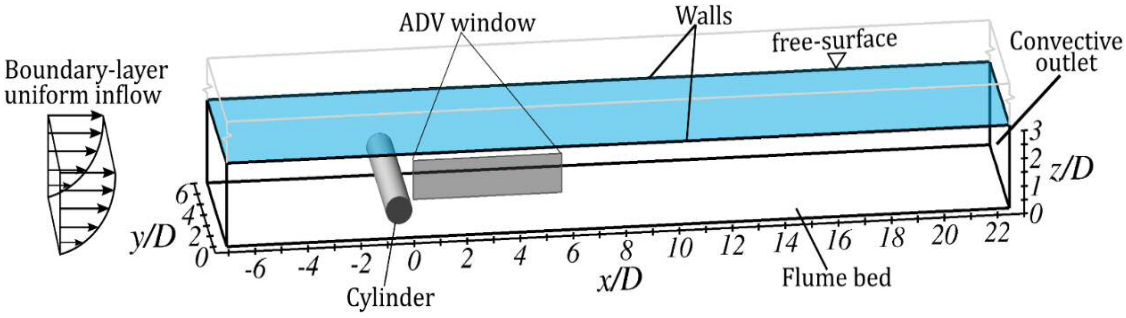

Figure 4.1. Schematic of the computational domain with the imposed boundary conditions showing location of horizontal cylinder and laboratory measurement control volume.

4.2.1 Approach flow conditions

At a longitudinal distance of three diameters (*3D*) upstream of the cylinder, vertical velocity profiles (z-direction) were measured as well as the lateral velocity distribution (y-direction) at the mid-flow depth (*0.5H*) to capture the upstream flow boundary conditions. Figure 4.2 presents a comparison of the measured approach flow profiles for the three discharges. The friction velocity (u_*) was obtained from the best-fit of the velocity measurements to a log-law (Figure 4.2b) that were measured for five flow conditions which included the three flow conditions modelled in this chapter (i.e. Re = 6,666, 10,000 and 13,333). Figure 4.2a shows that the friction velocity increased linearly with the bulk velocity and thus the velocity profile approaching the cylinder can be defined according to a log-law distribution as,

$$u(z)/u_* = \kappa^{-1} \ln(z\, u_*/\nu) \qquad \text{with} \qquad u_* = 0.1036\, U_0 + 0.00568 \qquad (4.1)$$

Here κ is the von-Karman constant equal to 0.41, z is the vertical coordinate considered and ν is the kinematic viscosity. Levels of streamwise velocity fluctuations were similar for all discharges, being largest close to the flume's bed and

decreased with increasing elevation (Figure 4.2c). The depth-averaged turbulence intensity, $\langle u' \rangle / U_0$, was found to be around 10% for all cases. Figure 4.2d shows that values of the cross-correlation of streamwise and vertical velocity fluctuations were largest for the lowest Reynolds number (Re = 6,666) while similar magnitudes were found for the Re = 10,000 and 13,333. Velocities measurements in the transverse direction showed a negligible variation in streamwise velocities, therefore the flow was assumed uniform across the flume width.

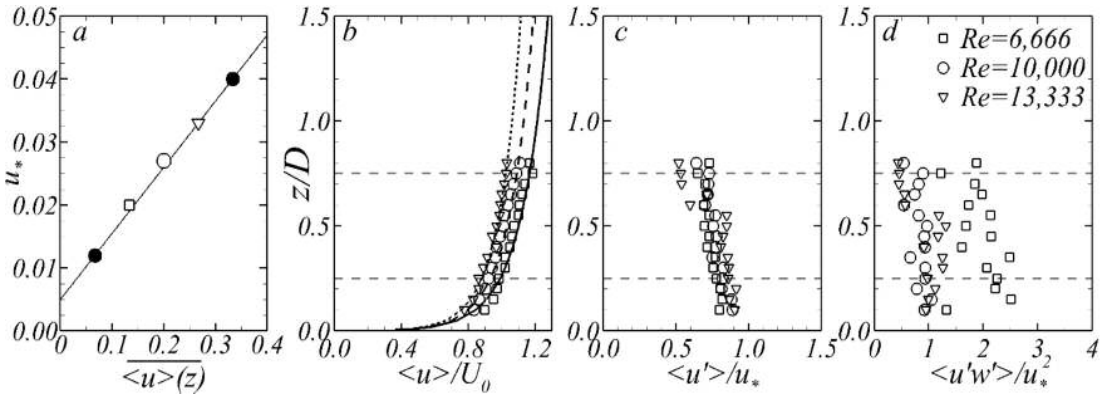

Figure 4.2. Approaching profiles experimentally measured at a distance of 3D upstream of the cylinder where (a) is the depth-averaged streamwise velocity against shear velocity derived from the velocity logarithmic profile fit for five flow conditions ranging from 3,333< Re < 16,666, (b) time-averaged streamwise velocity normalised by the bulk velocity, (c) streamwise velocity fluctuation normalised by shear velocity, and (d) vertical Reynolds shear stress normalised by the shear velocity squared for the three Reynolds number modelled in this study.

4.3 Computational background and setup

4.3.1 Numerical framework

Eddy-resolving simulations are accomplished using the in-house code Hydro3D which has been well-validated in hydro-environmental flows (Stoesser 2010;

Bomminayuni and Stoesser 2011; Kim et al. 2013; Kara et al. 2015; Ouro et al. 2017; McSherry et al. 2018). Hydro3D adopts the Large-Eddy Simulation (LES) approach to explicitly resolve the energy-containing flow structures while modelling the scales smaller than the grid size using a sub-grid scale model. The governing equations are the spatially filtered Navier-Stokes equations for incompressible, viscous flow that are solved in a Eulerian coordinate system and are as follows:

(4.2)

(4.3)

Here, $u_i = (u,v,w)$ and $x_i = (x,y,z)$ are the filtered fluid velocity and position in the three coordinates of space respectively, p denotes filtered pressure, v is the fluid kinematic viscosity, ρ is the fluid density, and τ_{ij} is the sub-grid scale stresses. The sub-grid scale stress tensor is approximated using the WALE subgrid scale model (Nicoud & Ducros, 1999) considering a filter size equal to the grid size. The forcing term f_i represents external forces calculated using the direct forcing Immersed Boundary (IB) method (Uhlmann, 2005), here used to represent the cylinder geometry (Ouro & Stoesser, 2017).

In Hydro3D the fluxes are calculated using a second-order central differencing scheme with staggered storage of the velocity components on a rectangular Cartesian grid. The fractional-step method is used with a three-step Runge-Kutta predictor to approximate convective and diffusive terms, and an efficient multi-grid technique is adopted to solve a Poisson pressure-correction equation as a corrector at the final step. Hydro3D uses the domain decomposition technique to divide the computational domain into rectangular sub-domains and is parallelised with Message Passing Interface (MPI) (Ouro, Fraga, Lopez-Novoa, & Stoesser, 2019). It also features a

local mesh refinement method (Cevheri et al. 2016) that permits a higher spatial grid resolution near the cylinder and a coarser grid resolution with increasing distance away from the cylinder, thus reducing the computational expense of large eddy simulation.

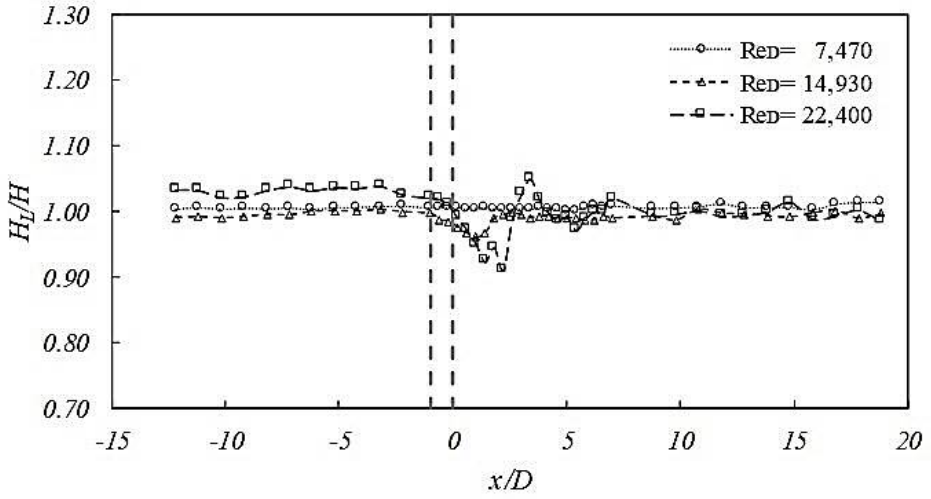

Figure 4.3. Experimental longitudinal surface water profile as a function of the Reynolds number. The vertical dotted lines denote the cylinder edges, H is the streamwise-averaged flow depth and H_L is the local flow depth.

Due to the presence of the cylinder and flow shallowness, surface standing waves were generated immediately downstream of the cylinder and were contained within a region of longitudinal distance 6D, throughout the test section (Figure 1.1), while the upstream flow depth remained constant and was only slightly elevated at higher Reynolds numbers (see Figure 4.2). The presence of surface waves resulted in a non-hydrostatic pressure field in the test section.

4.3.2 Computational setup

The computational domain presented in Figure 4.1 comprises 30*D* in the streamwise direction, 6*D* in the cross-streamwise direction and 3*D* in the vertical direction, therefore replicating the full flume width and the uniform flow depth used the experiments. Note the spanwise domain length (6*D*) is very close to the proposed length of $2\pi D$ required to fully capture the spanwise wavelength of the vortical structures in the cylinder wake (Aljure et al., 2017). The downstream end of the cylinder is located 7*D* from the upstream inlet and considered as the origin of the x-coordinates. The same grid resolution is adopted for the two lower Reynolds numbers (*Re* = 6,666 and 10,000) whilst the resolution is doubled for the highest Reynolds number case (*Re* = 13,333). Table 4.2 details the mesh resolution (Δz) for three flow conditions examined, grid resolution of the first cell off the wall in wall-units (Δz^+) and millions of fluid cells comprising the entire computational domain.

Table 4.2. Specification of the computational grid resolution used and total number of fluid cells for each of the cases analysed.

Re [-]	U_0 [ms^{-1}]	Δz [m]	Δz^+ [-]	Cells
6,666	0.1333	$6.250 \cdot 10^{-4}$	6.25	$14.32 \cdot 10^6$
10,000	0.2000	$6.250 \cdot 10^{-4}$	8.44	$14.32 \cdot 10^6$
13,333	0.2667	$3.215 \cdot 10^{-4}$	5.16	$82.94 \cdot 10^6$

The log-law velocity profile (Eq. 4.3) is prescribed at the inlet of the domain and adjusted for each of the examined flow discharges. A convective condition is used at the outlet and no-slip conditions were imposed at the bottom and lateral walls, which is justified from the values of $\Delta z+$ indicating that the first point off the wall is within

the viscous sub-layer. A shear-free rigid-lid condition is employed for representing the water surface as the influence of free-surface effects is considered small when the maximum *Fr* is relatively low (0.22).

The simulations are initially run until flow transients have vanished. First order statistics are then collected for a total simulation time in terms of non-dimensional time $t^* = tD/U_0$ of 260 equating to 32 eddy turn-over time ($t_e = H/u_*$). Second-order statistics are collected after t^*= 60 for a total of 200*D/U* representing approximately 170 shedding cycles. A Courant-Friedrichs-Lewy (CFL) condition of 0.7 was set to ensure numerical stability. The computations are performed on 170 Intel Skylake Gold 6148 @2.40GHz cores using Supercomputing Wales facilities with a total computational load of 225,000 CPU hours for the highest Reynolds number case (*Re* =13,333).

4.4 Results and discussion

4.4.1 Time-averaged nature of the flow

Results of the time-averaged flow developed around the cylinder for the *Re* = 6,666 case are shown in Figure 4.3 along the channel centreline plane i.e. *y/D* = 3. The distribution of streamwise velocities evidences how the approaching flow impinges the cylinder and accelerates over and beneath it, as depicted from Figure 4.3a. Flow streamlines indicate that the recirculation area immediately behind the cylinder is mostly symmetric and extends until approximately 1*D* downstream. After *x/D* = 1, the streamwise velocities significantly diminish outside of the wake bubble on the lower side of the wake, i.e. *z/D* <0.5, compared to the high-momentum region located above the wake (*z/D* = 1.5). Figure 4.3b presents the contours of time-averaged vertical velocities showing the asymmetry in the flow influenced upstream by the logarithmic distribution of the approaching flow and downstream by the closer

proximity of the cylinder to the channel bottom than free-surface layer. The area of high vertical velocities in the lower part of the near-wake is a result of the bed-effect as the fluid accelerates through the vertical gap between the cylinder and flume bed.

The lack of a more pronounced asymmetry in the recirculation bubble despite the small gap ratio (*G/D*) is somewhat expected as the present ratio *G/D* of 0.5 corresponds to the intermediate region in which the influence of the ground-effect in the time-averaged flow field is deemed small (Nishino et al. 2007; Oner et al. 2008). This can be observed from the streamlines in Figure 4.3a which show the lower half of the wake extending over the wake centreline, i.e. $z/D > 1$, until a distance $x/D = 5$, whilst in the upper layer near the free-surface layer the streamlines are nearly parallel. This asymmetric flow pattern is further supported by the distribution of the vertical velocities whose magnitude becomes notably reduced after $x/D = 1.5$. It is worth noting that no wall boundary layer separation upstream of the cylinder occurs, as the Reynolds numbers of the present flow conditions are well above the threshold of $Re = 1{,}400$ at which such separation vanishes (Price et al., 2002).

The examined cases are for Reynolds numbers within the sub-critical cylinder flow regime in which the shear layers are laminar whilst the wake is fully turbulent. Levels of computed streamwise turbulence intensity (Figure 4.3c) are larger than $\langle u' \rangle / U_0 = 0.6$ indicating that the near-wake is remarkably unsteady. There is also an uneven distribution of $\langle u' \rangle$ along the centreline of the cylinder wake ($z/D = 1$) with the turbulent region below this elevation extending almost twice the length than in the region higher up in the wake. Interaction between the cylinder-induced near-wake and the ground can be appreciated from the distribution of high $\langle u' \rangle$ values near the bed between $0 < x/D < 2$ reaching values up to 0.65.

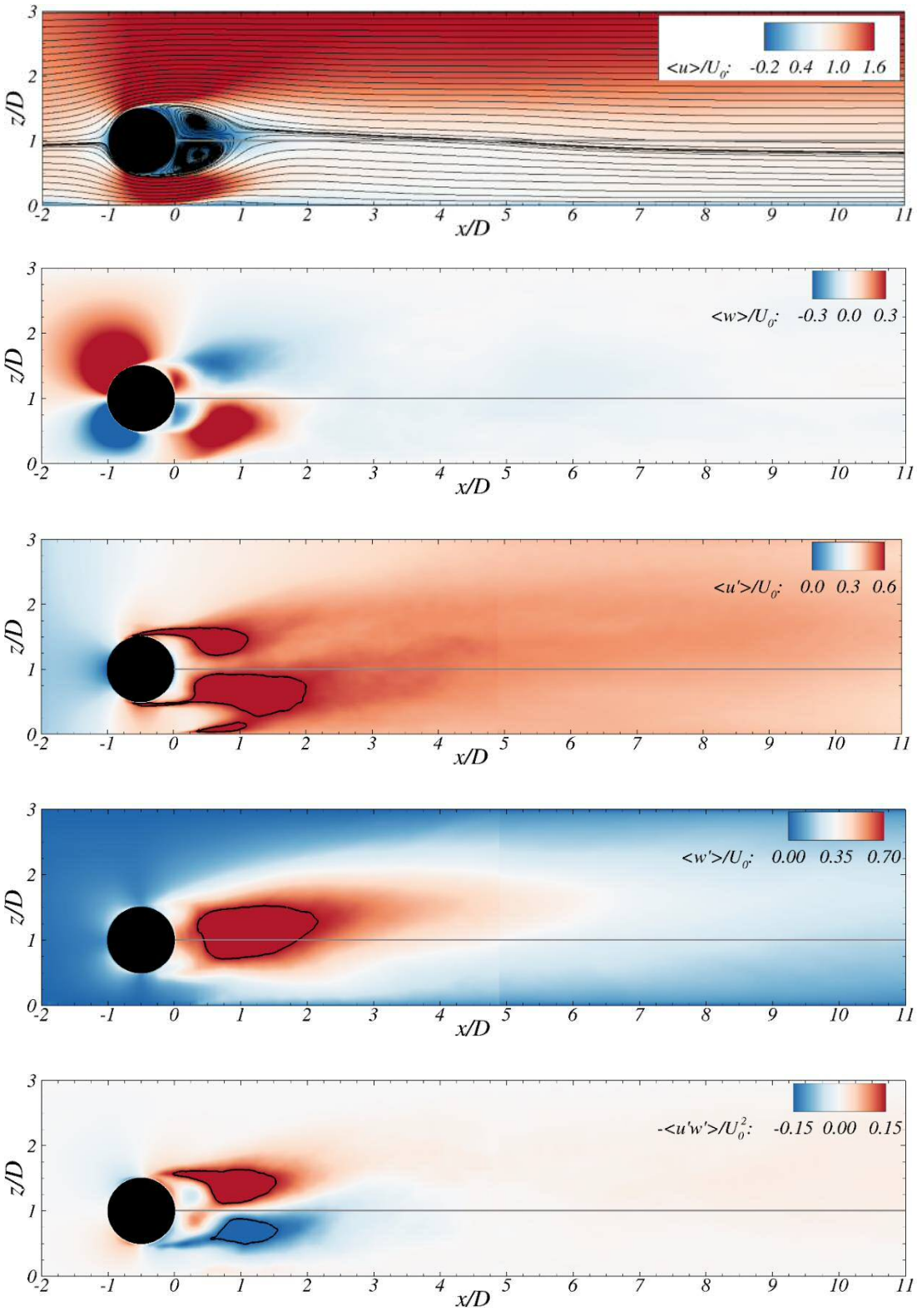

Figure 4.4. Side elevation contour plots of the computed (a) streamwise velocity, (b) vertical velocity, (c) streamwise turbulence intensity with lines denoting $<u'>/U_0 =$ 0.6, (d) vertical turbulence intensity with lines denoting $<w'>/U_0 =$ 0.7, and (e)

Reynolds shear stress with the solid lines corresponding to $\langle u'w' \rangle$ = +- 0.1, normalised by the bulk velocity for the Re = 6,666 case.

The asymmetry of the turbulent wake in the downstream direction is again depicted in the distribution of $\langle w' \rangle$ presented in Figure 4.3d with a well-defined area of $\langle w' \rangle / U_0 > 0.7$ found between $0.4 < x/D < 2.2$. Interestingly a larger portion of this high vertical turbulence intensity region is located above the cylinder centreline, z/D = 1, whilst predominantly below the centreline for the streamwise turbulence intensity (Figure 4.3c). This evidences that the ground-effect significantly affects the unsteady nature of the near-wake by changing the dynamics of the vortex generation and shedding which, in consequence, leads to an asymmetric wake distribution. A similar pattern is found in the distribution of vertical Reynolds shear stress ($\langle u'w' \rangle$); where higher Reynolds shear stresses values above z/D = 1 result from the higher momentum exchange between the flow overtopping the cylinder with the near wake than that with the flow going under the cylinder. Overall, the time-averaged second order statistics ($\langle u' \rangle$, $\langle w' \rangle$, $\langle u'w' \rangle$) indicate that the wake until x/D = 2 is very turbulent followed by a region between $2 < x/D < 5$ over which turbulence decays and is distributed uniformly over the water depth, as the wake expands over the entire water column.

Figure 4.4 presents the vertical profiles of $\langle u \rangle$ and $\langle u' \rangle$ at nine locations downstream of the cylinder obtained from the experiments and the LES for the cases of Re = 10,000 and 13,333. At the locations closest to the cylinder, i.e. $x/D < 1.2$, there is a significant velocity deficit behind the cylinder. LES captures well the distribution of $\langle u \rangle$ and $\langle u' \rangle$ over the water depth. The slight vertical offset of the computed wake is attributed to the fact LES treats the free-surface as a shear-free rigid lid whilst water surface waviness was present in the experiments, particularly immediately after the cylinder. Further downstream, the streamwise velocity tends to recover and approach

the unperturbed log-law profile found upstream of the cylinder. Until a distance of $x/D \approx 3$, the profiles of $\langle u' \rangle$ feature one peak over the cylinder top (i.e. $z/D > 1.5$) and another that is larger in magnitude at $z/D \approx 0.5$. Such asymmetrical distribution of $\langle u' \rangle$ evidences the ground-effect in the von-Karman street as also observed in Figure 4.3c. A more uniform distribution along the water column is found after $x/D = 3$ indicating that the shed vortices have merged as explained later in Section 4.4.3.

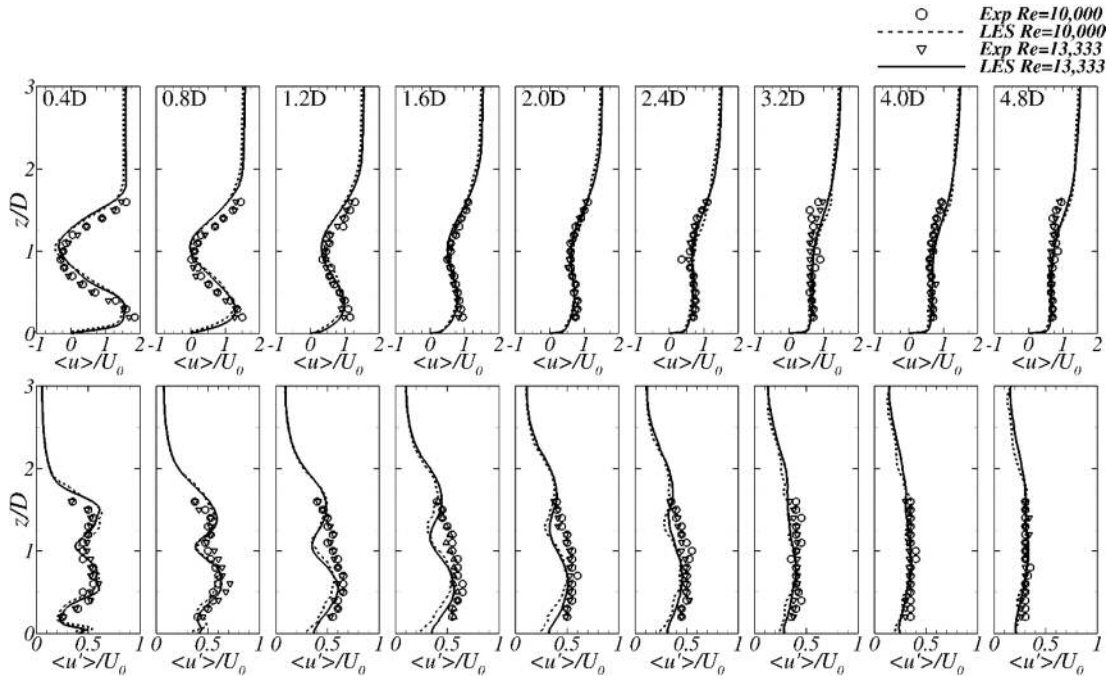

Figure 4.5. Vertical profiles of mean streamwise velocity $\langle u \rangle$ (top) and turbulence intensity $\langle u' \rangle$ (bottom) at different locations downstream of the cylinder for the Re = 10,000 and 13,333 cases. Comparison between experimental (symbols) and LES (lines) results.

The vertical distribution of mean vertical velocity ($\langle w \rangle$) and turbulence intensity ($\langle w' \rangle$) from the experiments and LES is shown in Figure 4.5 for the Re = 10,000 and 13,333 cases. Profiles immediately behind the cylinder show a marked upwards fluid motion below the cylinder centreline resulting from the flow acceleration through the

bed-cylinder gap. Vertical turbulence intensity profiles show that near the bluff body the maxima are attained along the cylinder centreline however further downstream the peak of $\langle w' \rangle$ shifts towards the free-surface as a result of the von-Karman vortices moving to the region of highest momentum. LES overpredicts the values of $\langle w \rangle$ close to the bed immediately behind the cylinder while there is a good match with the experimental results above the cylinder centreline (z/D = 1.0). A similar pattern is found for $\langle w' \rangle$ in the near-wake, although LES achieves an excellent match with experimental results immediately behind the wake bubble (x/D > 1.2). Overall, the normalised distribution of these mean quantities follows a very close distribution for the three cases.

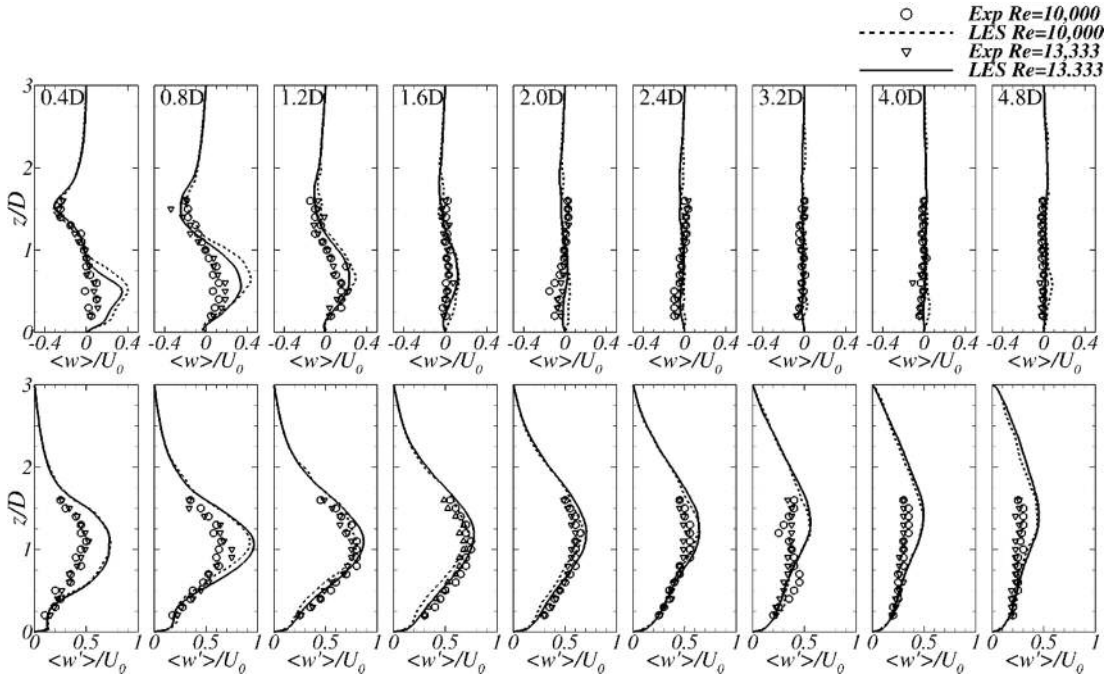

Figure 4.6. Vertical profiles of mean vertical velocity $\langle w \rangle$ (top) and turbulence intensity $\langle w' \rangle$ (bottom) at different locations downstream of the cylinder for the *Re* = 10,000 and 13,333 cases. Comparison between experimental (symboles) and LES (lines) results.

4.4.2 Recirculation region

Further insights into the asymmetric wake enclosed behind the cylinder for the different flow rates studied are given in Figure 4.6. The flow streamlines indicate that in all cases the two recirculating cells are not symmetrically distributed about the cylinder centreline and are slightly shifted towards the free-surface. This shift is more pronounced with increasing Reynolds number. The recirculation length (L_{rec}/D) shortens with increasing Reynolds number as presented in Table 4.3, and its values are similar to those reported for unconfined cylinder flows (Lehmkuhl et al. 2013; Aljure et al. 2017). Flow streamlines allow the precise location at which the boundary layers separate on both upper and lower halves of the cylinder. Both separation points move upstream with increasing Reynolds number, as shown in previous studies (Oner et al., 2008), and coincide with the successive reduction of the separation angles at the upper (θ^{up}) and lower (θ^{low}) half of the cylinder, as presented in Table 4.3. From Figure 4.6 it is also observed that the locus of the upper cell is closer to the cylinder than the bottom cell as the fluid flows faster under the cylinder than over it, which is again reflected in values of θ^{low} being larger than θ^{up}. Interestingly, for the three flow conditions studied, two laminar separation bubbles appear enclosed between the lee-side of the cylinder and the recirculation cells.

Table 4.3. Characteristics of the recirculation area for the different cases analysed: normalised recirculation length (L_{rec}/D) and upper (θ^{up}) and lower (θ^{low}) separation angles.

Re	L_{rec}/D [-]	θ^{up} [º]	θ^{low} [º]
6,667	1.389	95.7	101.3
10,000	1.348	92.9	97.6
13,333	1.233	86.6	95.7

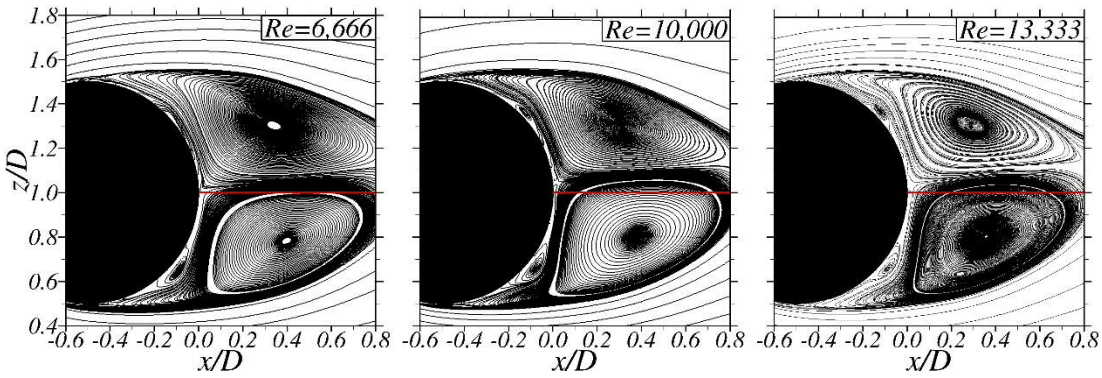

Figure 4.7. Mean recirculation region computed using LES. Red line indicates the cylinder centreline at z/D = 1.0.

4.4.3 Centreline profiles

The distribution of the mean flow field along the cylinder centreline (z/D = 1) with increasing downstream distance from the cylinder is shown in Figure 4.7 with longitudinal profiles of mean streamwise and vertical velocities, and turbulence intensities from both the experiments and LES. Figure 4.7a shows the velocity reversal in the attached recirculation area with a peak reversal of -0.4U_0. The recirculation area ends by 1D downstream of the cylinder as indicated by the positive streamwise velocity. For all cases analysed, the streamwise momentum has nearly recovered (i.e. $<u>/U_0 \approx 0.8$) by a downstream distance of 3D, and there is a good agreement between measured data and LES. Figure 4.7b shows that there is a similar trend in the evolution of $<u'>$ for cases of Re = 6,666 and 10,000, with experiments and LES data almost coinciding to a value close to $<u'> = 0.4U_0$ at a downstream distance of 3D, after which the streamwise turbulence intensities progressively decay with increasing downstream distance. However, in the near-wake the computed streamwise turbulence intensities are lower than the experiments, attributed to the lack of resolving the free-surface which may lead to a slight change in the vortex generation dynamics.

Centreline plots for <*w*> from Figure 4.7c show that in the region between 1-2*D* immediately downstream of the wake bubble, i.e. where the large-scale vortices are shed, there is a peak in positive <*w*> denoting predominant upwards fluid motion. The ground-effect is responsible for suppressing the symmetry in the vortex shedding mechanism compared to unbounded cylinder flows, which feature zero values of <*w*> along the cylinder centreline. By a downstream distance of 2*D*, the vertical velocities decrease and by 10*D* these are essentially zero for all three flow conditions. Regarding the distribution of vertical turbulence intensity (Figure 4.7d) the maxima are achieved at $x/D = 1$ for the LES and at $x/D = 1.5$ in the experiments, which are significantly larger than those found for the streamwise turbulence intensity. Close agreement between computed and measured results is observed by a downstream distance of 2D with <*w'*> attaining nearly $0.7U_0$ and progressively decaying until $0.2U_0$ further downstream.

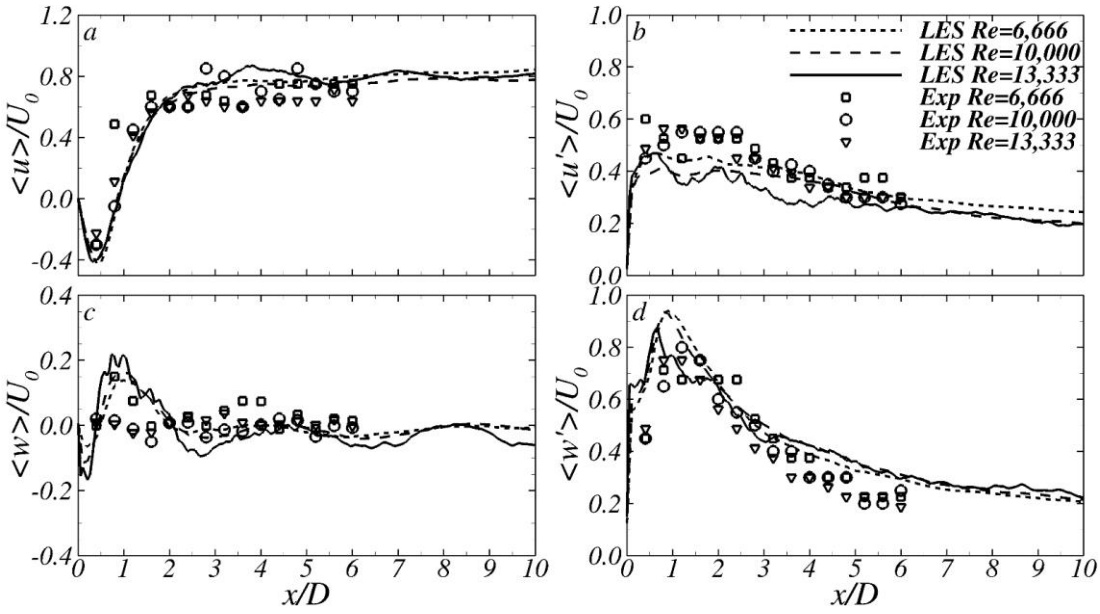

Figure 4.8. Centreline profiles of <*u*>, <*u'*>, <*w*> and <*w'*> from experiments and LES for the three Reynolds numbers.

4.4.4 Continuity equation terms analysis

The asymmetric near-wake recovery can be further characterised by considering the mean velocity terms in the continuity equation:

$$\overline{\qquad} \quad \overline{\qquad} \quad \overline{\qquad} \tag{4.4}$$

In an unbounded environment these terms should be symmetric to the cylinder centreline but are expected to change in the present case due to the proximity of the cylinder body to the flume bed. The term $\partial\langle v\rangle/\partial y$ is deemed much smaller than the other two as the main flow direction is in the XZ-plane. Figure 4.8 presents the contour plots of the terms $\partial\langle u\rangle/\partial x$ and $\partial\langle w\rangle/\partial z$ for the three flow cases examined. The regions of highest rate-of-change of $\langle u\rangle$ in the streamwise direction are found in the core of the near-wake between $0< x/D <2$ and $0.5< z/D <1.5$. These coincide with the regions of the largest negative rate-of-change of $\partial\langle w\rangle/\partial z$, as both terms need to balance in Eq. 4.4. A region of negative $\partial\langle u\rangle/\partial x$ develops over the upper shear layer until $x/D \approx 0.5$ indicating a decrease in x-velocities along the streamwise direction. In the gap between the flume's bed and cylinder such a region of $\partial\langle u\rangle/\partial x < 0$ extends until $x/D <1.5$ as a result of the wake dynamics affected by the close proximity to the ground. Upstream of the cylinder, an area of $\partial\langle u\rangle/\partial x >0$ is present as the approach flow accelerates. A reverse distribution is found for $\partial\langle w\rangle/\partial z$ in the near-wake of the cylinder. Both terms from the continuity equation show minor variations amongst the three flow discharges analysed.

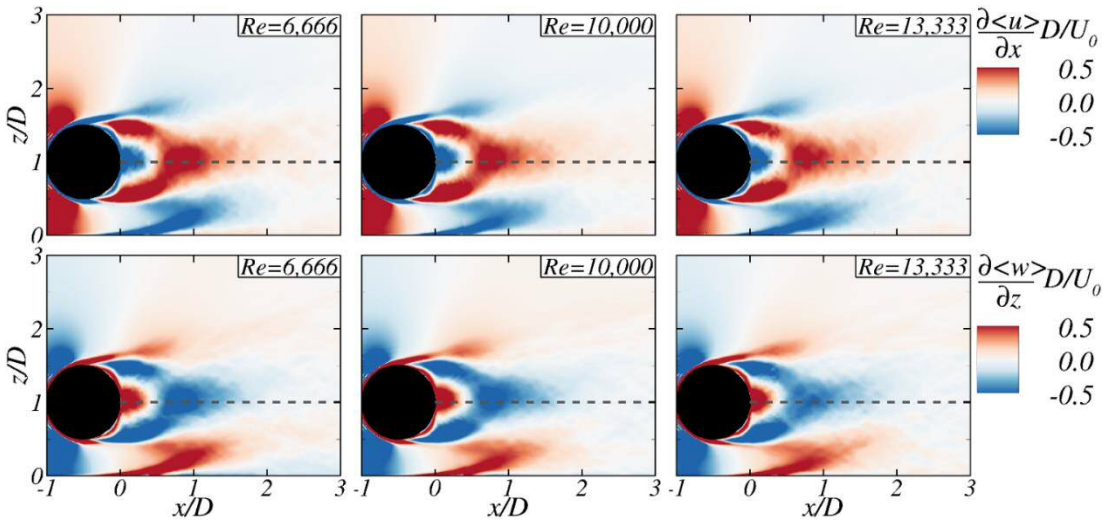

Figure 4.9. Continuity equation terms for the different Reynolds numbers.

4.4.5 Instantaneous flow structures

The three-dimensionality of the developed flow structures behind the cylinder are shown in Figure 4.9 with contours of y-vorticity at three different spanwise locations (y/D = 0.5, 3.0 and 5.0) for the case Re = 6,666, which shows the spanwise variation of the vortical structures. Laminar shear layers are developed along the cylinder surface and separate on the lee-side, becoming unstable due to the shear caused by the low-momentum near-wake and the fast-flowing fluid over the cylinder. Following a Kelvin-Helmholtz instability, the shear layers breakdown into small vortices that are convected downstream merging with the fully-turbulent near-wake between 0< x/D <1. Such flow separation is expected at these Reynolds numbers as they correspond to the sub-critical regime.

The laminar-to-turbulent transition and large-scale vortices generation are non-uniform across the entire spanwise length of the cylinder as observed from the spanwise-vorticity contours. The Kelvin-Helmholtz instability developed in the upper and lower shear layers is decoupled, i.e. at y/D = 0.5 the lower shear layer stays laminar until $x/D \approx 0.6$ whilst the upper one has transitioned shortly after its separation from the cylinder. Here only the Reynolds number 6,666 case is shown for

brevity. Nonetheless, similar instantaneous flow patterns in the near-wake are observed for all Reynolds numbers examined although there are some differences, e.g. more rapid breakdown of the shear layers with a higher Reynolds number, as indicated by the different separation angles show in Figure 4.6 and the values presented in Table 4.3.

In the region between $1< x/D <2$, the attached near-wake transitions to large-scale von-Kármán vortices, characteristic of the far-wake behind bluff bodies. Here the proximity of the cylinder to the flume bed leads to the generation of a ground-vortex (*GV*) as depicted in Figure 4.9. The *GV* originates from the low-pressure generated by the unsteady wake during the formation of the roller off the lower wall of the cylinder. This effect triggers the *GV* to lift-off the ground, constrain the formation of the lower roller while merging with the energetic structures as it is convected downstream to form a single vortical structure. This phenomenon is present for all three Reynolds numbers analysed although it is more pronounced for the highest Reynolds number case as the near-wake becomes more unstable closer to the cylinder, thus leaving more space for the *GV* to develop.

This ground-effect phenomenon has previously been observed in experimental studies (Choi and Lee 2000; Price et al. 2002; Oner et al. 2008; Nishino et al. 2007) and motivated computational analyses using Reynolds Averaged Navier-Stokes (RANS) (Kirkgoz et al., 2009), Detached-Eddy Simulation (DES) (T. Nishino et al., 2008) and LES (Sarkar & Sarkar, 2010). The present gap-to-diameter ratio (*G/D*) setup of 0.5 corresponds to the intermediate gap regime which relates the influence of the ground-effect on the cylinder's near-wake structure, and more specifically regulates whether large-scale von-Kármán vortices are shed or not (Oner et al. 2008; Nishino et al. 2007). For $G/D = 0.5$, the ground influence is relatively small allowing the large-scale vortices to be shed but their active interaction with each other (Figure 4.10) is in contrast to unbounded cylinder flows.

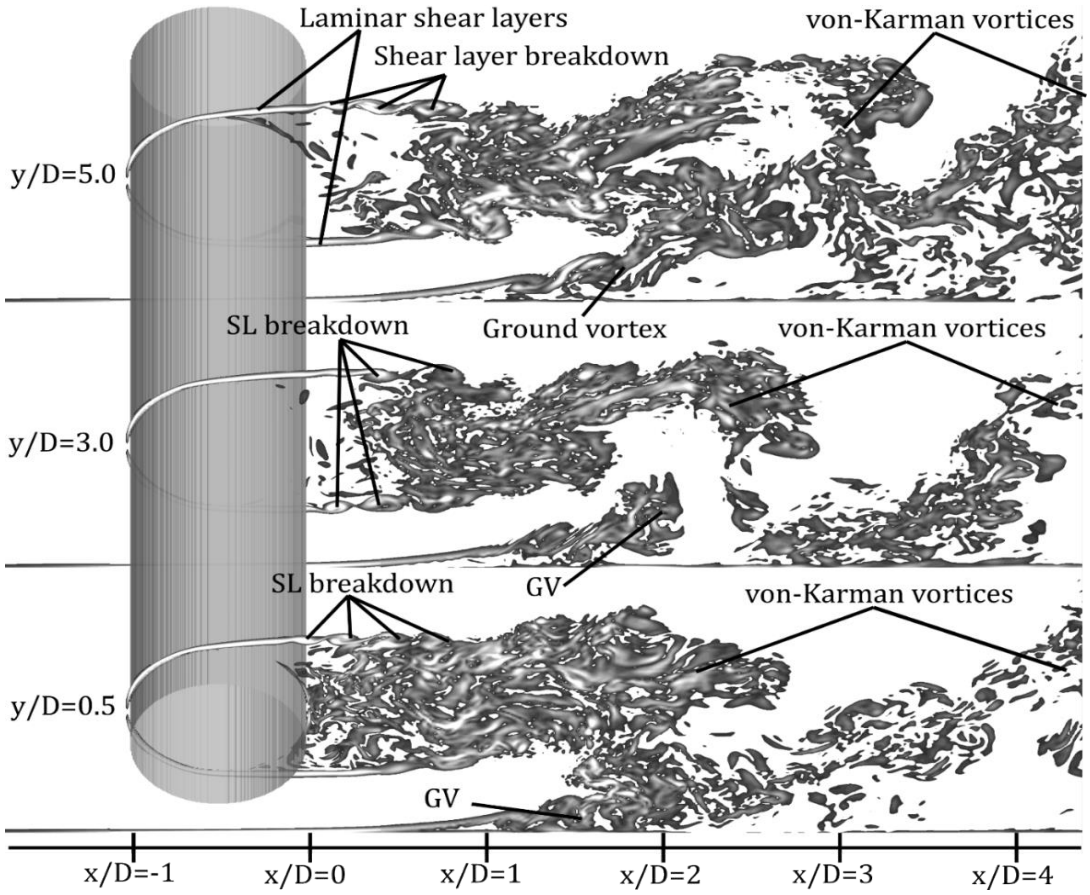

Figure 4.10. Contours of spanwise vorticity at different spanwise locations across the cylinder for the *Re* = 6,666 case.

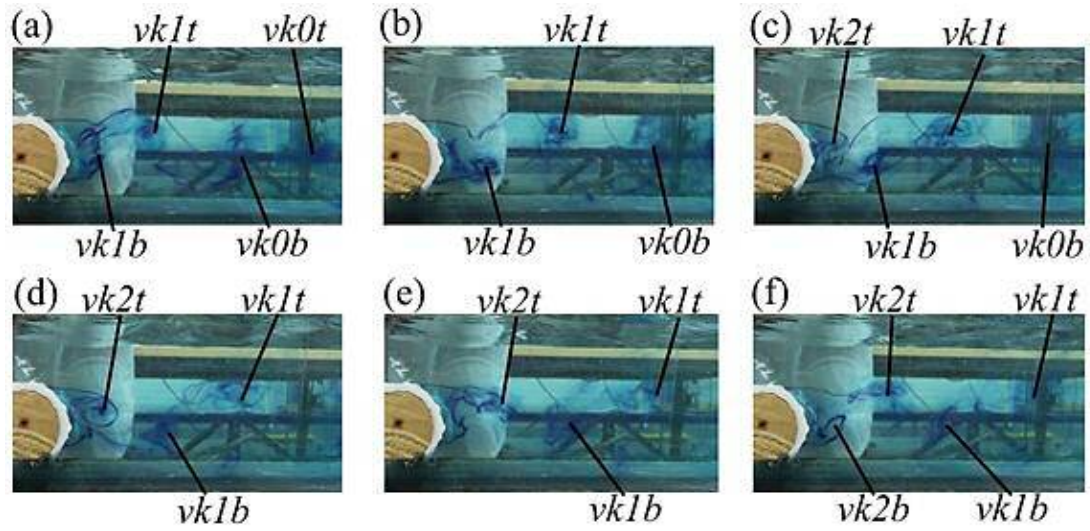

Figure 4.11. Flow visualization pictures in the cylinder wake at *Re* =14,930. Consecutive time frames are 0.1 s apart and cover an entire vortex shedding

cycle. *vk0t*, *vk1t* and *vk2t* denote vortices shed from the top shear layer whilst *vk0b*, *vk1b* and *vk2b* denote those from the bottom one.

The recurrent generation of instantaneous coherent turbulent structures were identified via Power Spectral Density (PSD) analysis of the time series of velocities at the sampling point x=6*D*, z=0.53*H* in the cylinder wake. Each time history was divided into six consecutive segments with each segment spanning 50s and the resulting spectra are the average of the PSD from each segment. Figure 4.14 shows the PSD of *u* and *w* velocities, i.e. E_{uu} and E_{ww} respectively, for the *Re*=18,600 case in which a single peak at 2Hz is observed for both velocity component spectra. At each discharge the frequency of these energy peaks related to the *vk* type vortex shedding and increased linearly with increasing *Re* with frequencies ranging from 0.46 to 4.05 s^{-1} (Figure 4.13), and corresponding Strouhal numbers remarkably constant irrespective of *Re* with a mean value of 0.31 ± 0.02 (mean ± s.d.) (Table 4.4). Note that these *St* values are higher than those for unbounded cylinder flows (*St* = 0.21) due to the proximity of the bed, in addition to the effects of free-surface dynamics.

Flow visualization of the wake for the *Re* = 14,930 case reveals the presence of the von-Kármán street with alternating coherent vortices shed off the cylinder's top and bottom, with shear layers referred to as "t" and "b" respectively (Figure 4.11). Figure 4.11a depicts a pair of *vk*vortices during the first stages of the vortex shedding cycle, i.e. *vk1t*-*vk1b*, and the pair of vortices *vk0t*-*vk0b* a downstream distance of 3*D*-4*D* where they have lost coherence during their downstream convection. The pathway of the vortex *vk1t* is tracked at different timeframes and the growth in vertical extent of the *vk* street towards the free-surface is shown in Figure 4.11. Such wake development is asymmetric as the vortices are constrained by the proximity of the bed and thus bottom vortices can only be horizontally propagated in the streamwise

direction. This complex flow pattern of energetic turbulent structures spanned across the entire flume's width and occupied a large extent of the water column.

Figure 4.12 shows the top-view of iso-surfaces of normalised Q-criterion (Hunt, Wray, & Moin, 1988) ($Q^* = QD^2/U_0^2 = 21$) coloured with relative elevation z/D for the Re = 13,333 case. The Kelvin-Helmholtz instability developed by the transition of shear layers coming off the edge of the cylinder into smaller rollers is shown, and this happens quicker for the Re = 13,333 case than the Re = 6,666 case (see Figure 4.9 and Figure 4.12). Thereafter, in the near-wake region spanwise rollers are formed with an undulating shape instead of being parallel to the cylinder edge (as marked with dotted line in Figure 4.12), which exhibits a wavelength λ of approximately πD/2. Interestingly, vortex dislocations caused by the large-scale von-Kármán vortices are irregularly distributed across the whole spanwise length. There is some correlation between the undulated spanwise roller and vortices dislocations, as those dislocations found at $y/D \approx 3.8$ or 1.0 are located further downstream in-line with low-momentum regions developed in the downstream roller at $x/D \approx 1$. At the time instance shown in Figure 4.10, the large-scale structures at elevations $z/D > 1$ found between $3 < x/D < 5$ are convected downstream in an oblique manner, i.e. with an angle relative to the cylinder edge. This is a well-known feature of the far-wake in cylinder flows (Williamson 1996) and interestingly occurs in the present case even though the flow is laterally constrained by the flume sidewalls, which also induce flow separation although its effect on the main wake structure is thought to be minimal.

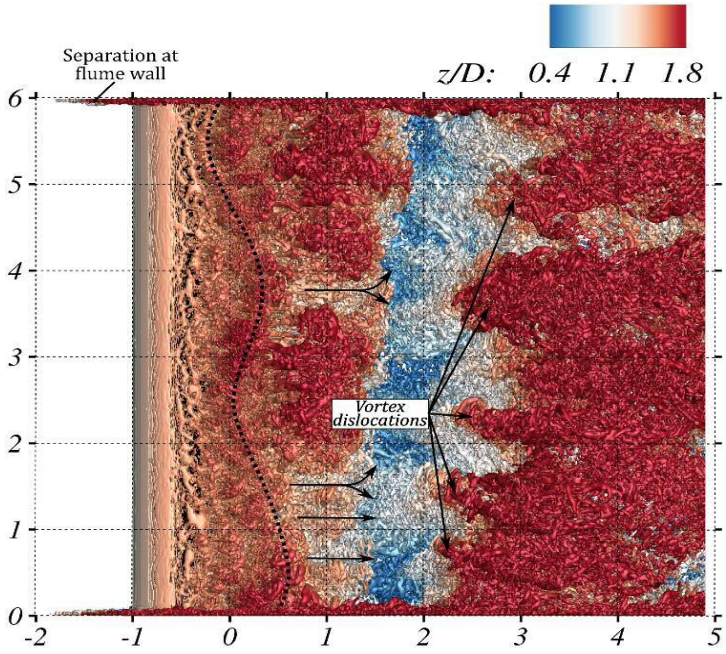

Figure 4.12. Top-view of iso-surfaces of Q-criterion ($Q^*=QD^2/U_0^2$ =21) coloured by the relative elevation z/D for the Re = 13,333 case. Arrows indicate the location of the vortex dislocations.

4.4.6 Dominant shedding frequency and hydrodynamic coefficients

The hydrodynamic forces generated on the cylinder are impacted by the asymmetric flow field developed around the cylinder owing to both its proximity to the bed and the upstream velocity logarithmic distribution. The cylinder forces are directly calculated from the immersed boundary method (Ouro et al., 2017) in the horizontal and vertical directions, F_x and F_z respectively, and are used to calculate the drag (C_D) and lift (C_L) coefficients given by:

$$C_D = Fx/(1/2 \cdot \rho \cdot B \cdot D \cdot U_0^2) \quad (4.5)$$

$$C_L = Fz/(1/2 \cdot \rho \cdot B \cdot D \cdot U_0^2) \quad (4.6)$$

where ρ is the fluid density and B is the cylinder's length. Values of the time-averaged hydrodynamic coefficients and their root-mean-square (rms) values are presented in

Table 4.4. The drag coefficient decreases with increasing Reynolds number, with values considerably lower than those found in unbounded cylinder flows due the proximity of the cylinder to the bed (Lei et al. 1999; Choi and Lee 2000), and the shallow flow conditions that increase the relative flow blockage of the cylinder. Time-averaged fluctuations of C_D are similar for the Re = 6,666 and 10,000 cases but decrease for the highest Reynolds number case (Re = 13,333). The ground-effect is responsible for the uplift force with time-averaged C_L values ranging from 0.011 and 0.019. The fluctuation of the C_L follows an analogous behaviour to that of C_D with the highest value being for the Re = 6,666 case and decreasing with increasing Reynolds number.

Table 4.4. Time-averaged and root-mean-square drag (C_D) and lift (C_L) coefficients, peak frequencies (f_p) and Strouhal number (St) obtained in the experiments and LES.

Re	C_D	rms(C_D)	C_L	rms(C_L)	f_p *(LES)*	f_p *(Exp)*	*St (LES)*	*St (Exp)*
[-]	[-]	[-]	[-]	[-]	[-]	[-]	[-]	[-]
6,666	0.3298	0.03330	0.0189	0.1168	0.819	0.85	0.321	0.32
10,000	0.2986	0.03474	0.0111	0.1225	1.105	1.21	0.307	0.30
13,333	0.1769	0.02090	0.0130	0.0673	1.490	1.61	0.298	0.30

Figure 4.14 presents the Power Spectral Distribution (PSD) of the vertical forces (F_z) experienced by the cylinder under the flow conditions considered. Distinct energy peaks are observed for each case with their frequency (f_p) becoming higher with increasing Reynolds number, and harmonics of these frequencies observed at $2f_p$ and $3f_p$ are more pronounced in the Re = 13,333 case. The Strouhal number ($St = f_pD/U_0$) associated with these peak frequencies is summarised in Table 4.4 with values around

0.30-0.32 which are above the $St = 0.21$ value reported for unbounded cylinder flows (Bearman & Zdravkovich, 1978). Experimental Strouhal values were obtained from the PSD of the time-history of vertical velocities at the sampling point located at $x/D = 6$, $z/D = 1.5$ and these are very close to the values from the simulations. The experimental and modelled results show a slight decline in Strouhal number with increasing Reynolds number which has been observed in lower Reynolds number studies (Price et al., 2002). Furthermore previous experimental studies reported increases in St as the G/D ratio decreased with values ranging between 0.20-0.28 for the present ratio of $G/D = 0.5$ although for lower Reynolds numbers (Price et al., 2002). It should be noted that the log-law distribution of the approaching flow also affects the values of the hydrodynamic forces (Lei et al., 1999), which also explains the present high St values and small hydrodynamic coefficients.

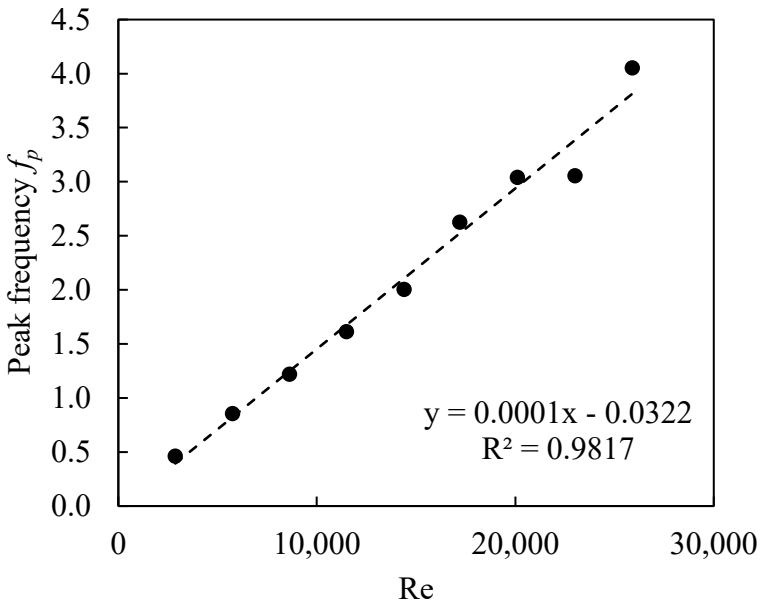

Figure 4.13. Peak vortex shedding frequencies from spectral analysis of experimental u and w velocity components for a point located at x = 6D, z = 0.53H downstream of the cylinder relative to Reynolds number. The sampling point location is shown in Figure 3.1.

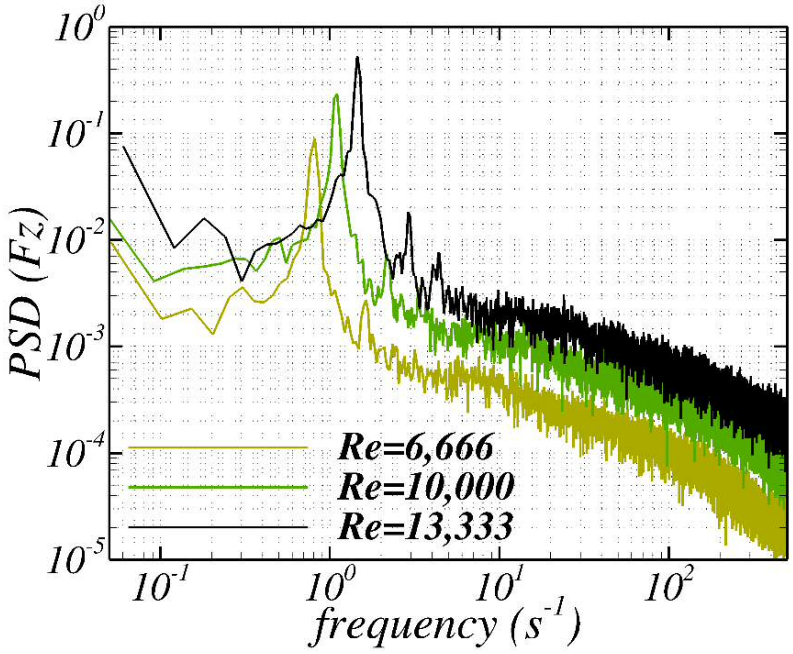

Figure 4.14. Spectral energy distribution of the vertical forces (*Fz*) in the cylinder computed from the LES for the three Reynolds number cases studied.

4.5 Conclusion

The nature of the turbulent wake behind a circular cylinder in close proximity to a solid boundary have been investigated using a combined experimental and large-eddy simulation study for Reynolds numbers in the range 6,666 to 13,333. The LES results agreed well with the experimental measurements for the time-averaged flow quantities and captured the streamwise velocity, its fluctuation in the recirculation bubble, and also the upward flow motion. The presence of the gap between the wall and cylinder, which remained fixed at a ratio of 0.5, significantly influenced the dynamics of the vortex generation and shedding which, in consequence, led to an increasingly pronounced asymmetric wake distribution with increasing Reynolds number. The boundary layer separation points on both the upper and lower halves of the cylinder move upstream with increasing Reynolds number, which is consistent with previous studies. Likewise, the enclosed recirculation bubble, was found to be slightly asymmetric by being larger in its lower part and decreasing in longitudinal

extent with increasing Reynolds number consistently with cylinder-wake flows. From the continuity equation, the rate of change of the mean velocity terms further characterised the asymmetric near-wake, whose distribution was similar for the three Reynolds numbers.

The Kelvin-Helmholtz instability developed in the upper and lower shear layers was shown to decouple with the lower and upper shear layers transitioning at different downstream distances. A more rapid breakdown of the shear layers occurred for the Re = 13,333 case than the Re = 6,666 case. In the near-wake region spanwise rollers were formed with an undulating pattern instead of being parallel to the cylinder edge, which was linked to the appearance of vortex dislocations. The ground-vortex formed as a result of the lower vortex inducing a difference in pressure that allows the former structure to lift-off the ground and merge with the von-Karman vortices to form a single vortical structure, which convected downstream with the flow. This phenomenon was present for all three Reynolds numbers examined and became more pronounced for the highest Reynolds number case as the near wake became more unstable closer to the cylinder. Spectral analysis revealed Strouhal numbers between 0.30-0.32 from both experiments and LES results, and which are higher that the value of 0.21 commonly found in unbounded cylinder flows owing to changes in the vortex shedding dynamics from the ground-effect. In this line, drag coefficient values lower than those for unbounded cylinder flows were obtained and an uplift force was present on the cylinder, both effects are consistent with previous studies conducted in proximity to a solid boundary.

Chapter 5. Temperature can outweigh velocity and turbulence effects on fish swimming performance

With the addition of data collected using Topmouth gudgeon (*Pseudorasbora parva*), this chapter will be part of a manuscript aimed at publication in *Water Research*. Authored by Thomas J Rhidian, Muhawenimana Valentine, Chapman, C. Amanda, Nefjodova Jelena, Wilson Catherine A.M.E., and Cable Jo. R.T, A.C and J.N conducted the fish behaviour tests; V.M and J.N collected and processed the hydrodynamics data, V.M analysed the data presented here and wrote the text of this chapter, all with supervision and comments from C.W and J.C.

Summary

Global climate change will impact freshwater thermal regimes, and the dependence of fish swimming behaviour on temperature will likely be transformed, particularly in altered, turbulent flows. In this study, a step velocity test in an open channel flume with Reynolds numbers ranging from 6,600 to 48,780 was used to evaluate the dependence of Pumpkinseed fish (*Lepomis gibbosus*) habitat choice and swimming performance on flow velocity and turbulence under thermal regimes of 15, 20 and 25^0C. ADV measurements showed that time averaged and depth averaged velocities of , , and and the velocity fluctuation increased with each velocity step. Differences in velocity metrics between the flume centreline and near wall were

minor, evident in terms of the variation of time averaged velocities and turbulent kinetic energy over the water column. Habitat choice was significantly affected by temperature since fish preferred the bottom 6 cm of the water column at 15^0C but preferred to swim at an elevation of 3-9 cm above the bed at 20 and 25^0C. This behaviour was linked to the presence of lower mean velocities within 3 cm near the bed, where fish gradually sought to swim as the step velocity increased, especially at the 15^0C temperature, which caused a vital physiological response to conserve energy. Fish size dependence of swimming performance was observed as larger fish took longer to fatigue at 20 and 25^0C, while the reverse occurred at 15^0C. Increase in temperature from 15^0C to 20^0C and 25^0C increased the time to fatigue by 41 and 37%, respectively. While low mean velocities were chosen to decrease swimming costs, velocity fluctuations significantly affected time to fatigue with having a negative effect, and and a positive effect. The current results show that thermal regimes alter fish swimming behaviour and water column usage and highlight the currently overlooked impact of temperature on fish-velocity interactions.

5.1 Introduction

Quantification of fish swimming behaviour relative to flow properties is critical for defining the hydro-engineering basis of fish habitat design and management. Despite the lack of consensus on the extent of the impact of flow alterations on fish habitat usage and swimming behaviour (Lacey et al. 2012), the alterations do change the magnitude and distribution of flow hydrodynamic properties and hence alter fish's natural response and behaviour (Nikora et al. 2003; Smith et al. 2005; Liao 2007; Tritico and Cotel 2010). Fish sustained, prolonged and critical swimming velocities are used as indicators of ability to navigate flows for short and long distance movements (Hammer 1995) and therefore are used to link fish swimming behaviour and altered flow hydrodynamics (Lupandin 2005; Nikora et al. 2003; Liao 2007;

Lacey et al. 2012; Tritico and Cotel 2010; Hockley et al. 2014). There are, however, difficulties in comparing swimming performance values amongst experimental studies with turbulent flows due to the variations in fish species, experimental methodologies, source and type of turbulence, time and velocity increments and duration of the tests (Lacey et al. 2012).

Fish swimming performance is highly depended on environmental factors, particularly water temperature, which can drastically alter fish physiology, a phenomenon studied extensively (Videler and Wardle 1991; Beddow et al. 1995; Hammer 1995; Alsop et al. 1999; Johnston and Temple 2002; Hammill et al. 2004; Tierney and Farrell 2004; Dembski et al. 2006). Since temperature directly affects fish metabolism (Figure 5.1) (Gollock et al. 2006), some species benefit from temperature increases, which increases their swimming velocities, while others respond negatively, depending on the species optimum temperature for improved performance (Hammer, 1995). This key effect of thermal regimes on swimming performance will likely intensify due to global warming, which will not only change river runoff regimes, precipitation frequency, timing and duration, but most importantly water temperatures, with direct impacts on aquatic ecosystems (Poff et al. 2002; Rahel and Olden 2008; Clarke 2009; Fobert et al. 2011).

The field of ecohydraulics and studies of fish swimming behaviour in altered and turbulent flows have largely overlooked the effects of thermal regimes, while basing design and management of fish passageways on fish swimming ability. Only a few studies have evaluated the changes in fish swimming performance under different thermal regimes in relation to flow velocity (Castro-Santos 2004; Haro et al. 2004; Enders et al. 2005). Findings varied widely from increased temperature and flow velocity resulting in increased swimming costs (Enders et al. 2005) to high variability of temperature effects leading to inconclusive results (Castro-Santos 2004; Haro et al. 2004).

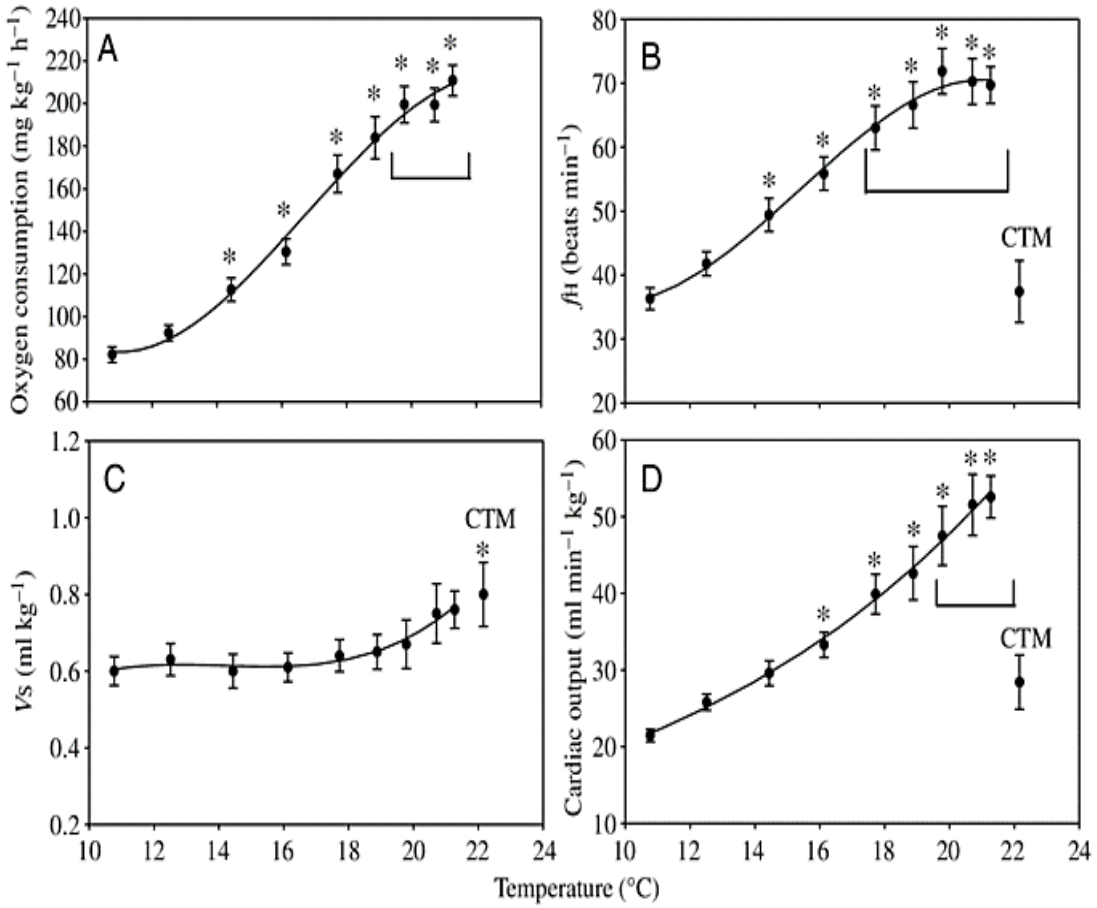

Figure 5.1. Example of the metabolic dependence of fish (Atlantic cod, *Gadus morhua*) on temperature in terms of rate of oxygen consumption (A), heart rate fH (B), stroke volume Vs (C) and cardiac output (D). CTM stands for critical thermal maximum. Figure reproduced from Gollock et al. (2006).

Climate change's impact on freshwater ecosystems thermal regimes will affect the dynamics of native and invasive species (Clarke 2009; Gallardo and Aldridge 2013). The present study focussed on the pumpkinseed (*Lepomis gibbosus*), a sunfish native to North America and one of the most invasive fish on mainland Europe (Copp, Fox, Przybylski, Godinho, & Vila-Gispert, 2004), although currently not considered as highly invasive in the UK due to its limited dispersal (Copp et al. 2004; Klaar et al. 2004; Tomeček et al. 2007). The effects of temperature on the pumpkinseeds' swimming performance are unknown, though warmer climates influence their growth

(Copp et al. 2004; Dembski et al. 2006; Copp and Fox 2007; Tomeček et al. 2007), and their phenotypic plasticity will likely benefit them compared to species native to the UK (Tomeček et al. 2007; Fox and Copp 2014). Oxygen consumption of pumpkinseeds, as a measure of metabolic cost, increases with increasing temperature (Roberts 1964) and swimming velocity (Brett and Sutherland 1965) as shown in Figures 5.2 and 5.3.

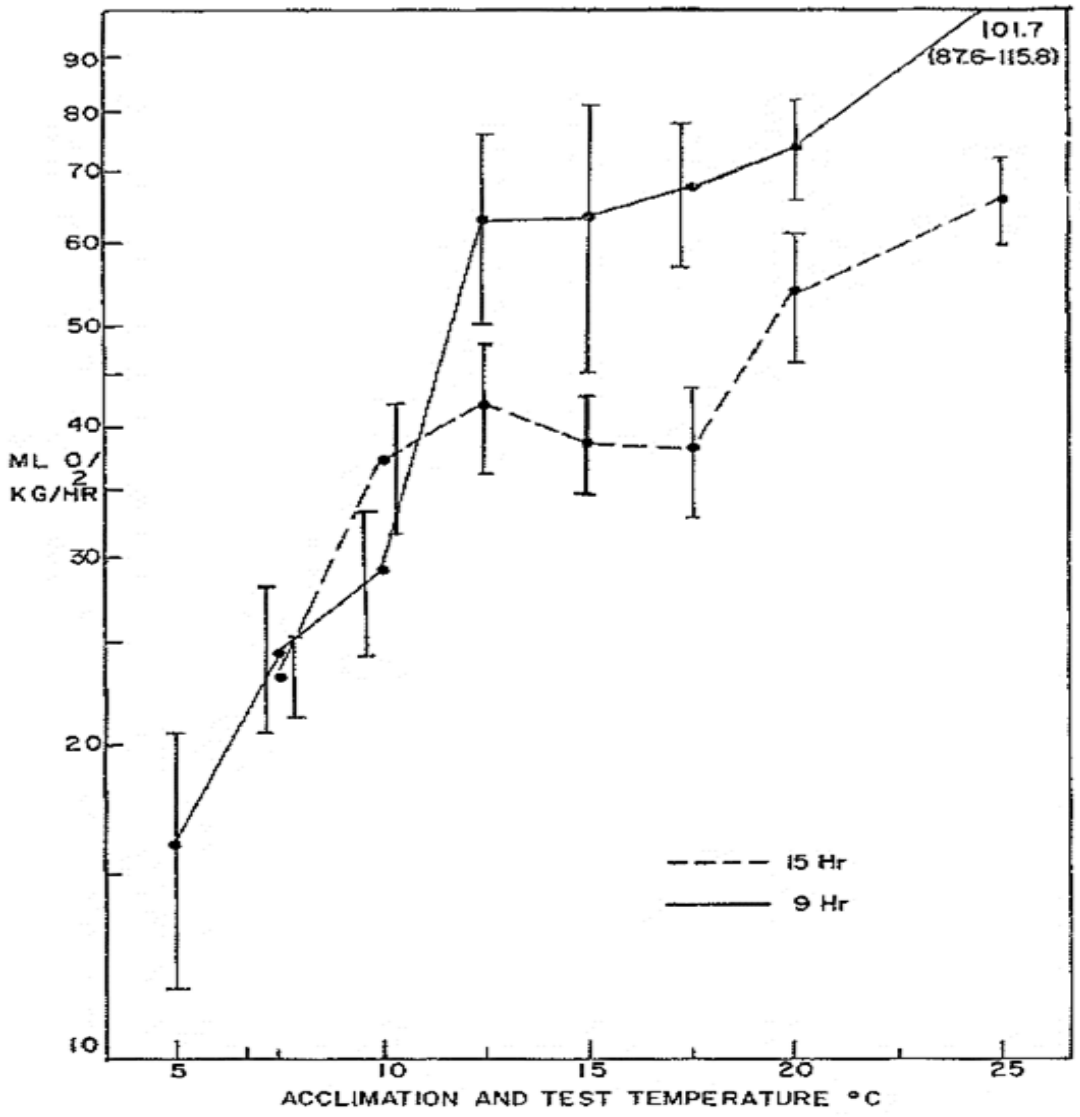

Figure 5.2. Respiration rates of the pumpkinseed (*Lepomis gibbosus*) in millilitres of Oxygen per kilogram per hour at various acclimation temperatures, with 9- and 15-hour photoperiod adaptations. Figure reproduced from Roberts (1964).

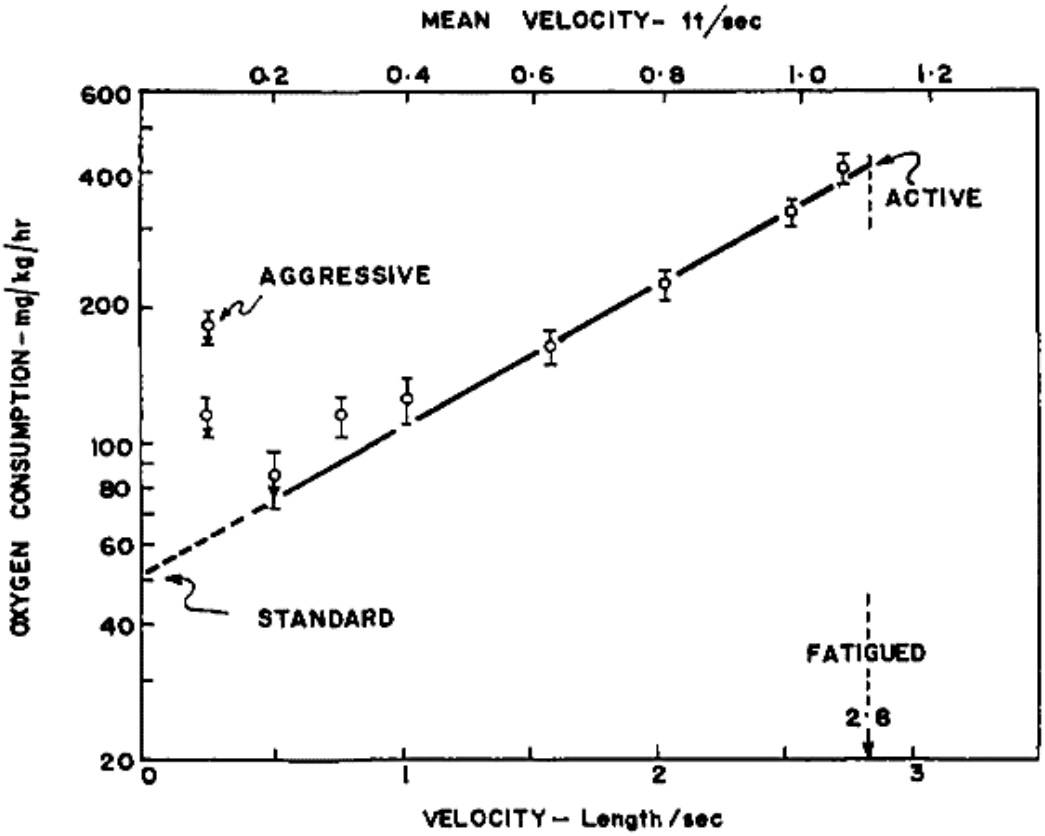

Figure 5.3. Pumpkinseed fish Oxygen consumption (milligrams per kilogram per hour) at various swimming velocities and behaviours. Figure reproduced from Brett and Sutherland (1965).

Due to the importance of thermal regimes impacts on fish, the predicted further alterations to aquatic ecosystems resulting from global climate change and the reliance of our understanding of fish-turbulence interactions on swimming performance, it is important to clarify fish swimming behaviour relative to flow velocity and turbulence under various water temperatures. Here, under the hypothesis that temperature affects fish habitat choice and swimming performance, we investigated these in terms of proportion of time spent in subsections of the test area, including water column position, and the fish's time to fatigue, for Pumpkinseed (*Lepomis gibbosus*) fish using a ramped velocity test at three temperatures (15, 20 and 25^0C). Measurements of local velocities quantified the flow properties to

determine the governing hydrodynamic metrics which affected habitat choice and swimming behaviour.

5.2 Methods

5.2.1 Flume setup

Experiments were conducted in a recirculating flume in the Hydro-environmental Research Centre laboratory, Cardiff School of Engineering. The flume was 10 m, 0.3 m, 0.3 m (length, width and depth) with 30 ls^{-1} discharge capacity. The flow depth was kept constant at 13.5 cm and velocity increments were made by increasing the discharge by 2 ls^{-1}. The step velocity test used to evaluate the critical swimming velocity of the fish and covered a velocity range of 9.28 cms^{-1} to 53.83 cms^{-1} as shown in Table 5.1. The test section, delimited by honeycomb flow diffusers, was 1.21 m long and was located between upstream 3.66 m and downstream 4.87 m from the flume inlet.

5.2.2 Fish swimming tests

Pumpkinseed (*Lepomis gibbosus*) (see Table 5.2) sourced from Silver Springs Fishery (Congresbury, UK) were tested using a standard step velocity test (Jain et al. 1997; Tierney et al. 2011) at three different temperatures of 15, 20 and 25^0C to assess their swimming performance. Prior to testing, the fish were maintained for at least one month at 15, 20 or 25^0C, corresponding with the flume flow temperature in the Cardiff School of Biosciences Aquarium. Fish were then transported to the flume in the School of Engineering one day prior to testing and acclimatised to the flume for 30 min at the lowest available discharge of 1.756 Ls^{-1}, which corresponds to a cross-sectional averaged velocity (U_0) of 4.335 cms^{-1}. The step velocity test used velocity increments of 5 cms^{1} and a 10 min time step, following the methods of Tierney (2011). The swimming tests were recorded using a MacBook Air laptop, positioned

to view the fish through the flume glass walls. Videos were analysed to quantify fish behaviour and habitat choice using JWatcher (version 1.0). The flume test area was divided into subsections (shown Figure 5.4) according to where fish preferred to swim and elevations in the water column. Time to fatigue, T_f, which was the duration fish were able to swim continuously throughout the step velocity test before exhaustion, is used here as a cumulative time indicator of fish swimming performance. Time to fatigue (T_f) can be obtained:

(5.1)

Where n is the number of velocity steps fully completed, t_i is the time fish swam at the fatigue velocity and t_{ii} is the step duration.

Table 5.1. Step velocity test details for Pumpkinseed swimming behaviour tests. T_s is the start time and T_e is the end time of each velocity step, Q is the discharge, U_0 is the cross-sectional average velocity, Re is the Reynolds number (Based on the hydraulic radius $R_0 = 0.071$, resulting from the flow depth of $H = 13.5$ cm). Fish acclimatisation was conducted at a discharge of 1.76 Ls^{-1} ($U_0 = 4.33$ cms^{-1}).

Step	T_s (min)	T_e (min)	Q (ls^{-1})	U_0 (cms^{-1})	Re (-)
	0	10	3.76	9.3	6,600
2	10	20	5.77	14.2	10,110
3	20	30	7.77	19.2	13,630
4	30	40	9.77	24.1	17,150
5	40	50	11.78	29.1	20,670
6	50	60	13.78	34.0	24,180
7	60	70	15.79	39.0	27,700
8	70	80	17.79	43.9	31,220
9	80	90	19.80	48.9	34,730
10	90	100	21.80	53.8	38,250
11	100	110	23.80	58.8	41,760
12	110	120	25.80	63.7	45,270
13	120	130	27.80	68.7	48,780

Table 5.2. Standard length, *SL* (mm) and weight, *W* (g) (mean ± stdev) of Pumpkinseed fish tested at three temperatures.

Temperature (^{0}C)	Number	*SL* (mm)	*W* (g)
15	10	69.4 (± 3.2)	3.9 (± 3.4)
20	13	63.8 (± 2.5)	7.2 (± 3.4)
25	9	61.4 (± 2.1)	6.5 (± 1.8)

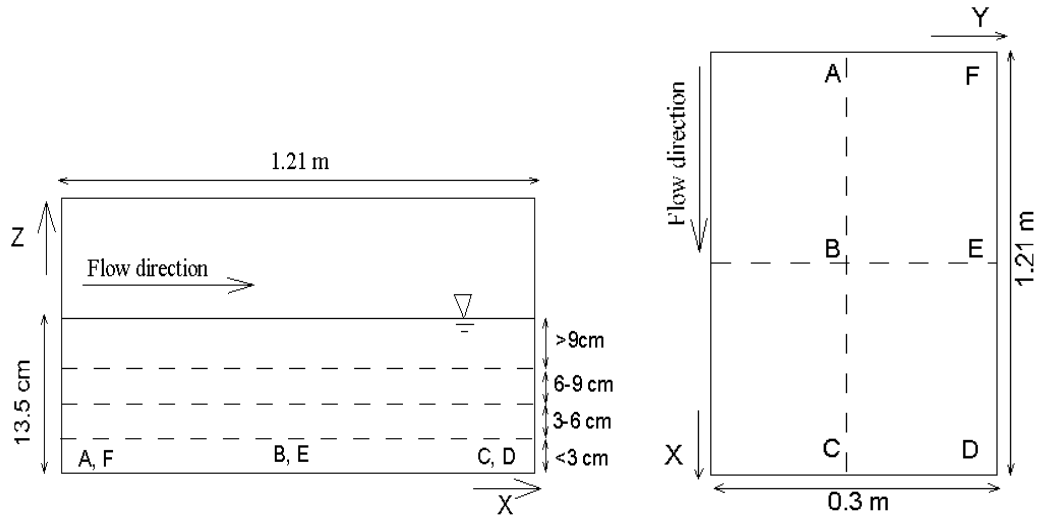

(i) (ii)

Figure 5.4. Side (i) and top (ii) views of the flume test section (not to scale) for fish behaviour and velocity measurements, which was 1.21 m long with a 13.5 cm flow depth. Also shown are the locations of velocity profiles along the flume centreline (A, B, and C) and near the flume wall (D, E, and F), with subsections of the water column used in the analysis of habitat choice.

5.2.3 Velocity data collection and post-processing

Velocity data was collected using a downward looking Nortek Acoustic Doppler Velocimeter (ADV) at 200Hz sampling frequency and 300 s sampling time. In the longitudinal direction (x), three measurement positions were located at 3.69, 4.26 and

4.86 m (A, B and C locations) from the flume inlet (Figure 5.4). At these longitudinal locations, measurements were made along the flume centre line and within 25 mm of the flume wall (D, E and F locations), marking two sampling positions in the transverse direction (y). In the vertical direction, 6 points, 10 mm apart were measured at each location. This made six profiles of six points each measured at every Reynolds number. Due to the configuration of the ADV, only a portion of the flow depth, with a height of 60 mm from the bed was measured and the remaining flow depth could not be measured. Filtering of the ADV data was performed using the Velocity Signal Analyser (MAJVSA version V1.5.62) based on thresholds of SNR and Correlation of 20 and 70%, respectively. Despiking used the Modified phase-space thresholding method by Goring and Nikora (2002 revised by Wahl 2003); followed by a 12 point average spike replacement (Jesson et al. 2013). Spikes that remained after this process were identified based on standard deviation from the mean profiles (Cea et al. 2007) and excluded from the dataset. Post-processed hydrodynamic properties MAJVSA included the turbulent kinetic energy (, longitudinal and spanwise turbulence intensity and respectively, and Reynolds shear stresses and ( ) for the horizontal and vertical components respectively. Note that overbar ( ) denotes time-averaging.

5.2.4 Statistical analysis

Generalised linear models (GLMs) with Gaussian family and Identity links were used to assess the effects of temperature, flow velocity and turbulence characteristics on the fish spatial preference and on their swimming performance in terms of time to fatigue. The models accounted for fish length and hydrodynamic flow properties of mean velocities in u, v, and w, components (x, y, z) and their fluctuations, as well as the turbulence intensity, turbulent kinetic energy, and vertical and horizontal

Reynolds stresses. Stepwise refinement of the models was used to drop variables until only statistically significant variables with $P<0.05$ remained. All statistical analysis were conducted in R statistics software 3.5.0 (R Core Team 2018), via RStudio (Version 1.1.447) (RStudio Team 2016).

5.3 Results

5.3.1 Flow hydrodynamic characteristics

ADV measurements of the open channel test section were made at three locations in the centreline and three locations near the wall in vertical profiles of six points (Figure 5.4) at all the discharges in Table 5.1. Figure 5.5 displays vertical profiles of time averaged velocity means , , , and fluctuations , , where the velocity means were similar in range and distributions along the centreline and wall. The velocity fluctuations showed increased variance near the wall compared to the centreline. The streamwise components and increased with increasing Reynolds number (Re) whilst the spanwise and vertical components ′ ′ , and were overall higher for lower Re. There was a predominance of negative velocities along the profiles for each Re while the other components were positive, and among the velocity fluctuations was the lowest. Similarly, Figure 5.6 shows profiles of turbulence statistics of turbulent kinetic energy *TKE* =) and the longitudinal and streamwise turbulence intensities in the centreline and near the flume wall. *TKE* and *TI* were similar in range and distribution in the centreline and near the wall, with a higher variance of these metrics for Z< 3 cm. The spanwise turbulence intensity TI_v was consistently two to three times higher than the longitudinal turbulence intensity TI_u.

Spatial averaging of velocities and turbulence metrics shown in Figure 5.7 for , , , and were performed according to the

flow volume zones (see Figure 5.4) for centreline locations of A, B and C and near wall locations of D, E, and F. Mean velocities and increased with increasing U_0 and were higher in the 3-6 cm elevation than the 0-3 cm near the bed, with increased scatter near the wall compared to the flume centreline. Turbulent shear stress overall increased with increasing U_0 and was predominantly positive in the centreline, while the reverse was observed near the flume walls. on the other hand, was nearly constant for all U_0 and slightly higher at the vertical elevation of 3-6 cm than 0-3 cm. Turbulence intensity was highest for the lower velocities, remained ≤ 2 from U_0 = 13.18 cms^{-1} and followed a similar distribution near the wall and in the flume centreline.

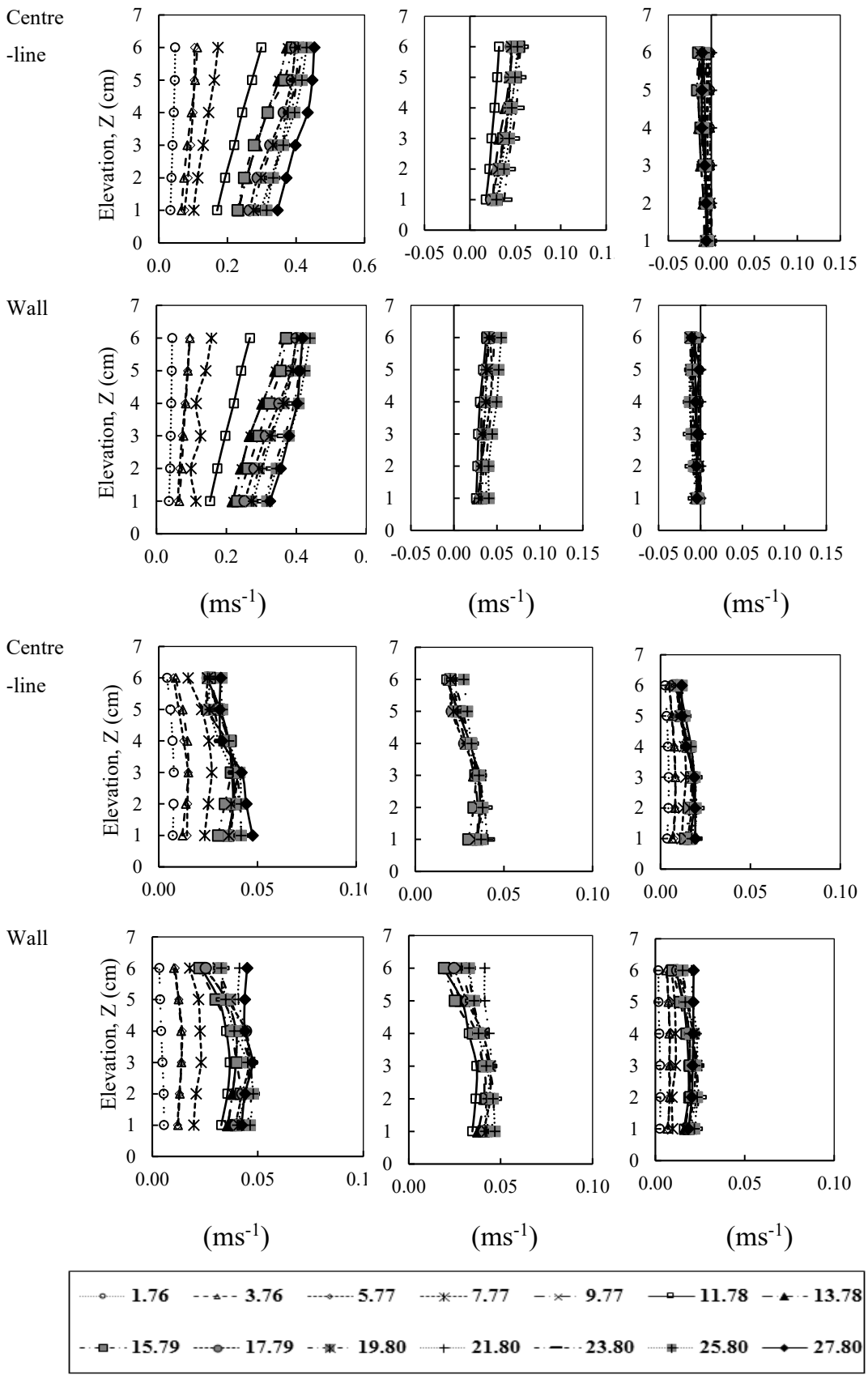

Figure 5.5. Vertical profiles of the flow time averaged velocities , <*v*> and <*w*> and velocity fluctuations <*u'*>, <*v'*> <*w'*> in the middle of the test section (longitudinal

distance of 4.265 m from the flume inlet), in the flume centreline and near wall for discharges of 1.75, 3.76, 5.76, 7.77, 9.77, 11.78, 13.78, 15.78, 17.79, 19.79, 21.80, 23.80, 25.80 and 27.80 Ls^{-1}.

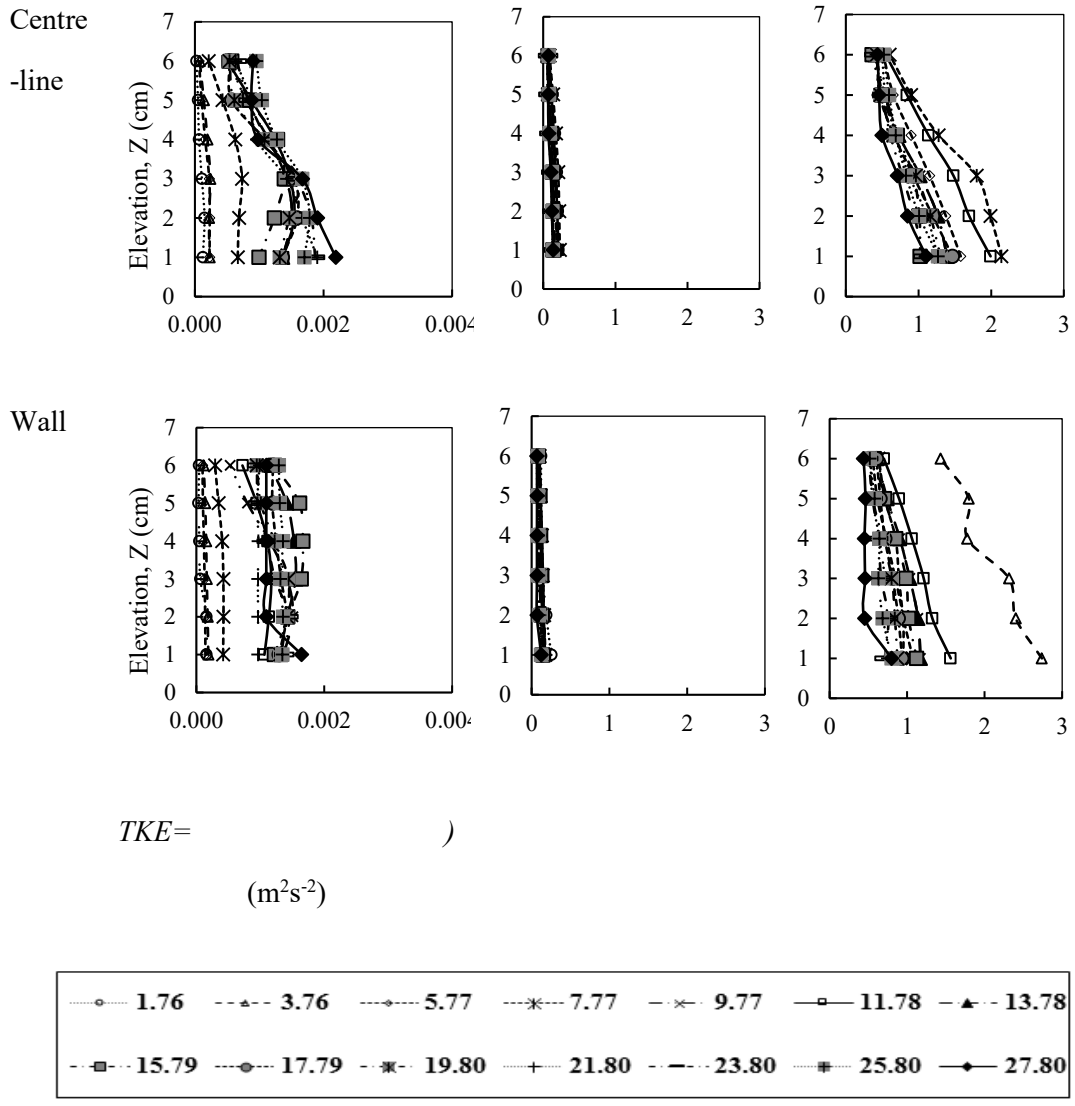

Figure 5.6.Vertical profiles of the flow turbulence properties of turbulent kinetic energy (*TKE*), streamwise turbulence intensity and spanwise turbulence intensity in the middle of the test section, in the flume centreline and near wall for all discharges of 1.75, 3.76, 5.76, 7.77, 9.77, 11.78, 13.78, 15.78, 17.79, 19.79, 21.80, 23.80, 25.80 and 27.80 Ls^{-1}.

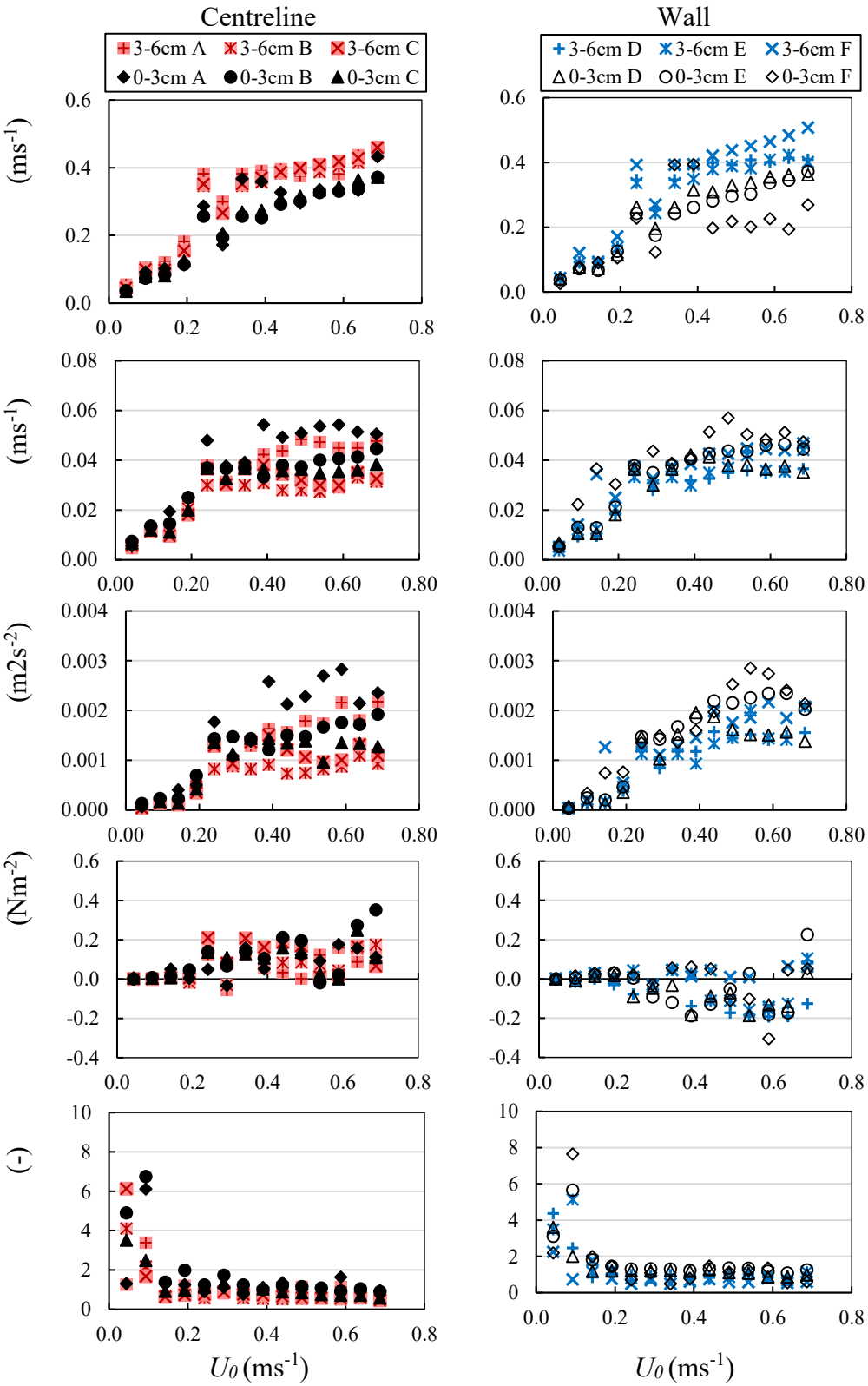

Figure 5.7. Flow velocities spatially averaged according to vertical zones of the water column at elevations of Z = 0-6 cm and 3-6 cm for all points along the centreline (A, B, C) and near the walls (D, E, F) for all the bulk velocities measured (shown in Table

1). Displayed are , < and where the overline (¯) indicates time averaging and brackets < > indicate spatial averaging.

5.3.2 Fish habitat choice and time to fatigue

Pumpkinseed swimming tests were conducted in a step velocity test with 13 steps in an open channel flume where cross-sectional area velocities ranged from 9.28 to 68.65 cms^{-1}, corresponding to Reynolds numbers ranging from 6,600 to 48,780 (Table 5.1) at three water temperatures (15, 20 and 25^0C). The distribution of fish occupancy in the water column relative to flow temperature and cross-sectionally averaged velocity at each step is shown in Figure 5.8, where the proportion of time fish occupied the volume zones throughout the step velocity test varied significantly in the water column (GLM, df=1, $P<0.05$).

The proportion of time varied only between 15^0C and the other two temperatures 20 and 25^0C (GLM, df=1, $P<0.05$). At 15^0C, pumpkinseeds preferred the 3-6 cm elevation at the lower velocity steps but changed their preference towards Z<3 cm with increasing velocity step, while their occupancy of the higher portion of the water column was limited throughout the step velocity test. At 20^0C, the proportion of time fish spent in the lower water column increased with increasing velocity, while it decreased in the 6-9 cm elevation; and preference for the 3-6 cm elevation was evident throughout the step velocity test. At 25^0C, the distribution of occupancy was similar to that at 20^0C, but with an increased preference for 3-6 cm elevation. At all temperatures, pumpkinseeds spent the least amount of time in the water column elevation above 9 cm (Figure 5.8). The flow turbulent fluctuations significantly affected the proportion of time fish spent in each flow volume zone, which increased with increasing (GLM, df=1, P=0.02) and (GLM, df=1, P=0.008) but decreased

with increasing (GLM, df=1, P=0.04) (Figure 5.9). Furthermore, the preference for swimming closer to the bed increased with increasing longitudinal turbulence intensity TI_u (GLM, df=1, P =0.03) and spanwise Reynolds shear stress τ_{uv} (GLM, df=1, P <0.05).

Time to fatigue (T_f) was negatively correlated with fish total length and weight at 15^0C, but positively correlated at 20 and 25^0C water temperatures (GLM, df=1, P<0.05) (Figure 5.10). T_f increased overall with increasing temperature (GLM, df=1, P=0.002) as fish swam on average 48.9 ±6.2, 83.6±7.7, and 77.4±3.6 min at 15, 20 and 25^0C, respectively; making T_f 41% and 37% lower for 15^0C than 20 and 25^0C, respectively. There was slight decrease in T_f of 6.2±4 min at 25^0C compared to 20^0C (Figure 5.11). Furthermore, T_f depended on the amount of time fish spent in the bottom 3 cm of the flume for 15 and 25^0C, but this correlation was negative at 20^0C (GLM, df=1, P<0.05) (Figure 5.12A). Time to fatigue (T_f) increased with increasing time in Z = 3-6 cm and 6-9 cm (GLM, df=1, p<0.05), indicating a positive correlation between T_f and the proportion of time spent at these elevations (Figure 5.12B). Figure 5.12C and D display similar temperature dependent variations and trends of the time to fatigue relative to the proportion of time fish spent in Z= 6-9 cm and Z>9 cm respectively. Mean velocity metrics did not significantly impact T_f (GLM, df=1, P>0.05). Conversely, T_f was negatively correlated with velocity fluctuations ( ) (GLM, df=1, P=0.001), indicating that had a diminishing effect on swimming performance. However, T_f was positively correlated with increasing and (GLM, df=1, P<0.05), which suggests that fish were not negatively affected by these turbulence components.

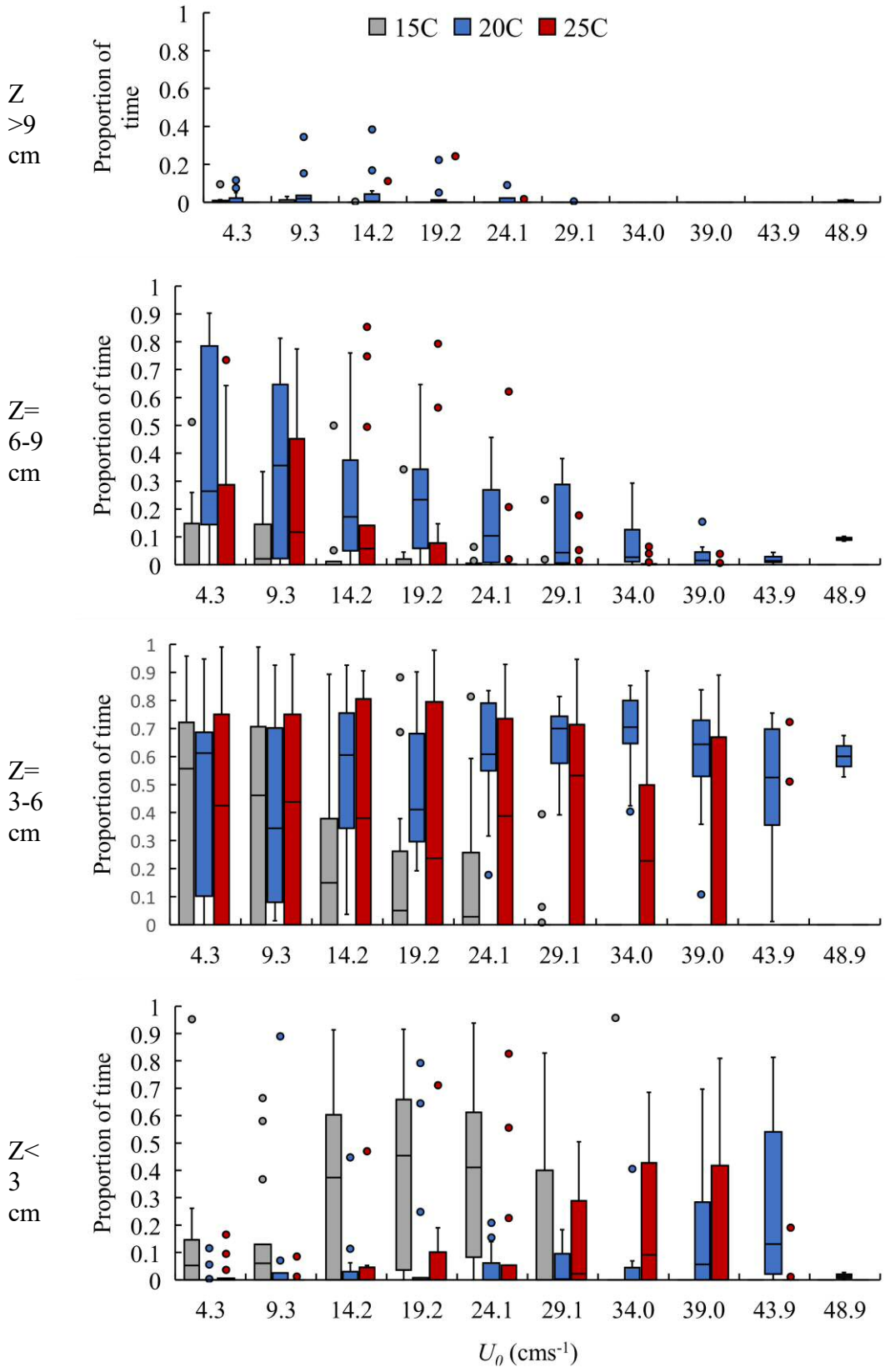

Figure 5.8. Proportion of time fish spent swimming in each subsection of the water column at the various flow temperatures throughout the velocity step test with U_0

ranging from 4.3 to 48.9 cms^{-1}, which was the final flow velocity at which any fish swam. Boxplots indicate, from bottom to top, minimum, first quartile, median, third quartile, and maximum.

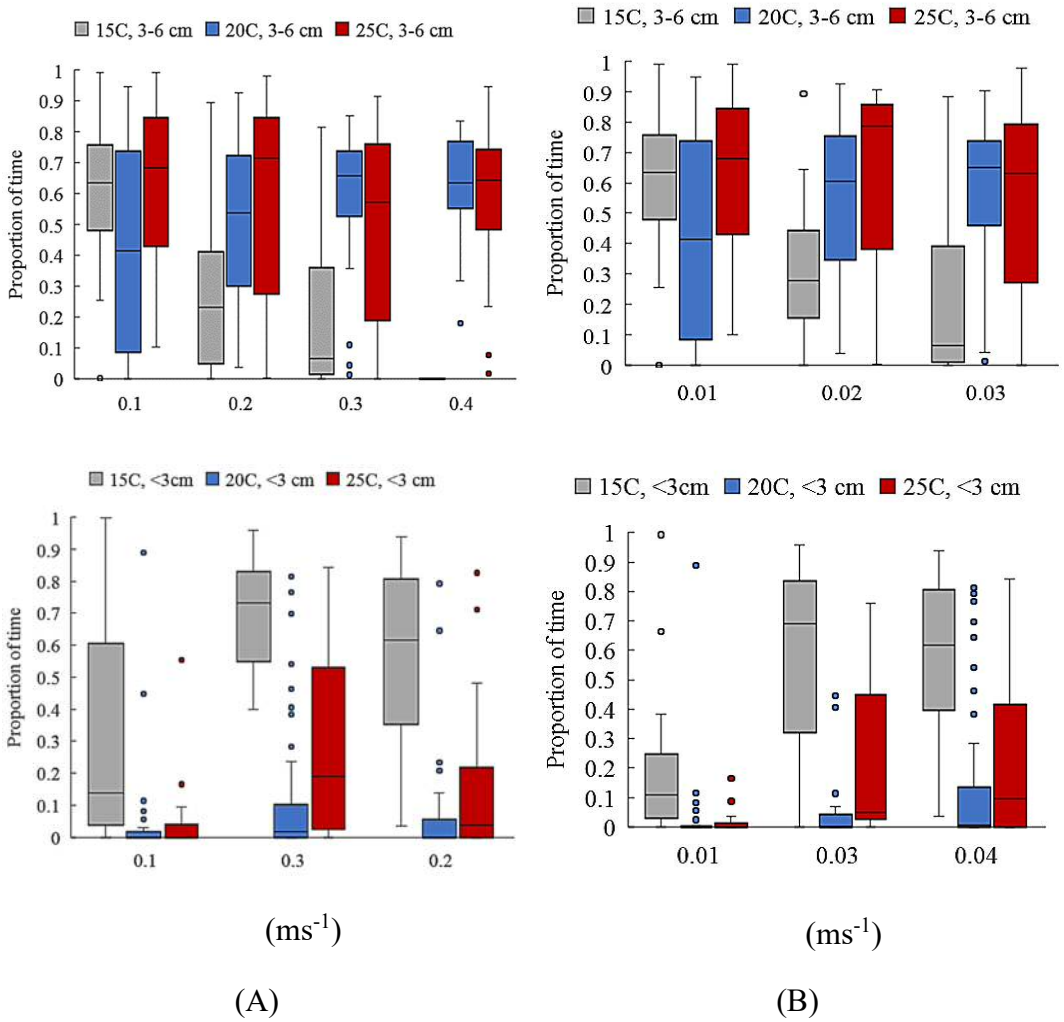

(ms^{-1}) (ms^{-1})

(A) (B)

Figure 5.9. Proportion of time fish spent in subsections of the water column Z < 3 cm and 3 <Z> 6 cm relative to the double-averaged velocity fluctuations of (A) and (B). where the overline (¯) indicates time averaging and brackets < > indicate spatial averaging. Boxplots indicate, from bottom to top, minimum, first quartile, median, third quartile, and maximum.

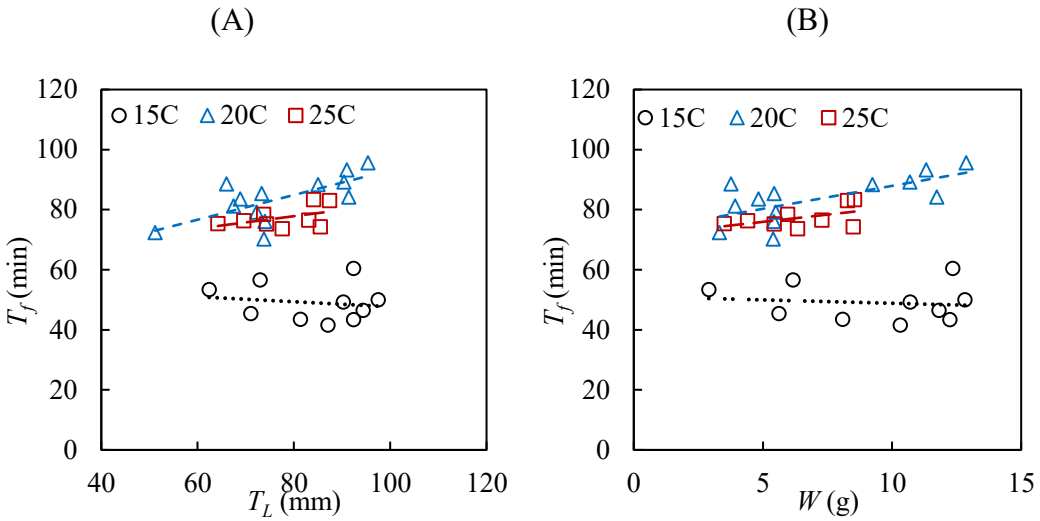

Figure 5.10. Time to fatigue T_f (min) relative to (A) fish total length, T_L (mm) and (B) fish weight, W (g).

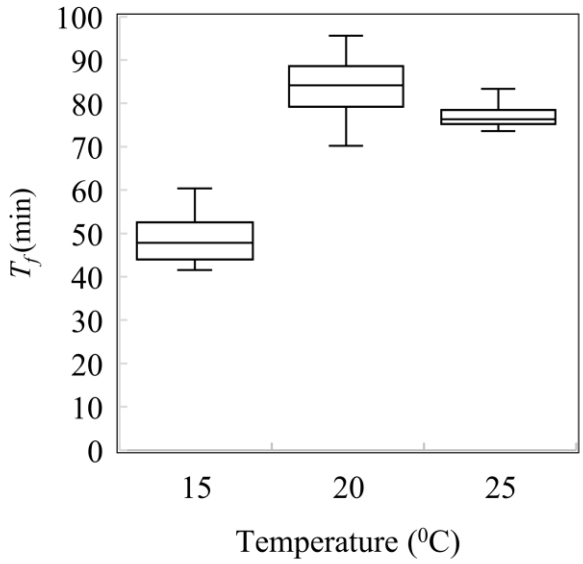

Figure 5.11. Time to fatigue (T_f) for Pumpkinseed fish tested at each temperature (15, 20 ad 25^{0}C).

(A) Time to fatigue and time in Z< 3cm

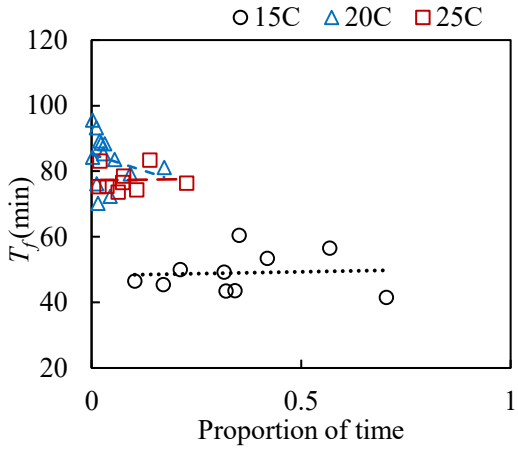

(B) Time to fatigue and time in Z = 3-6cm

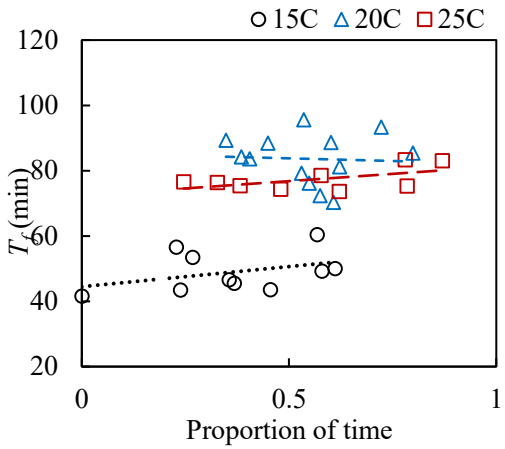

(C) Time to fatigue and time in Z= 6-9cm

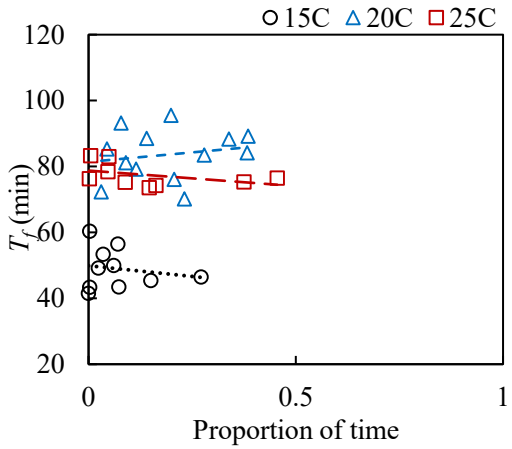

(D) Time to fatigue and time in Z>9cm

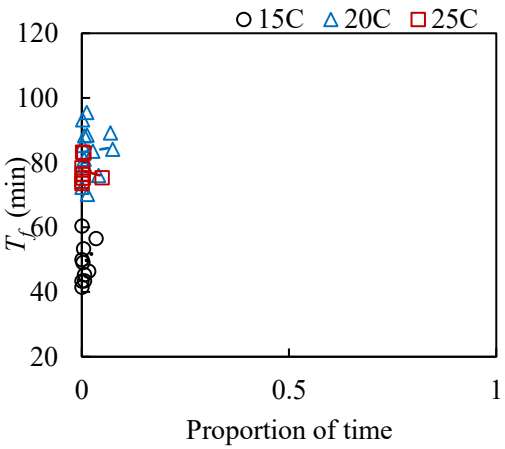

Figure 5.12. Time to fatigue in relation to fish habitat choice in terms of the proportion of time fish spent swimming in the water column at elevations of Z<3 cm (A), Z=3 to 6 cm (B), Z= 6 to 9 cm (C) and Z> 9 cm (D) for flow temperatures of 15, 20 and 25^{0}C.

5.4 Discussion

Using a step velocity test, the effects of flow temperature, velocity and turbulence on the swimming behaviour of pumpkinseed fish were evaluated in an open channel. Temperature affected fish habitat choice and swimming performance as the fish exhibited more exploratory behaviour at warmer temperatures. 20 and 25^0C temperatures also ensued a 41% and 37% increase in swimming time, respectively, compared to 15^0C. Swimming performance was dependant on fish size and temperature, larger fish took longer to fatigue at 20 and 25^0C, whereas the reverse occurred at 15^0C. Turbulence fluctuations governed fish swimming behaviour by affecting both habitat choice, which increased with and , but decreased with ; and time to fatigue was diminished by while positively correlated with and .

That the pumpkinseeds sought to conserve energy as a physiological response to the low temperature (Hammer 1995; Johnston and Temple 2002; Dembski et al. 2006) explains the predominant choice of the near bed region (Z< 3 cm) at 15^0C. This is further attributed to the presence of relatively lower mean velocities (and) (Figure 5.5A and B), which provided velocity refuge (Enders et al. 2003; Liao 2007). Incidentally, velocity fluctuations (and) were highest near the bed (Figure 5.5C and D), which contributed to lowering the fish's time to fatigue at 15^0C compared to 20 and 25^0C. Pumpkinseeds gradually spent more time near the flume bed with increasing step velocity (U_0) (Figure 5.8) as the energetic costs of swimming were increased by the increase in flow velocity (Brett and Sutherland 1965; Hammer 1995; Enders et al. 2003), which led the fish to seek relatively lower mean velocities.

The established fact that fish swimming ability increases with fish length and weight (Hammer, 1995) was observed for the higher two temperatures of 20 and 25^0C, but the opposite happened at 15^0C. This is perhaps due to the below optimum temperature, where the fish's metabolism might have been affected enough to hinder their swimming, and Pumpkinseed then utilised energy saving functions instead of

swimming, which would also explain the lower time to fatigue at 15^0C (Hammer 1995; Alsop et al. 1999; Johnston and Temple 2002; Tierney and Farrell 2004, Dembski et al. 2006). This is evidenced by the fish's increased preference for near-bed areas when the velocity steps increased under the 15^0C thermal regime compared to 20 and 25^0C, despite the presence of higher turbulent fluctuations at elevations less than 3 cm above the bed. Likewise, the elevated levels of turbulent kinetic energy and turbulence intensity are low enough not to impact on the energy saving benefits of the near bed zone. This also suggests that temperature effects might outweigh size effects for fish swimming in turbulent flows.

Pumpkinseed fish, originally from North America, are adapted to warm temperatures and are predicted to benefit from increasing temperatures because of climate change by dispersing further in European freshwaters (Dembski et al. 2006; Rahel and Olden 2008; Fobert et al. 2011; Fobert et al. 2013). Current results therefore might be affected by the fact that Pumpkinseed respond well to warm temperatures and were able to increase their swimming performance. This not unexpected, however, since temperature effects on fish swimming performance varies depending species (Videler and Wardle 1991; Castro-Santos 2004; Haro et al. 2004).

A distinction was made between the flume centreline and near wall due to the variations in hydrodynamic properties of the centre and sidewalls of open channels (Nezu, 2005) and the tendency for fish to seek velocity refuges near walls (Liao, 2007). However, in the current study, at 15, 20 and 25^0C fish only spent on average 4.22%, 0.27% and 1.62%, respectively, of the swimming tests in near wall areas, which suggests that these areas either did not provide refuge or fish were indifferent to them. This might be due to the similarities in distribution of local velocity and turbulence metrics between the flume centreline and the near wall areas. The flow hydrodynamic properties indicate the presence of a secondary currents in the channel (Figure 5.5, Figure 5.6, and Figure 5.7), which might have deterred the fish from

occupying the near-wall areas. The secondary currents are evident in the horizontal Reynolds shear stress as its direction near the flume wall is opposite that of the centreline, indicating flow circulation in the YZ plane, characteristic of secondary flows in open channels (Nezu, 2005).

Swimming performance serves as an indicator of fish endurance and ability to navigate various flow conditions and forms the basis for fish passage and other ecohydraulics measures. In addition to anthropogenic alterations of now highly turbulent river habitats, seasonal variations of water thermal regimes and the forecast increases in temperature due to global warming will further alter ecosystems. Considering that studies of thermal effects on fish swimming do not account for turbulence, and studies that evaluate turbulence-fish interactions overlook temperature effects, this study sought to bridge this gap. Under three temperatures, the habitat choice of pumpkinseeds was highly dependent upon temperature and swimming performance increased with increasing temperature. Evaluation of thermal regimes when studying fish-flow dynamics is recommended, since fish swimming behaviour will be impacted, and this will likely vary depending on fish species.

5.5 Conclusion

This study evaluated the effects the impact of temperature on fish-flow interactions and resulting habitat choice and swimming performance using a step velocity test for Pumpkinseed fish behaviour and ADV measurements for hydrodynamic flow characteristics. Time averaged and depth averaged velocities of , , and increased with each velocity step, and followed a similar pattern while and velocity fluctuations decreased. Differences between the flume centreline and near wall evident in the variance of time averaged velocities and turbulent kinetic energy were minor and did not create significant wall refuge for the fish. Size dependence of swimming performance was observed as increased length and weight resulted in

higher time to fatigue for the 20 and 25^{0}C, while the reverse occurred at 15^{0}C. Pumpkinseeds preferred the bottom 6 cm of the water column at 15^{0}C but preferred 3-9 cm water column elevations at 20 and 25^{0}C. Increased temperature from 15 to 20 and 25^{0}C resulted in increased time to fatigue by 41 and 37%, respectively. Fish used the region within 3 cm of the bed where reduced local mean velocities were present to conserve energy, particularly at the lowest temperature of 15^{0}C. Velocity fluctuations significantly affected time to fatigue with having a negative effect, and and having a positive effect. The current results show that fish swimming behaviour is not only dependent on flow hydrodynamic properties, but also on the thermal conditions, which might take precedence due to fishes' natural temperature preference. Hence, temperature effects might outweigh the effects of time-averaged velocities and fluctuations on habitat choice and swimming behaviour due to fish's physiological response toward low temperature, where energy saving might be necessary. In fishways and other river restoration schemes, fish might behave differently than anticipated due to regional and seasonal temperatures; therefore, current ecohydraulics design criteria can be improve by accounting for this temperature dependency of fish swimming behaviour.

Chapter 6. General Discussion: Synthesis and Future Research

6.1 Synthesis

Fragmentation of watercourses and freshwater habitats is one of the ecological consequences of hydraulic engineering infrastructures (Poff et al. 1997; Fuller et al. 2015). To remedy this, river restoration methods utilise fish passes and removal of barriers to increase habitat connectivity and restore biodiversity (Roni et al. 2002). The successful restoration of habitats and connectivity is hotly debated as current methods are not always efficient, as exemplified by fish passes which underperform for most fish species (Roscoe and Hinch 2010; Noonan et al. 2012; Kemp 2016). To aid flood defence, under the present shift from flood defence to flood risk management, new methods of Natural Flood Management (NFM) use flow attenuation obstructions, including Woody debris dams (WDD) (Pitt 2008; SEPA 2015; Burgess-Gamble et al. 2017). However, WDD designs and processes are not fully investigated or known, and their introduction into rivers highlights the currently unresolved questions of fish swimming behaviour in anthropically altered flows, which also form the design criteria for ecohydraulics methods, physical habitat tools (e.g. PHABSIM) and applications (Nestler et al. 2016).

This thesis evaluated the hydraulics of flood attenuation by WDD to determine the physical design characteristics that improve the hydraulic performance for natural flood management (Chapter 2). Designs of WDD, were defined based on the diameter, angle of orientation and the geometric arrangement of wood pieces, as well

as the overall channel blockage and the dam's porosity. Flood attenuation performance was measured as flow area afflux upstream of the dam under full-bank and 80% bankfull discharges, and this afflux was found to range from 0 to 30%. Findings indicated that the streamwise length of the dam, the cross-sectional channel blockage ratio and the dam's porosity increase afflux and it is therefore recommended that using these as criteria for designing WDD can maximise flood attenuation.

Furthermore, the question of further fragmenting river habitats through the use of channel obstructions for flood management as has been practiced in river engineering and water resources management, calls in to question the problem of fish-flow interactions, which are explored in Chapter 3. An idealised WDD in the form of a spanwise cylinder obstruction was used to evaluate fish (Nile tilapia, *Oreochromis niloticus*) behavioural response e.g. swimming stability and habitat usage to the altered flow conditions. Fish were found to chose areas with relatively low vorticity, turbulence intensity, turbulent kinetic energy, eddy size and Reynolds shear stress and losses of swimming stability occurred in the presence of downward Reynolds shear stresses and clockwise vortices. Results also highlighted the interplay between fish size and turbulence scale, as the loss of stability peaked when the ratio of turbulence length scale and fish length was 45 to 50%. The inclusion of these metrics in the design and refinement of hydro-engineering schemes is recommended (Chapter 3).

An in-depth look at the hydrodynamics of flow obstruction used numerical modelling with Large Eddy Simulation (LES) in combination with laboratory experiments to evaluate the fluid mechanics in the wake of the spanwise cylinder was undertaken in Chapter 4. The proximity of the ground to the cylinder rendered the wake asymmetric and led to different positions of the upper and lower shear layer separation points. Findings showed that a ground vortex lifts off the flume bed and merges with the von-Karman vortices. Experimental and numerical results matched well and

indicated that the lift force, drag coefficient and Strouhal numbers were higher than those for an unbounded cylinder or a vertical cylinder.

In Chapter 5, the limited understanding of fish-flow interactions was further addressed by evaluating the effects of thermal regimes on Pumpkinseed fish (*Lepomis gibbosus*) swimming behaviour and habitat usage in relation to flow velocity and turbulence. At temperatures of 15, 20 and 25^0C, fish sought relatively lower velocity areas, particularly at the lowest temperature where the physiological need to conserve energy was most evident. It was found that swimming performance, measured by time to fatigue depended on fish size, increased with temperature, but was negatively affected by the longitudinal component of velocity fluctuations. This indicated that velocities and turbulence affected fish habitat choice and swimming performance, but this interaction was entirely governed by temperature, and hence it is recommended that temperature ought to be a primary feature of fish-flow interaction evaluations.

Conclusions emerging from this thesis emphasize the complexities of altered and unnatural flows, which significantly alter fish behaviour. The hydraulic effect of WDD in terms of afflux reaching up to 30% surely changes the stream flow properties and provides flood attenuation benefits and spillage onto the upstream floodplains (Chapter 2). However, the channel confinement, resulting shear stresses and wake turbulence (Chapters 3 and 4), challenge fish swimming kinematics and habitat choice (Chapter 3). Therefore, it is necessary to balance both flood risk management and fish passage in the implementation of WDD for Natural Flood Management. Furthermore, the thermal regime effects on swimming performance suggest that our understanding of fish-behavioural responses to altered environments might ultimately be flawed by overlooking the physiologically demanding attributes of water temperature.

6.2 Future research

The research questions answered in this thesis could be complemented by replicating the experimental conditions with different fish species, as the findings herein will greatly vary with species differences (Hammer, 1995). For example, the fish-flow interactions described in Chapter 5 will vary depending on fish species' optimal temperature preference and acclimatisation, since species life and physiology affects fishes' interactions with their environment.

Evaluating fish behaviour in flows altered by WDD similar to those in Chapter 2 could determine the habitat enhancing abilities of the dams, in addition to the flood attenuation benefits demonstrated in this thesis. The vertical gaps between the dam and the flume bed was kept constant, however, gap ratios will change due to the blockage effect and wake hydraulics. Hence, evaluating more gap ratios and flow regimes could complement the findings presented herein. Other flow regimes in addition to the bankfull and 80% bankfull conditions could show the hydraulic processes of the WDD under a wide range of baseflow conditions, which are more likely to continue year-round, and yield continuous benefits to the ecosystem natural processes. Studying overbank flows conditions will quantify the floodplain flow storage and connectivity functions, as well as linking WDD performance to return periods to determine the range of flood events that can be successfully attenuated.

Measurements of the hydrodynamic flow field near a WDD are also necessary and would give insight to the hydrodynamics and physical process, to expand the results presented in this thesis and inform numerical flood modelling efforts. It is also necessary to perform field studies of engineered WDD as their hydraulic processes will depend on site-specific characteristic of flow, channel morphology and geometry e.g. meandering, soil type, riverbank and floodplain vegetation and wood nature and variety (Abbe and Montgomery 1996; Daniels and Rhoads 2004). Other key processes to consider are the geomorphological aspects as the shear forces such as

those observed in Chapters 3 and 4 would certainly enhance bed shear stresses and erosion in the wake of the dam.

Hydropower turbines create the most lethal environments for fish to pass through because they significantly alter their natural habitat in terms of flow rate, turbulence and shear stresses, pressure and dissolved gas levels (Abernethy *et al.* 2001; Cada and Odeh 2001). Research to further the study of the impact of hydro-turbines on fish behaviour and design fish-friendly turbines may employ methods used in this thesis and those of Maia et al. (2015) to evaluate the effect of swirl turbulence on fish swimming behaviour.

References

Abbe, T. B., & Montgomery, D. R. (1996). Large woody debris jams, channel hydraulics and habitat formation in large rivers. *Regulated Rivers: Research & Management*, *12*(23), 201–221. https://doi.org/https://doi.org/10.1002/(SICI)1099-1646(199603)12:2/3%3C201::AID-RRR390%3E3.0.CO;2-A

Abernethy, C. S., Amidan, B. G., & Cada, G. F. (2001). *Laboratory Studies of the Effects of Pressure and Dissolved Gas Supersaturation on Turbine-Passed Fish.* Report prepared for the U.S. Department of Energy, Idaho Operations Office.

Acreman, M. C., Harding, R. J., Lloyd, C., McNamara, N. P., Mountford, J. O., Mould, D. J., … Dury, S. J. (2011). Trade-off in ecosystem services of the Somerset Levels and Moors wetlands. *Hydrological Sciences Journal*, *56*(8), 1543–1565. https://doi.org/10.1080/02626667.2011.629783

Aljure, D. E., Lehmkhul, O., Rodríguez, I., & Oliva, A. (2017). Three dimensionality in the wake of the flow around a circular cylinder at Reynolds number 5000. *Computers & Fluids*, *147*, 102–118. https://doi.org/10.1016/j.compfluid.2017.02.004

Alsop, D. H., Kieffer, J. D., & Wood, C. M. (1999). The effects of temperature and swimming speed on instantaneous fuel use and nitrogenous waste excretion of the Nile Tilapia. *Physiological and Biochemical Zoology*, *72*(4), 474–483. https://doi.org/10.1086/316686

Angrilli, F., Bergamaschi, S., & Cossalter, V. (1982). Investigation of Wall Induced Modifications to Vortex Shedding From a Circular Cylinder. *Journal of Fluids Engineering*, *104*(4), 518–522. https://doi.org/10.1115/1.3241896

Armstron, G. S., Apahamian, M. W., Fewings, G. A., Gough, P. J., Reader, N. A., & Varallo, P. V. (2010). *Environment agency fish pass manual: guidance notes on the legislation, selection and approval of fish passes in England and Wales*. Bristol, UK: Environment Agency.

Barlow, J., Moore, F., & Burgess-Gamble, L. (2014). *Delivering Benefits thourgh Evidence: working with Natural Processes to reduce flood risk*. Retrieved from https://assets.publishing.service.gov.uk/government/uploads/system/uploads/at

tachment_data/file/338434/SC130004_R1.pdf

Bates, D., Mächler, M., Bolker, B., & Walker, S. (2015). Fitting linear mixed-effects models using lme4. *Journal of Statistical Software*, *67*(1). https://doi.org/10.18637/jss.v067.i01

Bearman, P. W., & Zdravkovich, M. M. (1978). Flow around a circular cylinder near a plane boundary. *Journal of Fluid Mechanics*, *89*(01), 33–47. https://doi.org/10.1017/S002211207800244X

Beddow, T. A., Van Leeuwen, J. L., & Johnston, I. A. (1995). Swimming kinematics of fast starts are altered by temperature acclimation in the marine fish *Myoxocephalus scorpius*. *The Journal of Experimental Biology*, *198*, 203–208. Retrieved from http://jeb.biologists.org/content/jexbio/198/1/203.full.pdf

Bernhardt, E. S., & Palmer, M. A. (2011). River restoration: the fuzzy logic of repairing reaches to reverse catchment scale degradation. *Ecological Applications*, *21*(6), 1926–1931. https://doi.org/10.1890/10-1574.1

Beveridge, O. S., Petchey, O. L., & Humphries, S. (2010). Mechanisms of temperature-dependent swimming: the importance of physics, physiology and body size in determining protist swimming speed. *Journal of Experimental Biology*, *213*(24), 4223–4231. https://doi.org/10.1242/jeb.045435

Bomminayuni, S., & Stoesser, T. (2011). Turbulence Statistics in an Open-Channel Flow over a Rough Bed. *Journal of Hydraulic Engineering*, *137*(11), 1347–1358. https://doi.org/10.1061/(ASCE)HY.1943-7900.0000454

Brett, J. R., & Sutherland, D. B. (1965). Respiratory Metabolisrn of Purnphinseed (*Lepornis gibbosus*) in Relation to Swirnrning Speedt. *Fisheries Research Board of Canada*, *22*(2), 0–4.

Breuer, M. (1998). Large eddy simulation of the subcritical flow past a circular cylinder: Numerical and modeling aspects. *International Journal for Numerical Methods in Fluids*, *28*(9), 1281–1302. https://doi.org/10.1002/(SICI)1097-0363(19981215)28:9<1281::AID-FLD759>3.0.CO;2-#

Bunn, S. E., & Arthington, A. H. (2002). Basic principles and ecological consequences of altered flow regimes for aquatic biodiversity. *Environmental Management*, Vol. 30, pp. 492–507. https://doi.org/10.1007/s00267-002-2737-0

Bunt, C. M., Castro-Santos, T., & Haro, A. (2012). Performance of fish passage

structures at upstream barriers to migration. *River Research and Applications*, *28*(4), 457–478. https://doi.org/10.1002/rra.1565

Bunt, C. M., Castro-Santos, T., & Haro, A. (2016). Reinforcement and Validation of the Analyses and Conclusions Related to Fishway Evaluation Data from Bunt et al. : 'Performance of Fish Passage Structures at Upstream Barriers to Migration.' *River Research and Applications*, *32*(10), 2125–2137. https://doi.org/10.1002/rra.3095

Burgess-Gamble, L., Ngai, R., Wilkinson, M., Nisbet, T., Pontee, N., Harvey, R., … Maslen, S. (2017). *Working with Natural Processes – Evidence Directory*. Environmental Agency, Report No. SC150005

Cada, G. F., & Odeh, M. (2001). Turbulence at Hydroelectric Power Plants and its Potential Effects on Fish. In *Report to Bonneville Power Administration*. https://doi.org/10.2172/781814

Castro-Santos, T. (2005). Optimal swim speeds for traversing velocity barriers: an analysis of volitional high-speed swimming behavior of migratory fishes. *Journal of Experimental Biology*, *208*(3), 421–432. https://doi.org/10.1242/jeb.01380

Castro-Santos, Theodore. (2004). Quantifying the combined effects of attempt rate and swimming capacity on passage through velocity barriers. *Canadian Journal of Fisheries and Aquatic Sciences*, *61*(9), 1602–1615. https://doi.org/10.1139/f04-094

Cea, L., Puertas, J., & Pena, L. (2007). Velocity measurements on highly turbulent free surface flow using ADV. *Experiments in Fluids*, *42*(3), 333–348. https://doi.org/10.1007/s00348-006-0237-3

Cevheri, M., McSherry, R., & Stoesser, T. (2016). A local mesh refinement approach for large-eddy simulations of turbulent flows. *International Journal for Numerical Methods in Fluids*, *82*(5), 261–285. https://doi.org/10.1002/fld.4217

Choi, J. H., & Lee, S. J. (2000). Ground effect of flow around and elliptic cylinder in a turbulent boundary layer. *Journal of Fluids and Structures*, *14*(5), 697–709. https://doi.org/10.1006/jfls.2000.0290

Chyu, C., Lin, J. -C., Sheridan, J., & Rockwell, D. (1995). Kármán vortex formation from a cylinder: Role of phase-locked Kelvin–Helmholtz vortices. *Physics of Fluids*, *7*(9), 2288–2290. https://doi.org/10.1063/1.868477

Clarke, S. J. (2009). Adapting to Climate Change: Implications for Freshwater Biodiversity and Management in the UK. *Freshwater Reviews*, *2*(1), 51–64. https://doi.org/10.1608/FRJ-2.1.3

Cooke, S. J., & Hinch, S. G. (2013). Improving the reliability of fishway attraction and passage efficiency estimates to inform fishway engineering, science, and practice. *Ecological Engineering*, *58*, 123–132. https://doi.org/10.1016/j.ecoleng.2013.06.005

Copp, G. H., & Fox, M. G. (2007). Growth and life history traits of introduced pumpkinseed (*Lepomis gibbosus*) in Europe, and the relevance to its potential invasiveness. In *Biological invaders in inland waters: Profiles, distribution, and threats* (pp. 289–306). https://doi.org/10.1007/978-1-4020-6029-8_15

Copp, G. H., Fox, M. G., Przybylski, M., Godinho, F. N., & Vila-Gispert, A. (2004). Life-time growth patterns of pumpkinseed *Lepomis gibbosus* introduced to Europe, relative to native North American populations. *Folia Zoologica*, *53*(3), 237–254. Retrieved from www.fishbase.org

Cotel, A. J., & Webb, P. W. (2015). Living in a Turbulent World—A New Conceptual Framework for the Interactions of Fish and Eddies. *Integrative and Comparative Biology*, *55*(4), 662–672. https://doi.org/10.1093/icb/icv085

Cotel, A. J., Webb, P. W., & Tritico, H. (2006). Do Brown Trout Choose Locations with Reduced Turbulence? *Transactions of the American Fisheries Society*, *135*(3), 610–619. https://doi.org/10.1577/T04-196.1

Coutant, C. C., & Whitney, R. R. (2000). Fish behavior in relation to passage through hydropower turbines: a review. *Transactions of the American Fisheries Society*, Vol. 129, pp. 351–380. https://doi.org/10.1577/1548-8659(2000)129<0351:FBIRTP>2.0.CO;2

Dadson, S. J., Hall, J. W., Murgatroyd, A., Acreman, M., Bates, P., Beven, K., … Wilby, R. (2017a). A restatement of the natural science evidence concerning catchment-based 'natural' flood management in the UK. *Proceedings of the Royal Society A: Mathematical, Physical and Engineering Science*, *473*(2199), 20160706. https://doi.org/10.1098/rspa.2016.0706

Daniels, M. D., & Rhoads, B. L. (2004). Effect of large woody debris configuration on three-dimensional flow structure in two low-energy meander bends at varying stages. *Water Resources Research*, *40*, 1–14.

https://doi.org/10.1029/2004WR003181

Daniels, M. D., & Rhoads, B. L. (2007). Influence of experimental removal of large woody debris on spatial patterns of three-dimensional flow in a meander bend. *Earth Surface Processes and Landforms*, *32*(August 2006), 460–474. https://doi.org/10.1002/esp

Daufresne, M., & Boët, P. (2007). Climate change impacts on structure and diversity of fish communities in rivers. *Global Change Biology*, *13*(12), 2467–2478. https://doi.org/10.1111/j.1365-2486.2007.01449.x

Dembski, S., Masson, G., Monnier, D., Wagner, P., & Pihan, J. C. (2006). Consequences of elevated temperatures on life-history traits of an introduced fish, pumpkinseed *Lepomis gibbosus*. *Journal of Fish Biology*, *69*(2), 331–346. https://doi.org/10.1111/j.1095-8649.2006.01087.x

Deng, Z., Guensch, G. R., McKinstry, C. A., Mueller, R. P., Dauble, D. D., & Richmond, M. C. (2005). Evaluation of fish-injury mechanisms during exposure to turbulent shear flow. *Canadian Journal of Fisheries and Aquatic Sciences*, *62*(7), 1513–1522. https://doi.org/10.1139/f05-091

Dixon, S. J., & Sear, D. A. (2014). The influence of geomorphology on large wood dynamics in a low gradient headwater stream. *Water Resources Research*, *50*(12), 9194–9210. https://doi.org/10.1002/2014WR015947

Dixon, S. J., Sear, D. A., Odoni, N. A., Sykes, T., & Lane, S. N. (2016). The effects of river restoration on catchment scale flood risk and flood hydrology. *Earth Surface Processes and Landforms*, *41*(7), 997–1008. https://doi.org/10.1002/esp.3919

Douglas, J. F., Gasiorek, J., Swaffield, J., & Jack, L. (2011). *Fluid Mechanics* (sixth). Harlow: Pearson Education.

Drucker, E. G., & Lauder, G. V. (1999). Locomotor forces on a swimming fish: three-dimensional vortex wake dynamics quantified using digital particle image velocimetry. *The Journal of Experimental Biology*, *202*(18), 2393–2412. Retrieved from http://www.ncbi.nlm.nih.gov/pubmed/10460729

Dynesius, M., & Nilsson, C. (1994). Fragmentation and Flow Regulation of River Systems in the Northern Third of the World. *Science*, *266*(5186), 753–762. https://doi.org/10.1126/science.266.5186.753

Enders, E. C., Buffin-Belanger, T., Boisclair, D., & Roy, A. G. (2005). The feeding

behaviour of juvenile Atlantic salmon in relation to turbulent flow. *Journal of Fish Biology*, *66*(1), 242–253. https://doi.org/10.1111/j.0022-1112.2005.00599.x

Enders, Eva C., Gessel, M. H., & Williams, J. G. (2009). Development of successful fish passage structures for downstream migrants requires knowledge of their behavioural response to accelerating flow. *Canadian Journal of Fisheries and Aquatic Sciences*, *66*(12), 2109–2117. https://doi.org/10.1139/F09-141

Enders, Eva C, Boisclair, D., & Roy, A. G. (2003). The effect of turbulence on the cost of swimming for juvenile Atlantic salmon (*Salmo salar*). *Canadian Journal of Fisheries and Aquatic Sciences*, *60*(9), 1149–1160. https://doi.org/10.1139/f03-101

Enders, Eva C, Boisclair, D., & Roy, A. G. (2004). The costs of habitat utilization of wild, farmed, and domesticated juvenile Atlantic salmon (*Salmo salar*). *Canadian Journal of Fisheries and Aquatic Sciences*, *61*(12), 2302–2313. https://doi.org/10.1139/f04-211

Enders, Eva C, Boisclair, D., & Roy, A. G. (2005). A model of total swimming costs in turbulent flow for juvenile Atlantic salmon (*Salmo salar*). *Canadian Journal of Fisheries and Aquatic Sciences*, *62*, 1079–1089. https://doi.org/10.1139/F05-007

Epps, B. P., & Techet, A. H. (2007). Impulse generated during unsteady maneuvering of swimming fish. *Experiments in Fluids*, *43*(5), 691–700. https://doi.org/10.1007/s00348-007-0401-4

Fagan, W. F. (2002). Connectivity, Fragmentation, and Extinction Risk in Dendritic Metapopulations. *Ecology*, *83*(12), 3243–3249. https://doi.org/10.2307/3072074

Floyd, T. A., MacInnis, C., & Taylor, B. R. (2009). Effects of artificial woody structures on Atlantic salmon habitat and populations in a Nova Scotia stream. *River Research and Applications*, *25*(3), 272–282. https://doi.org/10.1002/rra.1154

Fobert, E., Fox, M. G., Ridgway, M., & Copp, G. H. (2011). Heated competition: how climate change will affect non-native pumpkinseed *Lepomis gibbosus* and native perch *Perca fluviatilis* interactions in the U.K. *Journal of Fish Biology*, *79*(6), 1592–1607. https://doi.org/10.1111/j.1095-8649.2011.03083.x

Fobert, Emily, Zieba, G., Vilizzi, L., Godard, M. J., Fox, M. G., Stakenas, S., & Copp, G. H. (2013). Predicting non-native fish dispersal under conditions of climate change: Case study in England of dispersal and establishment of pumpkinseed *Lepomis gibbosus* in a floodplain pond. *Ecology of Freshwater Fish*, *22*(1), 106–116. https://doi.org/10.1111/eff.12008

Foley, M. M., Bellmore, J. R., O'Connor, J. E., Duda, J. J., East, A. E., Grant, G. E., … Wilcox, A. C. (2017). Dam removal: Listening in. *Water Resources Research*, *53*(7), 5229–5246. https://doi.org/10.1002/2017WR020457

Fox, M. G., & Copp, G. H. (2014). Old world versus new world: life-history alterations in a successful invader introduced across Europe. *Oecologia*, *174*(2), 435–446. https://doi.org/10.1007/s00442-013-2776-7

Franosch, J.-M. P., Hagedorn, H. J. A., Goulet, J., Engelmann, J., & van Hemmen, J. L. (2009). Wake Tracking and the Detection of Vortex Rings by the Canal Lateral Line of Fish. *Physical Review Letters*, *103*(7), 078102. https://doi.org/10.1103/PhysRevLett.103.078102

Fuller, M. R., Doyle, M. W., & Strayer, D. L. (2015). Causes and consequences of habitat fragmentation in river networks. *Annals of the New York Academy of Sciences*, *1355*(1), 31–51. https://doi.org/10.1111/nyas.12853

Gallardo, B., & Aldridge, D. C. (2013). The 'dirty dozen': socio-economic factors amplify the invasion potential of 12 high-risk aquatic invasive species in Great Britain and Ireland. *Journal of Applied Ecology*, *50*(3), 757–766. https://doi.org/10.1111/1365-2664.12079

Gippel, Christopher J. (1995). Environmental Hydraulics of Large Woody Debris in Streams and Rivers. *Journal of Environmental Engineering*, *121*(5), 388–395. https://doi.org/10.1061/(ASCE)0733-9372(1995)121:5(388)

Gippel, Christopher J., Finlayson, B. L., & O'Neill, I. C. (1996). Distribution and hydraulic significance of large woody debris in a lowland Australian river. *Hydrobiologia*, *318*(3), 179–194. https://doi.org/10.1007/BF00016679

Gippel, Christopher J., O'Neill, I. C., Finlayson, B. L., & Schnatz, I. (1996). Hydraulic Guidelines for the Re-Introduction and Management of Large Woody Debris in Lowland Rivers. *Regulated Rivers: Research & Management*, *12*(2–3), 223–236. https://doi.org/10.1002/(SICI)1099-1646(199603)12:2/3<223::AID-RRR391>3.0.CO;2-#

Gippel, Christopher James, Finlayson, B. L., & O'Neill, I. C. (1992). *The hydraulic basis of snag management*. Centre for Environmental Applied Hydrology, Department of Civil and ….

Giriat, D., Gorczyca, E., & Sobucki, M. (2016). Beaver ponds' impact on fluvial processes (Beskid Niski Mts., SE Poland). *Science of The Total Environment*, *544*, 339–353. https://doi.org/10.1016/j.scitotenv.2015.11.103

Gollock, M. J., Currie, S., Petersen, L. H., & Gamperl, A. K. (2006). Cardiovascular and haematological responses of Atlantic cod (*Gadus morhua*) to acute temperature increase. *Journal of Experimental Biology*, *209*(15), 2961–2970. https://doi.org/10.1242/jeb.02319

Goring, D. G., & Nikora, V. I. (2002). Despiking Acoustic Doppler Velocimeter Data. *Journal of Hydraulic Engineering*, *128*(1), 117–126. https://doi.org/10.1061/(ASCE)0733-9429(2002)128:1(117)

Gregory, K. J., Gurnell, A. M., & Hill, C. T. (1985). The permanence of debris dams related to river channel processes. *Hydrological Sciences Journal*, *30*(3), 371–381. https://doi.org/10.1080/02626668509491000

Hammer, C. (1995). Fatigue and exercise test with fish. *Comparative Biochemistry and Physiology Part A: Physiology*, *112*(1), 1–20. https://doi.org/https://doi.org/10.1016/0300-9629(95)00060-K

Hammill, E., Wilson, R. S., & Johnston, I. A. (2004). Sustained swimming performance and muscle structure are altered by thermal acclimation in male mosquitofish. *Journal of Thermal Biology*, *29*(4–5), 251–257. https://doi.org/10.1016/j.jtherbio.2004.04.002

Haro, A., Castro-Santos, T., Noreika, J., & Odeh, M. (2004). Swimming performance of upstream migrant fishes in open-channel flow: a new approach to predicting passage through velocity barriers. *Canadian Journal of Fisheries and Aquatic Sciences*, *61*(9), 1590–1601. https://doi.org/10.1139/f04-093

Hockley, F. A., Wilson, C. A. M. E., Brew, A., & Cable, J. (2014). Fish responses to flow velocity and turbulence in relation to size, sex and parasite load. *Journal of the Royal Society, Interface / the Royal Society*, *11*(November 2013), 20130814. https://doi.org/10.1098/rsif.2013.0814

Hoyt, J. W., & Sellin, R. H. J. (2000). Visualization of Flow Through a Cascade of Elliptical Cylinders. *Journal of Flow Visualization and Image Processing*, *7*, 1–

8.

Hulme, M., Jenkins, G., Turnpenny, J. R., Mitchell, T. D., Jones, R. G., Lowe, J., … Hill, S. (2002). Climate Change Scenarios for the United Kingdom: The UKCIP02 Scientific Repor. In *The UKCIP02 Briefing Report.* Retrieved from https://artefacts.ceda.ac.uk/badc_datadocs/link/UKCIP02_tech.pdf

Hunt, J. C. R., Wray, A. A., & Moin, P. (1988). Eddies, streams, and convergence zones in turbulent flows. *Center for Turbulence Research, Proceedings of the Summer Program*, 193–208. Retrieved from https://ntrs.nasa.gov/search.jsp?R=19890015184

Jager, H. I., Chandler, J. A., Lepla, K. B., & Van Winkle, W. (2001). A theoretical study of river fragmentation by dams and its effects on white sturgeon populations. *Environmental Biology of Fishes*, *60*(4), 347–361. https://doi.org/10.1023/A:1011036127663

Jain, K. ., Hamilton, J. ., & Farrell, A. . (1997). Use of a Ramp Velocity Test to Measure Critical Swimming Speed in Rainbow Trout (*Onchorhynchus mykiss*). *Comparative Biochemistry and Physiology Part A: Physiology*, *117*(4), 441–444. https://doi.org/10.1016/S0300-9629(96)00234-4

Jesson, M., Sterling, M., & Bridgeman, J. (2013). Despiking velocity time-series—Optimisation through the combination of spike detection and replacement methods. *Flow Measurement and Instrumentation*, *30*, 45–51. https://doi.org/10.1016/j.flowmeasinst.2013.01.007

Johnston, I. A., & Temple, G. K. (2002). Thermal plasticity of skeletal muscle phenotype in ectothermic vertebrates and its significance for locomotory behaviour. *Journal of Experimental Biology*, *205*, 2305–2322. Retrieved from http://jeb.biologists.org/content/205/15/2305

Kail, J., Hering, D., Muhar, S., Gerhard, M., & Preis, S. (2007). The use of large wood in stream restoration: Experiences from 50 projects in Germany and Austria. *Journal of Applied Ecology*, *44*(6), 1145–1155. https://doi.org/10.1111/j.1365-2664.2007.01401.x

Kara, S., Stoesser, T., Sturm, T. W., & Mulahasan, S. (2015). Flow dynamics through a submerged bridge opening with overtopping. *Journal of Hydraulic Research*, *53*(2), 186–195. https://doi.org/10.1080/00221686.2014.967821

Katopodis, C., & Williams, J. G. (2012). The development of fish passage research

in a historical context. *Ecological Engineering*, *48*, 8–18. https://doi.org/10.1016/j.ecoleng.2011.07.004

Kemp, P. S. (2016). Meta-analyses, Metrics and Motivation: Mixed Messages in the Fish Passage Debate. *River Research and Applications*, *32*(10), 2116–2124. https://doi.org/10.1002/rra.3082

Kemp, P. S., & O'Hanley, J. R. (2010, June 17). Procedures for evaluating and prioritising the removal of fish passage barriers: A synthesis. *Fisheries Management and Ecology*, Vol. 17, pp. 297–322. https://doi.org/10.1111/j.1365-2400.2010.00751.x

Kemp, Paul S., Gessel, M. H., & Williams, J. G. (2005). Fine-Scale Behavioral Responses of Pacific Salmonid Smolts as They Encounter Divergence and Acceleration of Flow. *Transactions of the American Fisheries Society*, *134*(2), 390–398. https://doi.org/10.1577/T04-039.1

Kim, D., Stoesser, T., & Kim, J.-H. (2013). The effect of baffle spacing on hydrodynamics and solute transport in serpentine contact tanks. *Journal of Hydraulic Research*, *51*(5), 558–568. https://doi.org/10.1080/00221686.2013.777681

Kirkgoz, M. S., Oner, A. A., & Akoz, M. S. (2009). Numerical modeling of interaction of a current with a circular cylinder near a rigid bed. *Advances in Engineering Software*, *40*(11), 1191–1199. https://doi.org/10.1016/j.advengsoft.2009.03.019

Kitts, D. (2010). *The hydraulic and hydrological performance of large wood accumulation in a low-order forest stream* (University of Southampton). Retrieved from http://eprints.soton.ac.uk/185791/

Klaar, M., Copp, G. H., & Horsfield, R. (2004). Autumnal habitat use of non-native pumpkinseed *Lepomis gibbosus* and associations with native fish species in small English streams. *Folia Zoologica*, *53*(2), 189–202.

Knight, D. W., & Demetriou, J. D. (1983). Flood Plain and Main Channel Flow Interaction. *Journal of Hydraulic Engineering*, *109*(8), 1073–1092. https://doi.org/10.1061/(ASCE)0733-9429(1983)109:8(1073)

Lacey, R. W. J., Neary, V. S., Liao, J. C., Enders, E. C., & Tritico, H. M. (2012a). The IPOS Framework: Linking Fish Swimming Performance In Aletered Flows From Laboratory Experiments To Rivers. *River Research and Applications*,

28(4), 429–443. https://doi.org/10.1002/rra.1584

Lane, S. N. (2017). Natural flood management. *Wiley Interdisciplinary Reviews: Water*, *4*(3), e1211. https://doi.org/10.1002/wat2.1211

Larinier, M. (2001). Environmental issues, dams and fish migration. In *FAO Fisheries Technical Paper* (Vol. 419)

Lauder, G. V. (2011). Swimming hydrodynamics: ten questions and the technical approaches needed to resolve them. *Experiments in Fluids*, *51*(1), 23–35. https://doi.org/10.1007/s00348-009-0765-8

Lauder, G. V., & Madden, P. G. A. (2007). Fish locomotion: kinematics and hydrodynamics of flexible foil-like fins. *Experiments in Fluids*, *43*(5), 641–653. https://doi.org/10.1007/s00348-007-0357-4

Lee, C. G., Farrell, A. P., Lotto, A., MacNutt, M. J., Hinch, S. G., & Healey, M. C. (2003). The effect of temperature on swimming performance and oxygen consumption in adult sockeye (*Oncorhynchus nerka*) and coho (*O. kisutch*) salmon stocks. *The Journal of Experimental Biology*, *206*(Pt 18), 3239–3251. https://doi.org/10.1242/jeb.00547

Lehmkuhl, O., Rodríguez, I., Borrell, R., Chiva, J., & Oliva, A. (2014). Unsteady forces on a circular cylinder at critical Reynolds numbers. *Physics of Fluids*, *26*(12). https://doi.org/10.1063/1.4904415

Lehmkuhl, O., Rodríguez, I., Borrell, R., & Oliva, A. (2013). Low-frequency unsteadiness in the vortex formation region of a circular cylinder. *Physics of Fluids*, *25*(8), 085109. https://doi.org/10.1063/1.4818641

Lei, C., Cheng, L., & Kavanagh, K. (1999). Re-examination of the effect of a plane boundary on force and vortex shedding of a circular cylinder. *Journal of Wind Engineering and Industrial Aerodynamics*, *80*(3), 263–286. https://doi.org/10.1016/S0167-6105(98)00204-9

Liao, J. C. (2007). A review of fish swimming mechanics and behaviour in altered flows. *Philosophical Transactions of the Royal Society B: Biological Sciences*, *362*(1487), 1973–1993. https://doi.org/10.1098/rstb.2007.2082

Liao, J. C., Beal, D. N., Lauder, G. V., & Michael S. Triantafyllou. (2003). The Kármán gait: novel body kinematics of rainbow trout swimming in a vortex street. *Journal of Experimental Biology*, *206*(6), 1059–1073. https://doi.org/10.1242/jeb.00209

Liao, J. C., Beal, D. N., Lauder, G. V., & Triantafyllou, M. S. (2003). Fish Exploiting Vortices Decrease Muscle Activity. *Science*, *302*(5650), 1566–1569. https://doi.org/10.1126/science.1088295

Lupandin, A. I. (2005). Effect of flow turbulence on swimming speed of fish. *Biology Bulletin*, *32*(5), 461–466. https://doi.org/10.1007/s10525-005-0125-z

Ma, X., Karamanos, G. S., & Karniadakis, G. E. (2000). Dynamics and low-dimensionality of a turbulent near wake. *Journal of Fluid Mechanics*, *410*, S0022112099007934. https://doi.org/10.1017/S0022112099007934

Maia, A., Sheltzer, A. P., & Tytell, E. D. (2015). Streamwise vortices destabilize swimming bluegill sunfish (*Lepomis macrochirus*). *Journal of Experimental Biology*, *218*(5), 786–792. https://doi.org/10.1242/jeb.114363

Manners, R. B., & Doyle, M. W. (2008). A mechanistic model of woody debris jam evolution and its application to wood-based restoration and management. *River Research and Applications*, *24*(8), 1104–1123. https://doi.org/10.1002/rra.1108

Manners, R. B., Doyle, M. W., & Small, M. J. (2007). Structure and hydraulics of natural woody debris jams. *Water Resources Research*, *43*(6), 1–17. https://doi.org/10.1029/2006WR004910

Masson-Delmotte, V., Zhai, P., Pörtner, H. O., Roberts, D., Skea, J., Shukla, P. R., & Waterfield, T. (2018). *Global warming of 1.5 C An IPCC Special Report on the impacts of global warming of 1.5 C above pre-industrial levels and related global greenhouse gas emission pathways, in the context of strengthening the global response to the threat of climate change*. Retrieved from https://www.ipcc.ch/site/assets/uploads/sites/2/2018/07/SR15_SPM_version_stand_alone_LR.pdf

McSherry, R., Chua, K., Stoesser, T., & Mulahasan, S. (2018). Free surface flow over square bars at intermediate relative submergence. *Journal of Hydraulic Research*, *56*(6), 825–843. https://doi.org/10.1080/00221686.2017.1413601

Mesquita, F. de O., & Young, R. J. (2007). The behavioural responses of Nile tilapia (*Oreochromis niloticus*) to anti-predator training. *Applied Animal Behaviour Science*, *106*, 144–154. https://doi.org/10.1016/j.applanim.2006.06.013

Miyazono, S., & Taylor, C. M. (2013). Effects of habitat size and isolation on species immigration-extinction dynamics and community nestedness in a desert river system. *Freshwater Biology*, *58*(7), 1303–1312.

https://doi.org/10.1111/fwb.12127

Moilanen, A., & Nieminen, M. (2002). Simple Connectivity Measures In Spatial Ecology. *Ecology*, *83*(4), 1131–1145. https://doi.org/10.1890/0012-9658(2002)083[1131:SCMISE]2.0.CO;2

Morita, K., & Yokota, A. (2002). Population viability of stream-resident salmonids after habitat fragmentation: a case study with white-spotted charr (*Salvelinus leucomaenis*) by an individual based model. *Ecological Modelling*, *155*(1), 85–94. https://doi.org/10.1016/S0304-3800(02)00128-X

Murchie, K. J., Hair, K. P. E., Pullen, C. E., Redpath, T. D., Stephens, H. R., & Cooke, S. J. (2008). Fish response to modified flow regimes in regulated rivers: research methods, effects and opportunities. *River Research and Applications*, *24*(2), 197–217. https://doi.org/10.1002/rra.1058

Murchie, K. J., Hair, K. P. E., Pullen, C. E., RedPath, T. D., Stephens, H. R., & Cooke, S. J. (2008). Fish response to modified flow regimes in regulated rivers: research methods, effects and opportunities. *River Research and Applications*, *24*, 197–217. https://doi.org/DOI: 10.1002/rra.1058

Nagayama, S., & Nakamura, F. (2010). Fish habitat rehabilitation using wood in the world. *Landscape and Ecological Engineering*, *6*(2), 289–305. https://doi.org/10.1007/s11355-009-0092-5

Naiman, R. J., Johnston, C. A., & Kelley, J. C. (1988). Alteration of North American Streams by Beaver. *BioScience*, *38*(11), 753–762. https://doi.org/10.2307/1310784

Nauen, J. C., & Lauder, G. V. (2002). Quantification of the wake of rainbow trout (*Oncorhynchus mykiss*) using three-dimensional stereoscopic digital particle image velocimetry. *The Journal of Experimental Biology*, *205*(21), 3271–3279

Neitzel, D. A., Richmond, M. C., Dauble, D. D., Mueller, R. P., Moursund, R. A., Abernethy, C. S., & Guensch, G. R. (2000). *Laboratory Studies on the Effects of Shear on Fish*. https://doi.org/10.2172/939056

Nestler, J. M., Stewardson, M. J., Gilvear, D. J., Webb, J. A., Smith, D. L., Nestler, J. M., … Webb, J. A. (2016). Ecohydraulics exemplifies the emerging " paradigm of the interdisciplines ." *Journal of Ecohydraulics*, *1*(December), 1–2, 5–15. https://doi.org/10.1080/24705357.2016.1229142

Nezu, I. (2005). Open-Channel Flow Turbulence and Its Research Prospect in the

21st Century. *Journal of Hydraulic Engineering-Asce*, *131*(4), 229–246. https://doi.org/10.1007/978-0-387-76495-5

Nicoud, F., & Ducros, F. (1999). Subgrid-scale stress modelling based on the square of the velocity gradient tensor. *Flow, Turbulence and Combustion*, *62*(3), 183–200. https://doi.org/https://doi.org/10.1023/A:1009995426001

Nienhuis, R. H., & Leuven, R. S. E. W. (2001). River restoration and flood protection: Controversy or synergism? *Hydrobiologia*, *444*, 85–99. https://doi.org/https://doi.org/10.1023/A:1017509410951

Nikora, V. I., Aberle, J., Biggs, B. J. F., Jowett, I. G., & Sykes, J. R. E. (2003). Effects of fish size, time-to-fatigue and turbulence on swimming performance: a case study of Galaxias maculatus. *Journal of Fish Biology*, *63*(6), 1365–1382. https://doi.org/10.1111/j.1095-8649.2003.00241.x

Nilsson, C., Reidy, C. A., Dynesius, M., Revenga, C., Nilsson, C., Reidy, C. A., … Revenga, C. (2005). Fragmentation and Flow Regulation of the World's Large River Systems. *Science*, *308*(5720), 405–408. https://doi.org/10.1126/science.1107887

Nisbet, T. R., Marrington, S., Thomas, H., Broadmeadow, S., & Valatin, G. (2011). Slowing the flow at Pickering. In *Final Report to Defra, Project RMP5455*.

Nishino, T., Roberts, G. T., & Zhang, X. (2008). Unsteady RANS and detached-eddy simulations of flow around a circular cylinder in ground effect. *Journal of Fluids and Structures*, *24*(1), 18–33. https://doi.org/10.1016/j.jfluidstructs.2007.06.002

Nishino, Takafumi, Roberts, G. T., & Zhang, X. (2007). Vortex shedding from a circular cylinder near a moving ground. *Physics of Fluids*, *19*(2), 025103. https://doi.org/10.1063/1.2710273

Noonan, M. J., Grant, J. W. A., & Jackson, C. D. (2012). A quantitative assessment of fish passage efficiency. *Fish and Fisheries*, *13*(4), 450–464. https://doi.org/10.1111/j.1467-2979.2011.00445.x

Norberg, C. (1994). An experimental investigation of the flow around a circular cylinder: influence of aspect ratio. *Journal of Fluid Mechanics*, *258*, 287–316. https://doi.org/10.1017/S0022112094003332

Nortek, A. S. (2009). *Vectrino velocimeter user guide*. Vangkroken, Norway.

Nyssen, J., Pontzeele, J., & Billi, P. (2011). Effect of beaver dams on the hydrology of small mountain streams: Example from the Chevral in the Ourthe Orientale

basin, Ardennes, Belgium. *Journal of Hydrology*, *402*(1–2), 92–102. https://doi.org/10.1016/j.jhydrol.2011.03.008

O'Hanley, J. R., Wright, J., Diebel, M., Fedora, M. A., & Soucy, C. L. (2013). Restoring stream habitat connectivity: A proposed method for prioritizing the removal of resident fish passage barriers. *Journal of Environmental Management*, *125*, 19–27. https://doi.org/10.1016/j.jenvman.2013.02.055

Odeh, M., Noreika, J. F., Haro, A., Maynard, A., Castro-Santos, T., & Cada, G. F. (2002). *Evaluation of the effects of turbulence on the behaviour of migratory fish, Final Report 2002.* Retrieved from http://www.efw.bpa.gov/cgi-bin/efw/FW/publications.cgi

Odoni, N. A., & Lane, S. N. (2010). *Assessment of the Impact of Upstream Land Management Measures on Flood Flows in Pickering Beck Using Overflow*.

Oner, A. A., Salih Kirkgoz, M., & Sami Akoz, M. (2008). Interaction of a current with a circular cylinder near a rigid bed. *Ocean Engineering*, *35*(14–15), 1492–1504. https://doi.org/10.1016/j.oceaneng.2008.06.005

Ouro, P., Fraga, B., Lopez-Novoa, U., & Stoesser, T. (2019). Scalability of an Eulerian-Lagrangian large-eddy simulation solver with hybrid MPI/OpenMP parallelisation. *Computers & Fluids*, *179*, 123–136. https://doi.org/10.1016/j.compfluid.2018.10.013

Ouro, P., & Stoesser, T. (2017). An immersed boundary-based large-eddy simulation approach to predict the performance of vertical axis tidal turbines. *Computers & Fluids*, *152*, 74–87. https://doi.org/10.1016/j.compfluid.2017.04.003

Ouro, P., Wilson, C. A. M. E., Evans, P., & Angeloudis, A. (2017). Large-eddy simulation of shallow turbulent wakes behind a conical island. *Physics of Fluids*, *29*(12), 126601. https://doi.org/10.1063/1.5004028

Palmer, M. A., Menninger, H. L., & Bernhardt, E. (2010). River restoration, habitat heterogeneity and biodiversity: A failure of theory or practice? *Freshwater Biology*, *55*(SUPPL. 1), 205–222. https://doi.org/10.1111/j.1365-2427.2009.02372.x

Pavlov, D. S., Lupandin, A. I., & Skorobogatov, M. A. (2000). The Effects of Flow Turbulence on the Behavior and Distribution of Fish. *Journal of Ichthyology*, *20*(2), 232–261. Retrieved from http://scholarworks.umass.edu/fishpassage_journal_articles/749

Pavlov, D. S., & Skorobogatov, M. A. (2009). Effect of the flow turbulence on the movement pattern of the caudal fin in fish. *Doklady Biological Sciences*, *428*(1), 464–466. https://doi.org/10.1134/S0012496609050214

Pelicice, F. M., & Agostinho, A. A. (2008). Fish-passage facilities as ecological traps in large neotropical rivers. *Conservation Biology*, *22*(1), 180–188. https://doi.org/10.1111/j.1523-1739.2007.00849.x

Pitt, M. (2008a). *Learning lessons from the 2007 floods*. Cabinet Office London.

Pitt, M. (2008b). Learning Lessons from the 2007 Floods. In *Floods Review*. https://doi.org/10.1007/s13398-014-0173-7.2

Plew, D. R., Nikora, V. I., Larned, S. T., Sykes, J. R. E., & Cooper, G. G. (2007). Fish swimming speed variability at constant flow: *Galaxias maculatus*. *New Zealand Journal of Marine and Freshwater Research*, *41*(2), 185–195. https://doi.org/10.1080/00288330709509907

Poff, N. L., Brinson, M. M., Day, J. W. (2002). *Aquatic ecosystems and global climate change: potential impacts on inland freshwater and coastal wetland ecosystems in the United States*. Retrieved from https://www.pewtrusts.org/-/media/legacy/uploadedfiles/wwwpewtrustsorg/reports/protecting_ocean_life/envclimateaquaticecosystemspdf.pdf

Poff, N. L., & Zimmerman, J. K. H. (2010). Ecological responses to altered flow regimes: a literature review to inform the science and management of environmental flows. *Freshwater Biology*, *55*(1), 194–205. https://doi.org/10.1111/j.1365-2427.2009.02272.x

Poff, N. LeRoy, Allan, J. D., Bain, M. B., Karr, J. R., Prestegaard, K. L., Richter, B. D., … Stromberg, J. C. (1997). The Natural Flow Regime. *BioScience*, *47*(11), 769–784. https://doi.org/10.2307/1313099

Poff, N. LEROY, & Hart, D. D. (2002). How Dams Vary and Why It Matters for the Emerging Science of Dam Removal. *BioScience*, *52*(8), 659–668. https://doi.org/https://doi.org/10.1641/0006-3568(2002)052[0659:HDVAWI]2.0.CO;2

Poff, N. LeRoy, & Schmidt, J. C. (2016). How dams can go with the flow Small changes to water flow regimes from dams can help to restore river ecosystems. *Science*, *353*(6304). https://doi.org/doi: 10.1126/science.aah4926

Pope, S. B. (2000). *Turbulent Flows*. https://doi.org/DOI:

10.1017/CBO9780511840531

Prasad, A., & Williamson, C. H. K. (1996). The instability of the separated shear layer from a bluff body. *Physics of Fluids*, *8*(6), 1347–1349. https://doi.org/10.1063/1.868942

Price, S. J., Sumner, D., Smith, J. G., Leong, K., & Paidoussis, M. P. (2002). Flow visualization around a circular cylinder near to a plane wall. *Journal of Fluids and Structures*, *16*(2), 175–191. https://doi.org/10.1006/jfls.2001.0413

Puttock, A., Graham, H. A., Cunliffe, A. M., Elliott, M., & Brazier, R. E. (2017). Eurasian beaver activity increases water storage, attenuates flow and mitigates diffuse pollution from intensively-managed grasslands. *Science of the Total Environment*, *576*, 430–443. https://doi.org/10.1016/j.scitotenv.2016.10.122

Quinn, P., O'Donnell, G., Nicholson, A., Wilkinson, M., Owen, G., Jonczyk, J., … Davies, G. (2013). *Potential Use of Runoff Attenuation Features in Small Rural Catchments for Flood Mitigation*. Retrieved from https://research.ncl.ac.uk/proactive/belford/newcastlenfmrafreport/reportpdf/June NFM RAF Report.pdf

Rahel, F. J., & Olden, J. D. (2008, June). Assessing the effects of climate change on aquatic invasive species. *Conservation Biology*, Vol. 22, pp. 521–533. https://doi.org/10.1111/j.1523-1739.2008.00950.x

Ranga Raju, K. G., Rana, O. P. S., Asawa, G. L., & Pillai, A. S. N. (1983). Rational assessment of blockage effect in channel flow past smooth circular cylinders. *Journal of Hydraulic Research*, *21*(4), 289–302. https://doi.org/10.1080/00221688309499435

Roberts, J. L. (1964). Metabolic responses of fresh-water sunfish to seasonal photoperiods and temperatures. *Helgoländer Wissenschaftliche Meeresuntersuchungen*, *9*(1–4), 459–473. https://doi.org/10.1007/BF01610057

Roni, P., Beechie, T. J., Bilby, R. E., Leonetti, F. E., Pollock, M. M., & Pess, G. R. (2002). A Review of Stream Restoration Techniques and a Hierarchical Strategy for Prioritizing Restoration in Pacific Northwest Watersheds. *North American Journal of Fisheries Management*, *22*(1), 1–20. https://doi.org/10.1577/1548-8675(2002)022<0001:AROSRT>2.0.CO;2

Roni, P., Beechie, T., Pess, G., & Hanson, K. (2015). Wood placement in river restoration: fact, fiction, and future direction. *Canadian Journal of Fisheries and*

Aquatic Sciences, *72*(3), 466–478. https://doi.org/10.1139/cjfas-2014-0344

Roscoe, D. W., & Hinch, S. G. (2010). Effectiveness monitoring of fish passage facilities: Historical trends, geographic patterns and future directions. *Fish and Fisheries*, *11*(1), 12–33. https://doi.org/10.1111/j.1467-2979.2009.00333.x

Roshko, A, Steinolfson, A., & Chattoorgoon, V. (1975). Flow forces on a cylinder near a wall or near another cylinder. *Proceedings of the 2nd US Nation Conference on Wind Engineering Research*, Paper IV-15. Fort Collins: California Inst Of Tech Pasadena.

Roshko, Anatol. (1961). Experiments on the flow past a circular cylinder at very high Reynolds number. *Journal of Fluid Mechanics*, *10*(03), 345. https://doi.org/10.1017/S0022112061000950

Sarkar, S., & Sarkar, S. (2010). Vortex dynamics of a cylinder wake in proximity to a wall. *Journal of Fluids and Structures*, *26*(1), 19–40. https://doi.org/10.1016/j.jfluidstructs.2009.08.003

Schalko, I., Schmocker, L., Weitbrecht, V., & Boes, R. M. (2018). Backwater Rise due to Large Wood Accumulations. *Journal of Hydraulic Engineering*, *144*(9), 04018056. https://doi.org/10.1061/(ASCE)HY.1943-7900.0001501

Schneider, C., Laizé, C. L. R., Acreman, M. C., & Flörke, M. (2013). How will climate change modify river flow regimes in Europe? *Hydrology and Earth System Sciences*, *17*(1), 325–339. https://doi.org/10.5194/hess-17-325-2013

SEPA. (2015a). *Natural Flood Management Handbook*. Scottish Environment Protection Agency (SEPA) Stirling.

SEPA. (2015b). *Natural Flood Management Handbook*. Scottish Environment Protection Agency (SEPA) Stirling.

Shields, F. D., & Alonso, C. V. (2012). Assessment of flow forces on large wood in rivers. *Water Resources Research*, *48*(4), 1–16. https://doi.org/10.1029/2011WR011547

Shields, F. D. J., & Gippel, C. J. (1995). Prediction of Effects of Woody Debris Removal on Flow Resistance. *Journal of Hydraulic Engineering*, *121*(4), 341–354.

Shields, F. D., Morin, N., & Cooper, C. M. (2004). Large Woody Debris Structures for Sand-Bed Channels. *Journal of Hydraulic Engineering*, *130*(3), 208–217. https://doi.org/10.1061/(ASCE)0733-9429(2004)130:3(208)

Shiono, K., & Knight, D. W. (1991). Turbulent open-channel flows with variable depth across the channel. *Journal of Fluid Mechanics*, *222*, 617–646. https://doi.org/10.1017/S0022112091001246

Silva, A. T., Katopodis, C., Santos, J. M., Ferreira, M. T., & Pinheiro, A. N. (2012). Cyprinid swimming behaviour in response to turbulent flow. *Ecological Engineering*, *44*, 314–328. https://doi.org/10.1016/j.ecoleng.2012.04.015

Silva, A. T., Lucas, M. C., Castro-Santos, T., Katopodis, C., Baumgartner, L. J., Thiem, J. D., … Cooke, S. J. (2018). The future of fish passage science, engineering, and practice. *Fish and Fisheries*, *19*(2), 340–362. https://doi.org/10.1111/faf.12258

Silva, A. T., Santos, J. M., Ferreira, M. T., Pinheiro, A. N., & Katopodis, C. (2011). Effects of water velocity and turbulence on the behaviour of Iberian barbel (*Luciobarbus bocagei*, Steindachner 1864) in an experimental pool-type fishway. *River Research and Applications*, *27*(3), 360–373. https://doi.org/10.1002/rra.1363

Silva, A. T., Santos, J. M., Ferreira, M. T., Pinheiro, A. N., & Katopodis, C. (2012). Passage efficiency of offset and straight orifices for upstream movements of Iberian barbel in a pool-type fishway. *River Research and Applications*, *28*(5), 529–542. https://doi.org/10.1002/rra.1465

Slow The Flow Calderdale. (2019). Engineered Leaky Woody Dams (WeLD's) on Rock Stream Beds - Slow The Flow Calderdale. Retrieved September 20, 2019, from http://slowtheflow.net/engineered-leaky-woody-dams-welds-on-rock-stream-beds/#

Smith, D. L., Brannon, E. L., & Odeh, M. (2005). Response of Juvenile Rainbow Trout to Turbulence Produced by Prismatoidal Shapes. *Transactions of the American Fisheries Society*, *134*(3), 741–753. https://doi.org/10.1577/T04-069.1

Smith, D. L., Brannon, E. L., Shafii, B., & Odeh, M. (2006). Use of the Average and Fluctuating Velocity Components for Estimation of Volitional Rainbow Trout Density. *Transactions of the American Fisheries Society*, *135*(2), 431–441. https://doi.org/10.1577/T04-193.1

SNIFFER. (2010). *WFD111 (2a) Coarse resolution rapid-assessment methodology to assess obstacles to fish migration Field manual level A assessment* (Vol. 111).

Retrieved from https://www.sniffer.org.uk/wfd111-phase-2a-fish-obstacles-manual-pdf

Stoesser, T. (2010). Physically Realistic Roughness Closure Scheme to Simulate Turbulent Channel Flow over Rough Beds within the Framework of LES. *Journal of Hydraulic Engineering*, *136*(10), 812–819. https://doi.org/10.1061/(ASCE)HY.1943-7900.0000236

Sumner, D. (2013). Flow above the free end of a surface-mounted finite-height circular cylinder: A review. *Journal of Fluids and Structures*, *43*, 41–63. https://doi.org/10.1016/j.jfluidstructs.2013.08.007

Taguchi, M., & Liao, J. C. (2011). Rainbow trout consume less oxygen in turbulence: the energetics of swimming behaviors at different speeds. *Journal of Experimental Biology*, *214*(9), 1428–1436. https://doi.org/10.1242/jeb.052027

Taniguchi, S., & Miyakoshi, K. (1990). Fluctuating fluid forces acting on a circular cylinder and interference with a plane wall. *Experiments in Fluids*, *9*(4), 197–204. https://doi.org/10.1007/BF00190418

Team, R. C. (2018). *R: A Language and Environment for Statistical Computing, R Foundation for Statistical Computing, Austria, 2015*. ISBN 3-900051-07-0: URL http://www. R-project. org.

Team, Rs. (2016). *RStudio: Integrated Development for R. Boston: RStudio Inc.; 2015*.

Thomas, H., & Nisbet, T. (2012). Modelling the hydraulic impact of reintroducing large woody debris into watercourses. *Journal of Flood Risk Management*, *5*(2), 164–174. https://doi.org/10.1111/j.1753-318X.2012.01137.x

Thomas, R., Vaughan, I., & Lello, J. (2013). Data analysis with R statistical software. In *A guidebook for scientists. Eco-explore*.

Tierney, K B, & Farrell, A. P. (2004). The relationships between fish health, metabolic rate, swimming performance and recovery in return-run sockeye salmon, *Oncorhynchus nerka* (Walbaum). *Journal of Fish Diseases*, *27*(11), 663–671. https://doi.org/10.1111/j.1365-2761.2004.00590.x

Tierney, Keith B., Kasurak, A. V., Zielinski, B. S., & Higgs, D. M. (2011). Swimming performance and invasion potential of the round goby. *Environmental Biology of Fishes*, *92*(4), 491–502. https://doi.org/10.1007/s10641-011-9867-2

Tierney, Keith B. (2011). Swimming Performance Assessment in Fishes. *Journal of*

Visualized Experiments, (51), 4. https://doi.org/10.3791/2572

Tomeček, J., Kováč, V., & Katina, S. (2007). The biological flexibility of the pumpkinseed: a successful colonizer throughout Europe. In *Biological invaders in inland waters: Profiles, distribution, and threats* (pp. 307–336). https://doi.org/10.1007/978-1-4020-6029-8_16

Tritico, H. M., & Cotel, A. J. (2010). The effects of turbulent eddies on the stability and critical swimming speed of creek chub (*Semotilus atromaculatus*). *Journal of Experimental Biology*, *213*(13), 2284–2293. https://doi.org/10.1242/jeb.041806

Uhlmann, M. (2005). An immersed boundary method with direct forcing for the simulation of particulate flows. *Journal of Computational Physics*, *209*(2), 448–476. https://doi.org/10.1016/j.jcp.2005.03.017

Unal, M. F., & Rockwell, D. (1984). Role of Shear Layer Stability in Vortex Shedding From Cylinders. *Physics of Fluids*, *27*(11), 2598–2599. https://doi.org/10.1063/1.864557

van der Hoop, J. M., Byron, M. L., Ozolina, K., Miller, D. L., Johansen, J. L., Domenici, P., & Steffensen, J. F. (2018). Turbulent flow reduces oxygen consumption in the labriform swimming shiner perch, *Cymatogaster aggregata*. *The Journal of Experimental Biology*, *221*(11), jeb168773. https://doi.org/10.1242/jeb.168773

Videler, J. J., & Wardle, C. S. (1991). Fish swimming stride by stride: speed limits and endurance. *Reviews in Fish Biology and Fisheries*, *1*(1), 23–40. https://doi.org/10.1007/BF00042660

Wahl, T. L. (2003). Discussion of "Despiking Acoustic Doppler Velocimeter Data" by Derek G. Goring and Vladimir I. Nikora. *Journal of Hydraulic Engineering*, *129*(6), 484–487. https://doi.org/10.1061/(ASCE)0733-9429(2003)129:6(484)

Wallerstein, N., & Thorne, C. R. (1997). *Impacts of woody debris on fluvial processes and channel morphology in stable and unstable streams*. Department of Geography, University of Nottingham (United Kindgom)

Wang, H., & Chanson, H. (2018). Modelling upstream fish passage in standard box culverts: Interplay between turbulence, fish kinematics, and energetics. *River Research and Applications*, *34*(3), 244–252. https://doi.org/10.1002/rra.3245

Wang, R. W., David, L., & Larinier, M. (2010). Contribution of experimental fluid

mechanics to the design of vertical slot fish passes. *Knowledge and Management of Aquatic Ecosystems*, (396), 02. https://doi.org/10.1051/kmae/2010002

Webb, P. W. (2004). Response latencies to postural disturbances in three species of teleostean fishes. *Journal of Experimental Biology*, *207*(6), 955–961. https://doi.org/10.1242/jeb.00854

Webb, P. W., & Cotel, A. J. (2010). Turbulence: Does Vorticity Affect the Structure and Shape of Body and Fin Propulsors? *Integrative and Comparative Biology*, *50*(6), 1155–1166. https://doi.org/10.1093/icb/icq020

Webb, Paul W. (1998). Entrainment by river chub nocomis micropogon and smallmouth bass Micropterus dolomieu on cylinders. *The Journal of Experimental Biology*, *201*(16), 2403–2412. Retrieved from http://jeb.biologists.org/content/201/16/2403.short

Webb, Paul W., & Cotel, A. J. (2011). Assessing possible effects of fish-culture systems on fish swimming: the role of stability in turbulent flows. *Fish Physiology and Biochemistry*, *37*(2), 297–305. https://doi.org/10.1007/s10695-011-9497-9

Webb, Paul W. (2002). Control of Posture, Depth, and Swimming Trajectories of Fishes. *Integrative and Comparative Biology*, *42*(1), 94–101. https://doi.org/10.1093/icb/42.1.94

Wenzel, R., Reinhardt-Imjela, C., Schulte, A., & Bölscher, J. (2014). The potential of in-channel large woody debris in transforming discharge hydrographs in headwater areas (Ore Mountains, Southeastern Germany). *Ecological Engineering*, *71*, 1–9. https://doi.org/10.1016/j.ecoleng.2014.07.004

Williams, J. G., Armstrong, G., Katopodis, C., Larinier, M., & Travade, F. (2012a). Thinking like a fish: a key ingredient for development of effective fish passage facilities at river obstructions. *River Research and Applications*, *28*(4), 407–417. https://doi.org/10.1002/rra.1551

Williams, J. G., Armstrong, G., Katopodis, C., Larinier, M., & Travade, F. (2012b). Thinking Like A Fish: A Key Ingredient For Development Of Effective Fish Passage Facilities At River Obstructions. *River Research and Applications*, *28*(4), 407–417. https://doi.org/10.1002/rra.1551

Williamson, C. H. K. (1996). Vortex Dynamics in the Cylinder Wake. *Annual Review of Fluid Mechanics*, *28*(1), 477–539.

Wohl, E. (2013). Floodplains and wood. *Earth-Science Reviews*, *123*, 194–212. https://doi.org/10.1016/j.earscirev.2013.04.009

Wohl, E., Angermeier, P. L., Bledsoe, B., Kondolf, G. M., MacDonnell, L., Merritt, D. M., … Tarboton, D. (2005). River restoration. *Water Resources Research*, *41*(10), 1–12. https://doi.org/10.1029/2005WR003985

Yen, B. C. (2002). Open Channel Flow Resistance 1. *Journal of Hydraulic Engineering*, *128*(1), 20–39. https://doi.org/Doi 10.1061/(Asce)0733-9429(2002)128:1(20)

Young, W. J. (1991). Flume study of the hydraulic effects of large woody debris in lowland rivers. *Regulated Rivers: Research and Management*, *6*(3), 203–211.

Zdravkovich, M. M. (1985). Forces on a circular cylinder near a plane wall. *Applied Ocean Research*, *7*(4), 197–201. https://doi.org/10.1016/0141-1187(85)90026-4